AFIT/GAE/ENY/99M-03.

FATIGUE RESPONSE OF REPAIRED THICK ALUMINUM PANELS WITH BONDLINE FLAWS

THESIS

David S. Conley
Captain, USAF

AFIT/GAE/ENY/99M-03.

Approved for public release; distribution unlimited

Disclaimer

The views expressed in this dissertation are those of the author and do not reflect the official policy or position of the United States Air Force, the Department of Defense, or the United States Government.

AFIT/GAE/ENY/99M-03.

FATIGUE RESPONSE OF REPAIRED THICK ALUMINUM PANELS WITH BONDLINE FLAWS

THESIS

Presented to the Faculty of the Graduate School of Engineering of the Air Force Institute of Technology Air University In Partial Fulfillment for the Degree of

Master of Science

David S. Conley

Captain, USAF

Air Force Institute of Technology

Wright-Patterson AFB, Ohio

March 8, 1999

Sponsored by both the Fatigue and Fracture Group, Air Vehicle's Directorate (AFRL/VASE) and the Mission Support Group, Material's Directorate (AFRL/MLSA)..

AFIT/GAE/ENY/99M-03.

FATIGUE RESPONSE OF REPAIRED THICK ALUMINUM PANELS WITH BONDLINE FLAWS

David S. Conley

Captain, USAF

Approved:

Dr. Shankar Mall
Committee Chairman

3/5/99
Date

Dr. Anthony N. Palazotto
Committee Member

3/5/99
Date

Maj Jeffrey S. Turcotte
Committee Member

5 Mar 99
Date

Dedication

I dedicate this work to my friend Brian Cramer, who taught me just about everything I know about bonded repairs.

Acknowledgments

There are a large number of people whom I would like to thank for all the help they provided during thecourse of this project. This could take a while, so please be patient. I would like to thank Dr. Tom Mills for his encouragement, expertise, advise and jumbalaya. He designs a mean patch and an even meaner stew. Lt Jim Ryan was kind enough to provide machining work and a sharp wit (at no extra charge). I have tried to match wits with him on several occasions but always seem to leave the fray pummeled and beaten...someday Jim. Maj Joel Schubbe was instrumental in furthering my understanding of both finite elements and composite patching. His Jeep is the posterchild for aging systems damage. If he can keep that thing running, he should definitely be working on airplanes. Without help from Sam Naboulsi, the finite element portion of this work would never have been completed. And despite what some might think, I do not hold his being a Buckeyes fan against him, very much. I would like to thank Mr. Mark Derriso for properly educating me on the use of the MTS 458 controller, which was promptly exchanged out for a newer model as soon as I was up to speed. Go figure. I would like to thank Jim Mazza, Dan McCray, Lt Jason Avram and the Soche students Kylie and Mike for all their help. A brighter group of people would be hard to find; that and they put together a pretty good paint-ball party. John Brausch and Dan Laufersweiler both went well beyond the call of duty in taking care of all my NDI needs. Their willingness to take time out of their personal lives to help me was much appreciated. Next on my list is the AFIT lab staff. Jay Anderson made sure I had the equipment and training I needed to do my experimentation (safety briefing? what safety briefing). Thanks to Dan Rioux for buying the new tools and toys that made my work easier. That Tennessee Vols obsession can be cured by a good bout of pshychotherapy, so you do not need to worry. I would like to thank Andy Pitts, not for any particular work done but for the pointless stories, the bad jokes and the fond memories. Thanks

also to Kris Larsen who made sure all my computer resource needs were taken care of. I would also like to acknowledge the people who introduced me to the field of bonded repairs, Capt Jason Denney (a.k.a. botog) and Lt. Col Rob Fredell. I would like to thank my advisor Dr. Shankar Mall for being patient and supportive of this work. Last but not least, there was the support at home. I would like to thank my dog Sonny for not getting upset at all the missed walks because I had to do some writing. I want to thank my cat Duke for keeping his cool under pressure. And most importantly, I would like to thank my soon to be Fiance (its a secret so do not tell her yet) Caroline Groth. Her love and support made everything a whole lot easier. All this goes to prove one thing, given a large enough group of people, even I can get through a Masters program. Thanks everybody.

David Conley

Table Of Contents

List of Figures

Page

Page

List of Tables

List of Symbols

English Symbols

a	Half Crack Length
$^{\circ}C$	Degree Celsius
$^{\circ}F$	Degree Fahrenheit
E	Young's Modulus (MPA)
G	Strain Energy Release Rate
K	Stress Intensity Factor
r	Radius (crack tip to point of interest)
c	Material Constant
m	Material Constant or Meter
M	Moment (N*m), or Mega ($1*10^6$)
Pa	Pascal
S	Stiffness Ratio
T	Force (N) or Temperature ($^{\circ}C/^{\circ}F$)
u	Displacement Along X-Axis
v	Displacement Along Y-Axis
$\frac{da}{dN}$	Crack Growth Rate (m/cycle)
t	Thickness (mm)

Greek Symbols

α	Coefficient of Thermal Expansion of LEFM Correction Constant for Geometry
σ	Stress (MPA)

π	Pi (radians)
θ	Plane Rotation (radians), or Elevation Angle from Crack Plane to Point of Interest
υ	Poisson's Ratio
Δ	Delta (parameter range)
ρ	Radius of Curvature

Subscripts

I	Mode I
II	Mode II
III	Mode III
L	Longitudinal Direction
T	Transverse Direction
x	X-Axis Designator
y	Y-Axis Designator
z	Z-Axis Designator
xy	X-Y Plane Designator
max	Maximum
r	Repair Property Values
p	Plate Property Values

Superscript

u	Extensional Designator
c	Leading Node Quantity
t	Total Designator

θ	Rotational Designator
i	Wildcard Designator for Plate, Adhesive, or Patch Properties

Abbreviations

ABDR	Aircraft Battle Damage Repair
AFIT	Air Force Institute of Technology
AFRL	Air Force Research Laboratory
AMRL	Aeronautical and Maritime Research Laboratory
ASTM	American Society for Testing and Materials
CD	Center Disbond
CTD	Crack Tip Disbond
CTE	Coefficient of Thermal Expansion
FBP	Fully Bonded Patch
FAA	Federal Aviation Administration
FWD	Full Width Disbond
GBS	Grit Blast Silane
GDP	Gross Domestic Product
LEFM	Linear Elastic Fracture Mechanics
NASA	National Aeronautics and Space Administration
PAA	Phosphoric Acid Anodize
PABST	Primary Adhesively Bonded Structure Technology
PACS	Phosphoric Acid Containment System
PTD	Patch Tip Disbond
RAAF	Royal Australian Air Force

AFIT/GAE/ENY/99M-03.

Abstract

In today's environment of dwindling budgets and expanding missions, new tools need to be developed to aid in the maintenance of the Air Force's aging aircraft fleet. As the service lives of these aircraft are extended beyond their original design lives, the integrity and safety of their structures becomes a looming issue. Structure that has broken or been damaged must be repaired or replaced, with repair being the more cost effective option. Bonded composite repair of metallic structures is one of the candidate technologies which has demonstrated enormous potential in this area and is the subject of this study.

Analytical, numerical and experimental research has been conducted in characterizing fatigue response and damage tolerance of bonded composite repair to thin metallic structure. Thick structure, while not being ignored, has not enjoyed the same attention. The effectiveness of bonded repairs in extending the lives of thick structural components is not in doubt. Applications however have been limited because of questions concerning the tolerance of these repairs to application or manufacturing defects. This limitation on the technology is mainly due to a lack of research in this area. The purpose of this study was to expand the knowledge base by: 1) experimentally investigating the fatigue response of repaired thick aluminum panels with bondline flaws and, 2) investigating the accuracy of current finite element modeling techniques in predicting the life of repaired thick aluminum panels.

The experimental portion of this study involved the fatigue testing of precracked 559x178x6.35mm (22x7x0.25in), 2024-T351 aluminum panels repaired with partially bonded, unidirectional 18 ply Boron/Epoxy composite patches. Panels with no repair were also tested to establish a baseline for comparison. The debonds were introduced into the adhesive bondline using teflon inserts. The

repaired panels were subjected to constant amplitude fatigue testing with a peak stress of 120 MPa. Five different debond location configurations were tested, with debonds ranging in size from 5% to 20% of the total bond area. Test specimens underwent ultrasonic inspection during the course of testing to track debond growth. Out of plane displacements caused by thermal mismatch between the patch and panel were also measured.

Results from the experimentation showed that crack growth rate was influenced by how much of the crack was covered or bridged by the adhesive and patch. Debond locations away from the crack showed little or no impact on repair life. In these configurations, the crack was bridged restricting crack tip opening displacement and thus crack growth. Debond locations around the crack allowed greater crack tip opening displacement, resulting in increased crack growth rates and shorter repair life. Ultrasonic inspection showed no noticeable growth in the artificially induced debonds for any of the debond configurations during fatigue testing.

The numerical analysis portion of this study involved the finite element modeling of the repaired aluminum panel. The repaired panel was modeled using three layers of 2D 4 noded Mindlin plate elements, with separate layers modeling the aluminum panel, the adhesive and the composite patch. The layers were connected at the nodes using through-the-thickness constraint equations that satisfied both Mindlin plate assumptions and compatibility along the plate-adhesive and adhesive-patch interfaces. Debonds were simulated in the model by releasing nodes in the debond area from the appropriate constraint equations. Displacement results from the model were used with the modified indirect crack closure method to calculate the strain energy release rate at the crack tip. The stress intensity factor at the crack tip was then calculated from the strain energy release rate. Crack growth rate data was then calculated from the stress intensity factor using the Paris Law. Results from the finite element model were shown to very closely match experimental data.

In summary, this study showed that debond size and location had a definite impact on the life of a repaired specimen. It showed that current repair design practices, originally developed for thin structure, resulted in repairs that were tolerant of very large debonds when applied to thick structure. However, the experimental results also suggest that there is much work left to be done in the area of repair-design optimization for thick structure. The numerical analysis showed that current modeling techniques can adequately predict stress intensity factors and crack growth rates of bonded composite repairs for thick structure.

FATIGUE RESPONSE OF REPAIRED THICK ALUMINUM PANELS WITH BONDLINE FLAWS

Chapter 1 - Introduction

1.1 Aging Aircraft

One of the key factors in aircraft design is how long the aircraft is to be in service. For commercial and military aircraft, an expected life of twenty years is typical. The aircraft is designed with an economic life that equals the expected service time. The economic life of an aircraft is reached when it is no longer fiscally viable to keep the aircraft in service. In other words, when the cost of maintaining an aircraft becomes greater than the revenues and services provided by the aircraft, or greater than the cost of purchasing a new aircraft, it has reached the end of its economic life.

The increasing cost of purchasing new aircraft serves to extend the economic lives of existing airframes. This being the case, it becomes economically necessary to keep current aircraft inventories flying. The reasons for this are really quite obvious. In the case of commercial airlines, in order to remain competitive, costs must be kept down. As generating a profit is the goal of commercial airlines, they stand to make more money by using the aircraft they have now, as opposed to purchasing new. For the military, the reasons are somewhat different.

Procurement buying power is at a fifty year low and continues to drop. Figure 1 shows defense spending over the past fifty years. As defense budgets dwindle, the funding available for new procurements becomes scarce. This means that newer aircraft cannot be purchased that will replace those that are retired due to age, or become unserviceable through damage or obsolescence.

The immediate problem that is seen from this is despite the reduction in resources, the scope of the military's mission never decreases. The only real solution for the military is to extend the service lives of their current inventory. At first this does not sound troubling until one notices that service lives are being extended far beyond what their original designs intended.

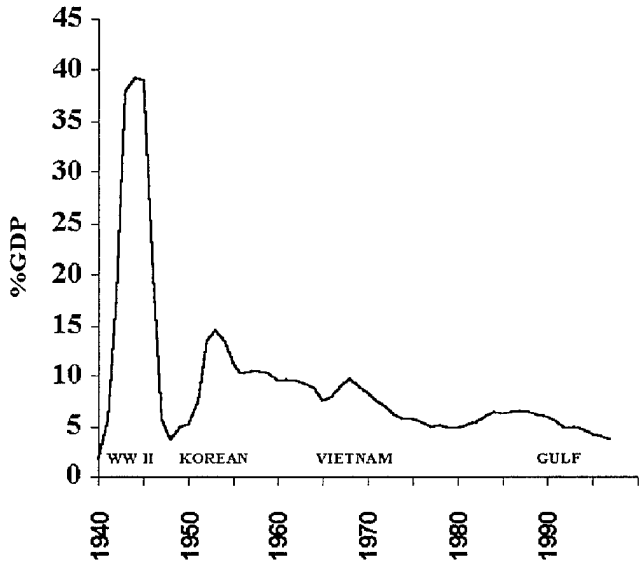

Figure 1. Military Spending as % of Gross Domestic Product

This practice of extending the service lives of older aircraft has caused the problem now known as Aging Aircraft. Aging aircraft covers a wide range of topics from outdated and obsolete avionics to fatigued and weakened structures. This writing will concentrate on the structural aspect of the Aging Aircraft problem.

The Aging Aircraft problem really gained attention in April, 1988 when Aloha Airlines' Flight 243 [1] lost a large portion of its forward fuselage in mid-flight. It was subsequently discovered that the accident was caused by extensive fatigue cracking in the lap joints joining the upper and lower portions of the fuselage. This accident illustrated to the world how potentially dangerous the aging aircraft problem was, and as a direct result, the U.S. Government established the Na-

tional Aging Aircraft Research Program under the Federal Aviation Administration (FAA) and the Airframe Structural Integrity Program under the National Aeronautics and Space Administration (NASA). The Air Force, aware of its own inventory of aging aircraft, established its own Aging Aircraft Program. Table 1 [2] shows the age and expected future use of some of the Air Force's current aircraft.

Table 1. Age Chart

Aircraft	Year Fielded	Average Age	Proposed Retirement	Retirement Age
C/KC-135	1956	35.0	2040	79
B-52H	1961	34.3	2030	68
T-38	1961	28.5	2020	52
C-141	1965	29.5	2003	36
E-3	1977	16.3	2025	45
F-16	1979	7.6	2025	36

In order to keep these aircraft safe as they grow older, aggressive maintenance technologies and programs are required. The Air Force Research Laboratory has programs in place directed at stemming the structural damage caused by aging, i.e. fatigue cracking, stress corrosion, etc. [3]. This technology is being transferred to the aircraft maintainers who will field and apply it within their maintenance programs. However, maintenance programs do not have unlimited funding; therefore the technologies they employ must both do the job and be cost effective.

Aircraft maintainers have basically three choices when dealing with aircraft structures in need of service: 1) replace, 2) repair or 3) scrap. Scrapping a part runs the risk of removing the aircraft from service and is therefore undesirable. Replacing a part would be the most desirable choice, but doing so is not always possible. In some cases, the aircraft is no longer in production and replacement parts are very difficult to come by. In other cases, the parts are simply no longer available. The maintainer can then expect to pay heavily to either purchase the part or have it custom made. With funding levels low, this is also undesirable. This leaves the final less expensive option of repair.

The majority of structural repairs performed on Air Force aircraft are accomplished using mechanically (bolted/riveted) fastened doublers. This technology is well known and established in the maintenance community. Mechanically fastened repairs have the advantage that they are easily designed, fabricated and installed. However, installation requires the drilling of holes into the parent structure. These holes constitute a loss of material, directly affecting the load carrying capability of the damaged structure. Moreover, the holes are sites of increased stress concentrations which can cause further fatigue cracking. An improperly designed or applied bolted/riveted repair can potentially cause more damage than it repairs. An alternative technology pioneered by the Australian Aeronautical and Maritime Research Laboratory (AMRL) provides structural reinforcement by bonding composite doublers to damaged structure. Composites, with their combination of high strength, low weight and excellent fatigue properties, make for good repair material. Added benefits are the ability to customize or tailor the design to fit the application. The process of bonding the repair does not require any drilling and eliminates the high stress concentrations introduced by mechanical fasteners. This technology has been in service in the Australian military for many years and has met with great success [5, 6]. The U.S. military and commercial industry, confronted with the same problems faced by the Australians, namely decreased funding and aging aircraft, are now employing bonded repairs in their maintenance practices. It must be noted, however, that bonded repairs are not without disadvantages. Strict process controls are required to ensure the composite is securely bonded to the parent structure. Deviations can cause flaws in the adhesive bondline, commonly referred to as debonds, which result in a drop in repair efficiency and a shortening of the life-span of the repair.

The transfer of bonded technology into the military is progressing slowly. Many in the maintenance community are trained and become highly skilled in applying bolted repairs. They populate the sheet metal shops found at nearly every Air Force base. Due to lack of exposure, many

are unfamiliar and still uncomfortable with bonding composites onto airplanes. For this reason, bonded repairs in Air Force applications, with the exception of a few programs [7, 8], are still confined to thin, secondary, non-critical structures, i.e. fuselage skins. Thick heavily loaded structure (primary structure), when damaged, is either replaced or repaired using mechanically fastened reinforcements

Research performed by the Australians [9] and recent Air Force studies [10–12], show the benefits of applying fully bonded repairs to thick heavily loaded structure. There is little question about the potential of the technology, however there are still questions concerning the tolerance of bonded repairs to flaws. Denney [11] investigated the effects of debonds in thin structures ($t \leq$ 1mm). This work was carried further by Mills and Ryan [12] (1mm $\leq t \leq$ 3.175mm). Schubbe [10] characterized the performance of fully bonded repairs to thick structure (3.175mm $\leq t \leq$ 6.35mm). The current study was performed to characterize the effects of debonds on the fatigue life of thick structures ($t = 6.35$mm). A finite element analysis was also performed to investigate the accuracy of current analysis tools in predicting the life of thick repaired structures.

Thick aluminum panels were precracked and then repaired with composite patches. Disbonds were intentionally placed within the bondline to simulate flaws. Disbonds were placed in different areas under the repair to investigate the effect of location on fatigue life. Fully bonded repairs and precracked panels with no repair were also tested to establish a baseline. The repair configurations tested are shown in Figure 2. The aluminum panels were AL2024-T351 with nominal dimensions of 558.8x177.8x6.35mm. The patch was an eighteen ply boron/epoxy lay-up with nominal dimensions of 182x101.6x2.286mm. The test specimens were subjected to constant amplitude fatigue cycling until panel failure.

This thesis has been separated into six chapters, each summarizing a different part of the study. This first chapter presented the motivation and goal of the study. The second chapter discusses

both theory and past efforts into bonded repair technology. Chapter three provides details about all experimental work and associated experimental procedures. The fourth chapter presents and discusses the results of the experimental work. Chapter five details and summarizes the results of the finite element modeling approach. Chapter six closes the document with a brief summary of the work done and includes a discussion of avenues of future research.

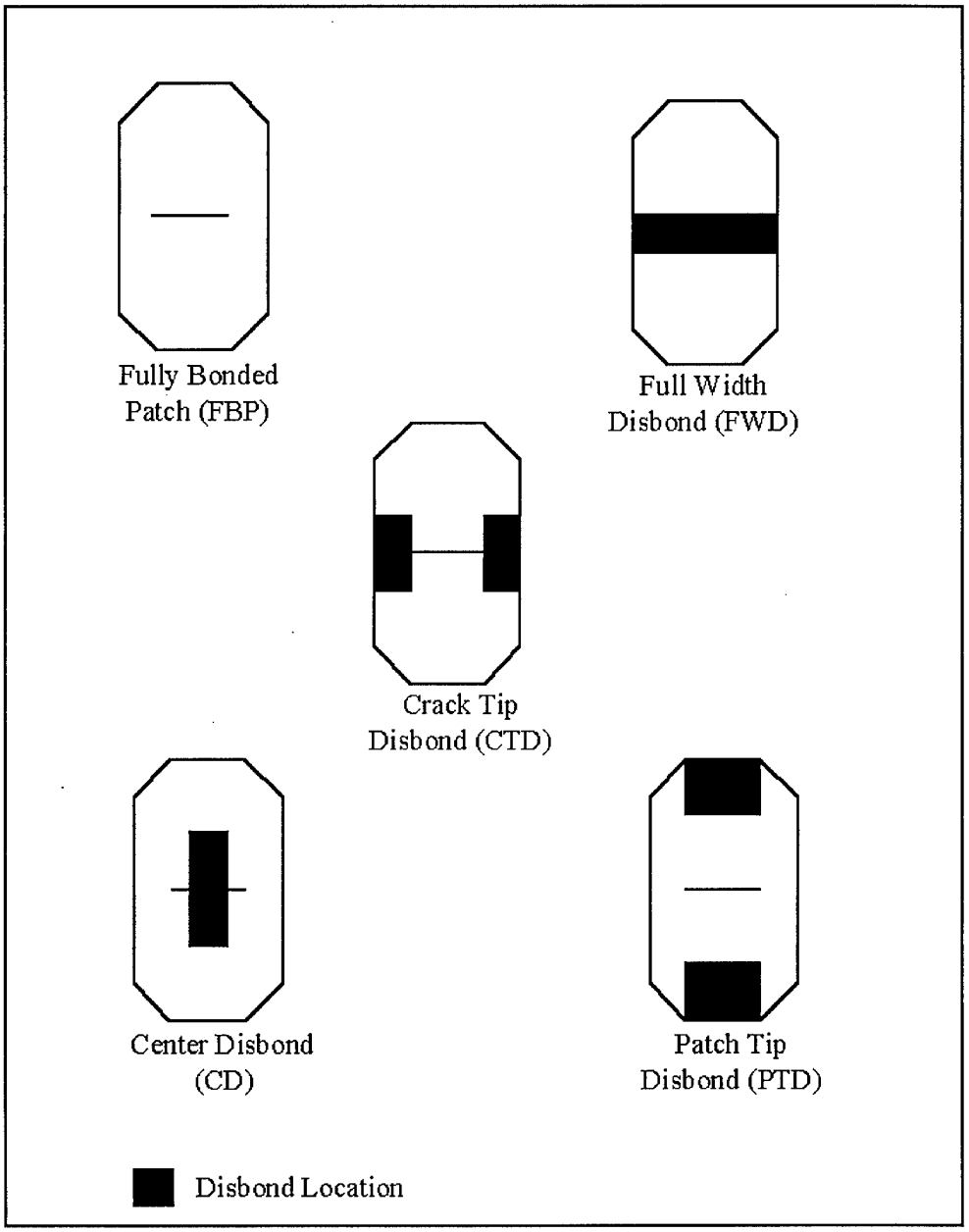

Figure 2. Repair Configurations

Chapter 2 - Background

2.1 Theory

To understand how a repair works, it is helpful to be familiar with some of the basic concepts of fracture mechanics. Fracture mechanics, as the name implies, is the study of fracture (crack growth) in structures. This discussion will focus on the area of fracture mechanics known as Linear Elastic Fracture Mechanics (LEFM) and the concept of the Stress Intensity Factor (K).

Consider a piece of structure that has a crack in it. This crack could be caused by loading, environment or a combination of both. If the structure is continuously subjected to these conditions, the crack will grow. Figure 3 shows crack growth as a function of time/loading cycles. As the crack grows, the load carrying ability, the residual strength and the time to failure of the structure is decreased. When the residual strength of the structure is no longer strong enough to carry the apploed load, the structure will fail.

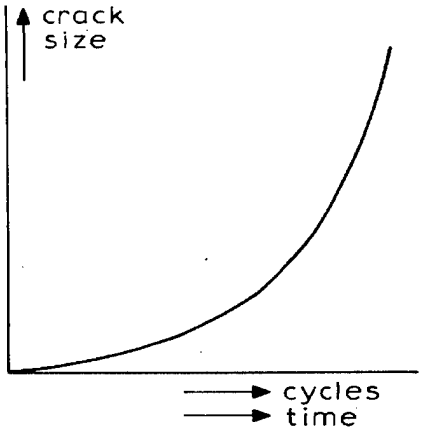

Figure 3. Crack Length versus Time/Loading Cycles [13]

Stress can be applied to a crack in three different loading modes. These modes are shown in Figure 4. In Mode I, the load is tensile, in-plane and perpendicular to the crack, causing it to "open." Mode II represents an in-plane load, parallel to the crack that causes a "sliding" motion.

In Mode III, the load is parallel to the crack, but out of plane causing a "tearing" motion. Mode I is the dominant loading condition in this study. For more detail on Modes II and III, the reader is referred to any fracture mechanics textbook. Consider the case of an infinite plate with a crack

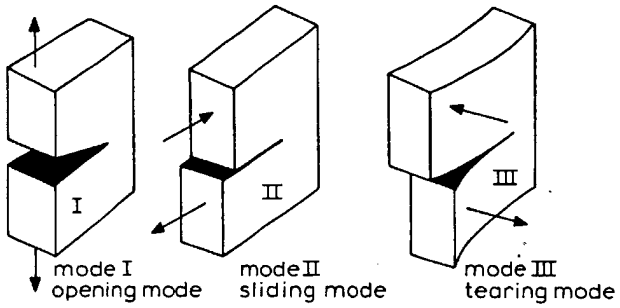

Figure 4. Crack Opening Modes [13]

subject to the uniaxial far field stress σ as seen in Figure 5. For the infinite plate Mode I condition, Linear Elasticity defines the stress intensity factor K_I as:

$$K_I = \sigma\sqrt{\pi a} \tag{1}$$

where σ=the applied stress and a=half the crack length.

Using this, it can also be shown [13] that the stresses at the crack tip are:

$$\sigma_x = \frac{K_I}{\sqrt{2\pi r}}\sqrt{\frac{a}{2r}}cos\frac{\theta}{2}[1 - sin\frac{\theta}{2}sin\frac{3\theta}{2}] \tag{2}$$

$$\sigma_y = \frac{K_I}{\sqrt{2\pi r}}\sqrt{\frac{a}{2r}}cos\frac{\theta}{2}[1 + sin\frac{\theta}{2}sin\frac{3\theta}{2}] \tag{3}$$

$$\tau_{xy} = \frac{K_I}{\sqrt{2\pi r}}sin\frac{\theta}{2}cos\frac{\theta}{2}cos\frac{3\theta}{2} \tag{4}$$

$$\sigma_z = 0 \text{ (plane stress)} \tag{5}$$

or

$$\sigma_z = \nu(\sigma_x + \sigma_x) \text{ (plane strain)} \tag{6}$$

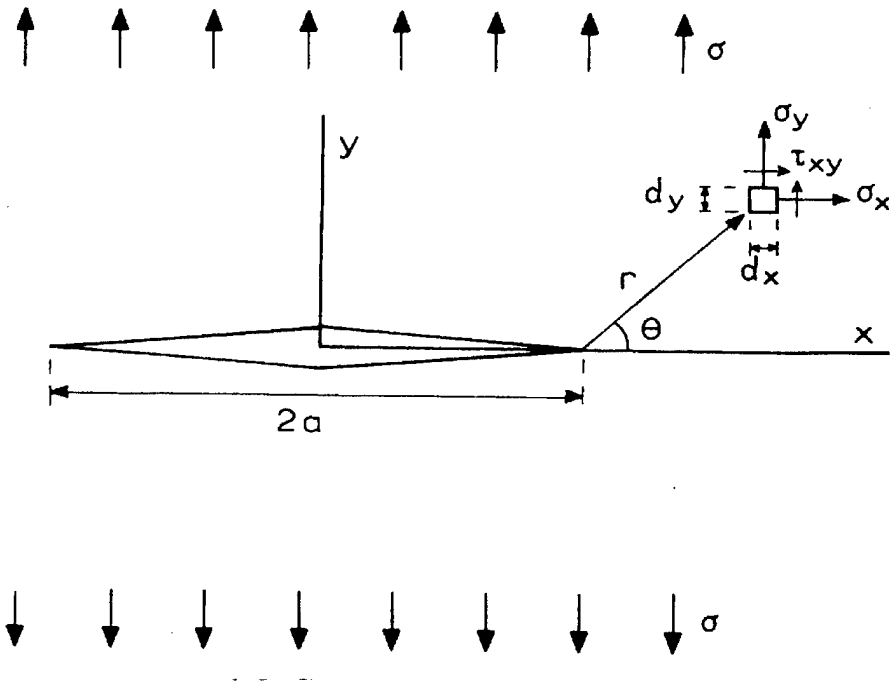

Figure 5. Crack in Infinite Plate [13]

The stress component of interest in Mode I is σ_y. This is the stress that causes the opening of the crack. The stress intensity factor K has the units of $stress * \sqrt{length}$. It can be difficult at first to recognize a physical relationship for K. The best way to describe it is to look at Figure 6 and know that K characterizes or describes the shape of the stress field σ_y in front of the crack tip.

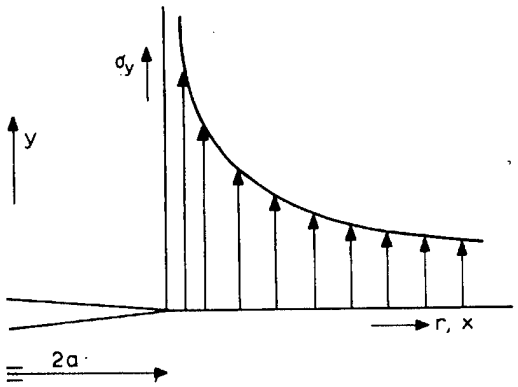

Elastic stress σ_y at the crack tip

Figure 6. Stress Field σ_y at the Crack Tip [13]

As there are very few infinite plates in reality, the following relation can be defined from elasticity which takes finite geometries or modal variations of the crack growth into consideration.

$$K = \alpha\sigma\sqrt{\pi a} \tag{7}$$

where α=correction constant for specimen geometry or crack opening mode.

This correction factor has already been calculated for many different geometries and can be generally found in fracture handbooks and textbooks. There are many different ways to relate K to crack growth, but for engineering purposes the most common is the Paris Law.

$$\frac{da}{dN} = c\Delta K^m \tag{8}$$

where da=change in crack length

dN=change in number of loading cycles

c, m =material constants

Now that the connection between stress and crack growth has been established, consider a cracked plate that has been repaired. As the plate is loaded, the load that would have flowed around the crack tip is re-routed. Instead, the load is attracted into the repair through the adhesive. The repair provides an alternate load path. The load that would have gone into opening the crack is now distributed between the panel and the repair, effectively reducing the stresses around the crack tip. Reducing the stress reduces the stress intensity factor, which in turn reduces the crack growth. A properly designed and applied repair can significantly slow down the growth of a crack and, in some cases, retard it entirely.

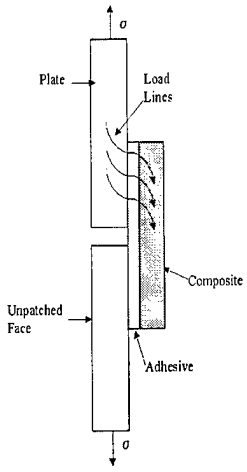

Figure 7. Load Flow into a Repair

2.2 Bonded Composite Repair versus Mechanically Fastened Repairs

Traditional structural repairs use metallic materials and mechanical fasteners to fix damaged structure. These repairs are normally designed to satisfy only one criterion, that of restoring static strength to the damaged component. The effects of dynamic loading and environment are not taken

into account. This approach is no longer acceptable as the effects of fatigue and corrosion are more evident than ever because of the aging state of most of the Air Force's aircraft.

The majority of structural repairs done today, as in the past, still use metal doublers and mechanical fasteners. Despite the absence of fatigue and corrosion considerations in the design process, this approach does have its advantages. The wealth of experience that maintainers have applying "bolted" repairs stems back to the introduction of the modern metallic airplane. As these repairs seek only to restore static strength, they are relatively quick and easy to design. The equipment and infrastructure needed to apply them has been in place for decades, making them easy to both apply and remove. Bolted repairs can be assembled in nearly any environment [14]. The materials used are highly available and not subject to limited shelf lives. The application process does not pose any serious environmental concerns as few chemicals other than solvent and sealant are needed to apply a repair. Moreover, they can be used in high temperature areas where composites would be prone to heat related damage. However, there are also some serious drawbacks to be considered when using metal/mechanical repairs. The first is in the aforementioned design process which neglects fatigue and corrosion. The repair, being metallic, becomes susceptible to the same fatigue loading and corrosion that damaged the original structure. Another problem lies in the application process where it is necessary to drill holes into the parent structure. This has two effects. The first being that material has been removed from the parent structure reducing its load carrying ability. The second and potentially more serious is that the holes become areas of high stress concentrations. These sites become prime areas for the nucleation and growth of new cracks. Corrosion will still be a problem as, at the repair interface, galvanic corrosion may occur. This damage becomes difficult to detect, because the corrosion is obscured by the repair. From this discussion, it becomes apparent that it is actually possible to worsen the damage on a structure by applying a metal/mechanical repair.

Bonded composite repairs solve many of the problems introduced by bolted repairs. Modern composites provide the maintainer with a high strength, fatigue resistant, low weight material with which to assemble repairs. This high strength means composite repairs can be smaller, more streamlined and lighter than their equivalent metal repairs, an important aspect when dealing with aerodynamic or weight sensitive structure. Composite repairs are highly tailorable. They can be made to match surfaces with complex geometry. Also, given the designer knows the stresses at a given repair location, the repair can be oriented such that the loading directions and fiber directions coincide, allowing the composite to more efficiently transfer load away from the damaged structure. Imagine, instead of transferring the load through a finite number of points inside the repair area, the load is transferred at every point inside the repair area. This eliminates the stress risers found in bolted repairs and is the advantage gained by bonding. Also, problems associated with interface corrosion are minimized, as most composites do not react with metal. This combination of attributes allows the bonded composite to restore static strength, improve fatigue resistance, and minimize corrosion damage; the elements required of a properly applied repair. As a testament to their effectiveness, there are currently over 6500 composite patches flying on fuselage skins, either as structural reinforcements or as crack arrestors [15].

Composites are not perfect however and also have their disadvantages. Training is required to learn how to properly handle the composite material. The composite material is more costly and less readily available when compared to metal. The damaged surface must be properly prepared (surface preparation) before a repair can be applied. This surface preparation requires specialized equipment and training and is very process/environment sensitive. Any deviation from the process or contamination from the environment can severely degrade the quality of the repair. Chemicals are used in the surface preparation that must be carefully and professionally handled in order to avoid environmental concerns. The choice of adhesive type, whether it be film or paste, is also

important. Film adhesives are preferred as they provide a good thin uniform bondline with less opportunity for porosity. However, most film adhesives require elevated cure temperatures, which can cause adverse residual thermal stresses in both the repair and damaged structure [16]. Problems associated with elevated temperatures can be removed by using room-temperature cure paste adhesives, but the trade off is reduced strength, bondline non-uniformity, and increased bondline porosity susceptibility. Most adhesives and composites must be stored in a freezer and have a shelf life of approximately one year. Lastly, bonded repairs, once applied, are very difficult to remove [14, 16–18].

2.3 Composite Repair Design

Some of the major factors that should be taken into consideration when using bonded composite repairs are listed below.

- Design
- Patch Material Selection
- Adhesive Selection
- Surface Preparation

2.3.1 Design

"The goal of a properly designed bonded repair is to restore the damaged structure's ultimate load carrying capability. Damage growth should either be arrested or significantly retarded. The repair must be carried out without causing further damage or creating a weak link in the structure. In short, the repair allows the structure to fulfill its original intended function [19]."

Understanding the loads that act on a repair aid greatly in the patch design. Consider the case of a single sided repair undergoing Mode I loading, the configuration investigated in this study. Both the repaired structure and the repair are experiencing tensile stresses. The load is transferred from the parent structure to the patch through shear in the adhesive. This is shown in Figure 8.

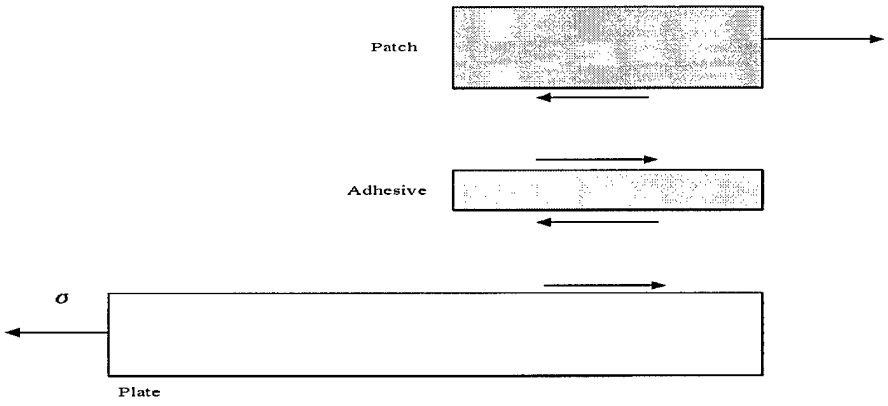

Figure 8. Repair Load Transfer

The plate is tensilly loaded, however the application of the repair causes a shift of the neutral axis through the repaired area. This shift introduces a bending moment between the plate and patch. This bending, shown in Figure 9, adds a component of load normal to the adhesive, its weakest load carrying direction. Moreover, the normal load occurs near the patch tip, the area of highest shear stress.

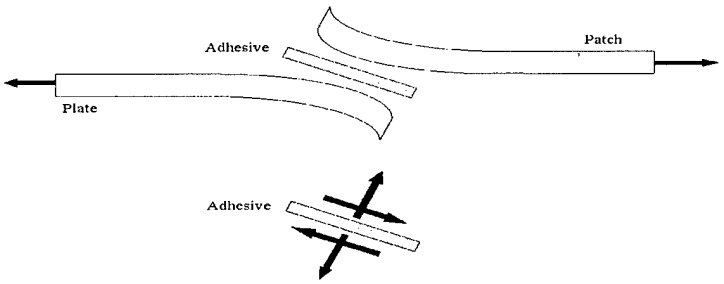

Figure 9. Bending Caused by Neutral Axis Shift in Single Sided Repair

This combination of normal and shear loading can lead to two common modes of bondline failure, peel and cleavage. Peel represents the combination of shear and tensile loads acting on the thin adhesive, while cleavage is the result of the offset tensile load [19]. Both failure modes are shown in Figure 10.

By tapering the edge of the patch, load can be more gradually transferred from the parent structure to the patch. This will reduce the high stresses that contribute to peel and cleavage fracture. Increasing the overlap length of the repair spreads the load out over a larger bond area, again reducing the stresses that cause peel and fracture. It should be noted however that increasing the overlap length can have negative side effects. Schubbe [10] showed that, in thick structure,

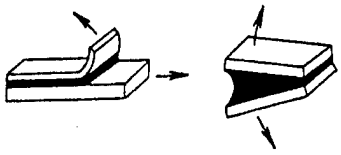

Figure 10. Peel and Cleavage Fracture [19]

long overlap lengths can induce adverse residual thermal stresses during the bonding process that decrease the life of the repair.

Some general guidelines, or "rules of thumb", have been established to aid in the successful design of composite repairs. These include:

- Choose repair materials that have static load-carrying capability greater than or equal to that of the parent material
- Use a double lap arrangement whenever practical. This eliminates the bending problems associated with the offset neutral axis.
- Use overlap distances of roughly 30 times the thickness of the parent structure for double lap repairs and 80 times for single lap repairs.
- Taper the thickness of the repair patch at its ends to relieve adhesive peel stresses. The slope of the taper should be about 1:10.
- Make sure a smooth fillet is produced in the bonding process. The fillet helps to reduce the Mode I stress concentrations that occur at the edge of the overlap.
- Maintain a stiffness ratio (S) of $E_r t_r / E_p t_p \geq 1$, where E_r and E_p are the moduli of the repair and plate respectively and t_r and t_p are the thicknesses of the repair and plate [10, 19].

2.3.2 Patch Material Selection

Two of the factors which should be considered when choosing which composite to use in a repair are: 1) Strength/Stiffness Requirements and 2) Operational Environment.

Higher strength composites have allowed for the design of smaller, lighter, thinner repairs. This is advantageous where the repair area is confined by surrounding structure, or where there may be aerodynamic concerns. The thin repair also adds the benefit of causing less bending due to neutral axis shift. However, the strength and stiffness of the patch should be carefully matched to the application. A patch that is too stiff will attract load that could damage the structure around it, whereas a patch that is not stiff enough will not carry enough load. In structure where large thermal gradients might be encountered, it is recommended that the designer try to match the thermal properties of the patch and the parent structure. This will avoid adverse loading of the bonded joint caused by thermal expansion mismatch. Table 2 shows some current patch materials

and their properties. The subscripts L and T refer to the materials' longitudinal and transverse properties respectively.

Table 2. Patch Materials

Material	E_L/E_T (GPa)	Strength(MPA)	Poisson Ratio (υ)	CTE, α_L,($10^{-6}/^{\circ}C$)
2024-T3	72.4/72.4	324	0.33	22.7
Glass/Epoxy	50/14.5	1130	0.30	6.1
Graphite/Epoxy	138/14.5	1447	0.20	-1
GLARE 2	65.6/50.7	390	0.33	17.9
Boron/Epoxy	210/25	1590	0.168	4.5

2.3.3 Adhesive Selection

Adhesive selection is based on

- Good strength and toughness in the expected operating temperature range (-50$^{\circ}C$ to 80$^{\circ}C$ for most aircraft applications)
- Resistance to environment (humidity) and/or aircraft fluids (fuel, hydraulic)
- Bonding ability with chosen surface preparation agents
- Lowest possible cure temperature [10]

An adhesive with a high shear modulus reduces the stresses in both the patch and parent structure. This leads to a reduction in K and crack growth. Low modulus adhesives make the repair more compliant, allowing greater crack tip opening displacement and thus faster crack growth. As mentioned earlier, the adhesive should also have good peel properties to withstand any bending loads caused by a neutral axis shift. Cure temperature is important and should also influence the adhesive choice. High temperature cure adhesives usually exhibit both greater strength and durability than low temperature adhesives. There are drawbacks though, as the elevated temperatures can cause unwanted residual thermal stresses, bending and damage to the surrounding structure from heat exposure. Moreover, at low operating temperatures high temperature adhesives may become brittle. Low temperature (room temperature) cure adhesives are not as strong as their counterparts, and have poor environmental durability. At high temperatures, low temperature cure adhesives may become more plastic allowing greater crack opening and thus faster crack growth. Low tem-

perature adhesives are best utilized as temporary repairs e.g. aircraft battle damage repair (ABDR), where either equipment or materials are not in place to use a high temperature cure adhesive. For permanent repairs, high temperature cure adhesives should always be used.

Adhesives used in structural bonding can be found in three different physical forms: 1) foam, 2) paste and 3) film adhesives. Foam adhesives have the property that they expand during the curing process. This is useful when repairing rough or damaged bondlines. Paste adhesives normally come in one or two parts mixtures. Two part paste adhesives must first be measured out, mixed and then manually spread using a flat instrument e.g. a spatula. There is ample opportunity for human error to occur in both the mixing and spreading stages of the adhesive application. Improper portioning of the parts may result in degraded bond strength and manual spreading can result in a non-uniform bondline. Advantages of paste adhesives are that refrigerated storage is not required and that they can be cured at both room and elevated temperature. This makes them useful in the application of temporary repairs. Film adhesives exhibit the best strength and durability properties. They are supplied in tape form, are easy to apply and provide a uniform bondline thickness. Their drawbacks include higher cost, required refrigerator storage, and the need for both heat and pressure during curing. Table 3 shows examples of each type of adhesive and their properties.

Table 3. Structural Adhesives

Adhesive	**Adhesive Type**	**Cure Time/Temp**	**Storage**	**Supplier**
FM-39	Foam	1 hr/121°C	6 months/-18°C	American Cyanamid
EC-1386	Paste (one-part)	1 hr/177°C	4.5°C or below	3M
EA-9309	Paste (two part)	3 days/room temp or 1hr/66°C	12 months/room temp	Dextor Corp/Hysol
FM-73	Film	1 hr/121°C	6 months/-18°C	American Cyanamid
AF163-2M	Film	1 hr/121°C	6 months/-18°C	3M

2.3.4 Surface Preparation

"Surface preparation of the metal adherend is the keystone upon which the structural adhesive bond is formed [20]." In other words, if the bonding surfaces are not properly treated, the likelihood of repair degradation and failure is greatly increased. Good surface preparations should have these features:

- Repair produces highly durable bond for the given environment
- No noxious chemicals are used, due to closed repair areas or close handling
- Curing and fabrication should be as close to ambient temperature as possible
- Patch must resist or discourage corrosion cracking
- Repair must produce no electrical sparking, due to fuels tanks, etc.
- The overall process must be non-specific, applicable to several adherends [16]

To sum it up, the process should be safe, simple and effective.

Three of the most widely used surface treatments for adhesive bonding are:

- Phosphoric acid anodizing (PAA)
- Phosphoric acid containment system (PACS)
- Grit Blast Silane (GBS)

All of these follow the same basic steps in their application process. These are:

- degrease - rinse
- deoxidize - rinse
- chemical etch/anodize - rinse and dry
- prime [20]

The three processes each have their advantages and disadvantages although all produce strong, environmentally durable bonds. PAA requires that the damaged structure be removed and placed in an acid bath during the anodizing process. This in not always convenient. This was remedied by the introduction of PACS. PACS allows the anodizing step be done on aircraft but introduces the problem of chemical migration, i.e. acid could become trapped in areas where it cannot be easily removed (honeycomb structure, under fastener heads). GBS uses alumina grit blast, silane

coupling agents and corrosion inhibiting primer to prepare the surface. The GBS process avoids the risks associated with using acids on airplanes and is also the most environmentally friendly.

2.4 Past Studies/Efforts

2.4.1 Experimentation

Much effort has been put into the characterization of bonded repairs, both experimental and theoretical. Some of the first research aimed at this technology originated with Baker at the Australian Aeronautical and Maritime Research Laboratory [5, 9, 16, 20].

Baker's experiments characterized crack growth in aluminum panels. He assumed that bending would be negligible in on-aircraft repaired components due to surrounding, stiffening structure and this influenced his test specimen design. His test specimens were edge cracked panels bonded together over a honeycomb core. This sandwich specimen allowed him to run two tests simultaneously and eliminate bending caused by the adhesive curing process. His results showed constant crack growth rates while the crack was underneath the patch. This indicated that the repaired stress intensity factor, henceforth referred to as ΔK_r, was reasonably constant while the crack was underneath the patch. This data was corroborated by Denney [11] for repaired thin panels. He has also performed work investigating the effects of debonds and elevated temperature on repair life as well as studying the residual strength of patched panels. His disbond studies showed that life decreased with increased disbond size and that very little disbond growth was noted at the end of the tests where the specimens were disassembled for inspection. Baker's elevated temperature tests also showed a decrease in life most likely due to an increase in ΔK_r caused by a decrease in adhesive shear modulus and yield stress and change in crack propagation properties of the alloy itself. His residual strength tests, which were performed on AL2024-T3 panels immediately after repair, showed an increase in yield strength. His research has led to the application of bonded repairs

on the Royal Australian Air Force (RAAF) F-111 [5], Mirage III [22] and even reinforcement of cracked superstructure of a Royal Australian Navy FFG-7 class frigate [9], amongst others. More importantly, his work validated bonded repairs as an alternative to mechanically fastened repairs and paved the way for those to follow.

The Primary Adhesively Bonded Structure Technology (PABST) program of 1978 was one of the U.S. Military's first forays into using adhesive bonding technology. The purpose of the study was to investigate the effects of different surface treatments, adhesives and adhesive primers on the durability of bonded joints. During the course of the program, which involved the construction and assembly of a bonded fuselage section, it was discovered that adhesive bonds were far more tolerant than previously thought. For the structure, the shear strength of the adhesive was greater than the shear strength of the two adherends (thin aluminum) and was therefore not the weak link in the joint. The bondline was tolerant of damage in the form of small debonds, so long as the debonds did not decrease the shear strength of the adhesive below that of the aluminum. Debonds became more prevalent in thicker, more heavily loaded structure due to greater loading of the adhesive. The program also monitored three disbonds located in fuselage splice joints to determine their impact on the structure. These debonds showed no decrease in joint strength and no increase in adhesive shear stress or strain. It was concluded, that most disbonds can go unrepaired except those at the edges of the bonded joint. In this case, a sealant, not an adhesive, should be used to protect the bondline from environmental attack [23, 24].

Other experimental programs have looked at other aspects of the bonded repair problem. Fredell conducted tests using both Boron/Epoxy and Glare to investigate the effects of coefficient of thermal expansion (CTE) mismatch on the life of repaired structure. Glare is a hybrid composite made up of alternating layers of aluminum and fiberglass. His tests showed that by trying to match the CTEs of the repair material and parent structure, residual thermal stresses caused by the cur-

ing process could be reduced. This lead to a noticeable increase in repair life. Moreover, in the case of transport aircraft that cruise at high altitudes and low temperatures, this CTE match would prolong the life of the repair when compared to repair with a large CTE mismatch (low CTE when compared to parent structure). The greater CTE mismatch caused greater stresses in the parent material, adhesive and patch. It could also cause the crack to open, thus reducing the life of the repair. His efforts lead directly to a demonstrator program where two Glare patches were applied to stress corrosion cracks found on the aft upper crown of a C-5A [25].

Denney [11] performed a series of tests aimed at determining the effects of disbond size and location on thin aluminum panels (t=1mm) repaired with Boron/Epoxy patches. He also examined the effects of different adhesives, high temperature cure films and room temperature cure paste on repair life. Debonds were introduced into the adhesive bondline of his specimens with teflon inserts. After the curing process, the specimens were fatigued tested. Denney's results showed that both disbond size and location had an impact on repair life, although much less than was anticipated. Even in the cases of gross disbonds and worst case locations, the life of the repaired specimens was much greater than that of an unrepaired panel. His tests also supported the findings of Baker concerning ΔK_r and debond growth. Denney recorded constant crack growth rates while the crack was under the patch, and C-scan and post failure inspections showed little or no growth of the artificially induced debonds.. His investigations into the different adhesives showed that film adhesives, while creating greater residual thermal stresses, were still stronger and performed better than the paste adhesives.

Mills and Ryan [12] took Denney's work a step further and considered greater thicknesses ($1mm \leq t \leq 3.15mm$). Using the same method as Denney, they introduced debonds into the bondline of their test specimens. Their results also showed decreased life with increased debond

size (still with significant increases in life over the unrepaired case) and little to no growth of the artificially induced debond.

Ratwani [26,27] approached the bonded repair problem with an empirically weighted analytical method which used experimental results from both thick and thin plate regimes to formulate the empirical weighting factor for his model. In the formulation of his model, bending was considered negligible but was reinstated in the weighting factor. He used a semi-analytical method involving through-the-thickness stress-distribution and strip model of the plate to determine different back face stress intensity factors for plates of different thicknesses with a single sided repair. His results for ΔK_r compared well with experimental data for thin plates but lost accuracy as thicknesses increased.

Schubbe [10] investigated the effects of repair geometry and stiffness ratios on single sided repair of thick plates ($3.15mm \leq t \leq 6.35mm$). His work showed, that for thicker plates, a stiffness ratio of one, not the commonly advised 1.4 as used for most thin cases, provided the largest improvement in life. This was due to reduced thermal stresses and bending, which showed to have a noticeable impact on repair life. He also developed an analysis that employed a finite element modelling technique known as the 3-Layer technique, which will be discussed in more detail later, in conjunction with empirical data to formulate an empirical weighting factor for the prediction of ΔK_r and hence life of repaired structure.

2.4.2 Analysis

On the analysis side, one of the first and still most popular analytical models for analyzing bonded repairs is the Rose Model [21]. Rose's model is based on the original inclusion analogy by Muki and Sternberg [28]. By making simplifying assumptions, the model estimates the values of ΔK_r, the maximum adhesive shear strain, the maximum tensile stress in the patch and parent

material, and the change in stiffness due to the presence of a crack and bonded repair. His model has been expanded to include residual thermal stresses due to adhesive curing and out-of-plane bending caused by single sided repair. Results of this model compare well with experimental data for thin plates but loses accuracy with increased plate thickness.

Many of the finite element approaches utilize two-dimensional elements in a layering technique to model the bonded repair. This was done to avoid the larger computational requirements of the 3D models and the problems that arose from modelling the thin adhesive, choosing between unreasonably high aspect ratio elements or a denser more computationally expensive mesh. Sun [29] was one of the first to utilize the layering technique. His model used two-dimensional Mindlin plate elements for the plate and patch and shear springs for the adhesive. The adhesive elements connected the nodes of the plate to the patch using displacement constraint equations that satisfied Mindlin plate assumptions. This lay-up can be seen in Figure 11. The model provided displacement data which was used with the indirect crack closure model to solve for ΔK_r.

The crack closure model, based on Irwin's crack closure integral [30], was first introduced by Rybiki and Kanninen [31] and modified by Sun to included rotational effects for two dimensional Mindlin plate elements. The crack closure model states that the energy absorbed to extend a crack tip by an amount Δa is equal to the work required to close the crack to its original length. The indirect crack closure model solves for K_r by first solving for the strain energy release rates (G) and then relating G to K_r through Westergarrd's representation. Contributions from both the central plane displacements and rotation of the 2D elements are used in the calculation of G. The strain energy release rate for Modes I and II are:

$$G_I^u = \lim_{\Delta a \longrightarrow 0} \frac{1}{2\Delta a} T_y^c \Delta v^c \tag{9}$$

$$G_{II}^u = \lim_{\Delta a \longrightarrow 0} \frac{1}{2\Delta a} T_x^c \Delta u^c \tag{10}$$

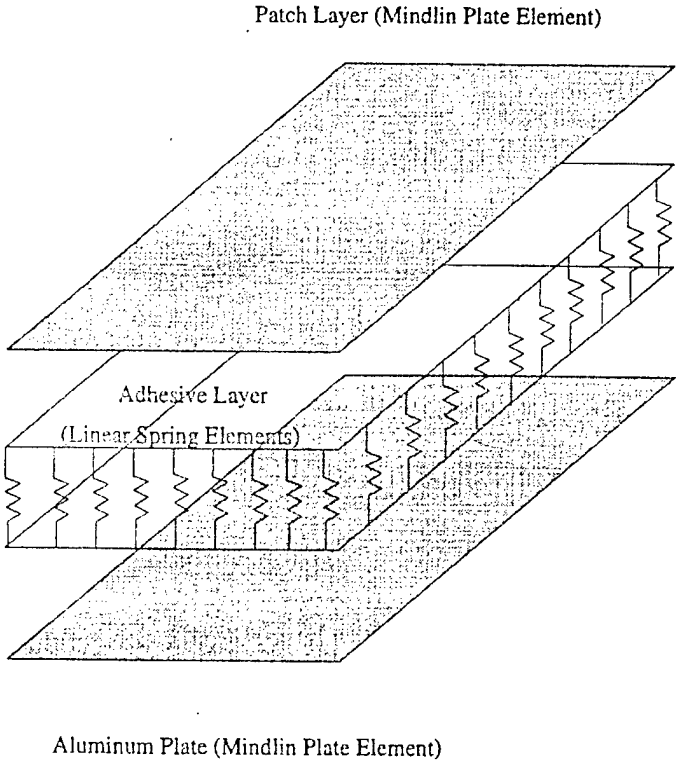

Figure 11. Sun's Plate/Spring Model [10]

and the rotational contributions are:

$$G_I^\theta = \lim_{\Delta a \longrightarrow 0} \frac{1}{2\Delta a} M_x^c \Delta\theta_x^c \tag{11}$$

$$G_{II}^\theta = \lim_{\Delta a \longrightarrow 0} \frac{1}{2\Delta a} M_y^c \Delta\theta_y^c \tag{12}$$

where u = contribution due to displacement at the element mid-plane

Δa = virtual crack extension due to displacement at the mid-plane of the element

Δu_c = crack opening displacement at first node ahead of crack along the x-axis

Δv_c = crack opening displacement at first node ahead of crack along the y-axis

T_x^c = force in the x direction required to close the crack

T_y^c = force in the y direction required to close the crack

$\Delta\theta_x^c$ = crack rotation along Δa about the x-axis

$\Delta\theta_y^c$ = crack rotation along Δa about the y-axis

M_x^c = moment about the x-axis required to close the crack

M_y^c = moment about the y-axis required to close the crack

For a Mode I crack opening, the total strain energy release rate becomes:

$$G_I^t = G_I^u + G_I^\theta \tag{13}$$

Incorporating Irwin's crack closure into Westergarrd's representation yields:

$$K_I^2 + K_{II}^2 = \frac{GE}{\beta} \tag{14}$$

where β equals unity for plane stress and (1-ν^2) for plane strain and E is Young's Modulus. If it is assumed that there is no interaction between Modes I and II, the above equation reduces to:

$$K_I = \left(\frac{GE}{\beta}\right)^{\frac{1}{2}} \tag{15}$$

Sun compared his results using this method to experimental data and found they again compared well with thin plates, but lost accuracy as plate thickness increased.

Naboulsi and Mall [32] expanded upon Sun's method and modeled the adhesive using 2D Mindlin plate elements. The three mindlin plate layers are connected again using displacement

constraint equations that satisfy mindlin plate assumptions. By modelling the adhesive as a continuum, thermal effects, progressive damage and varied non-linear behavior of the adhesive could be included in the analysis. Their results for thin plates compared well with experimental data generated by Denney [33]. Schubbe employed this modelling technique combined with his empirical weighting factor to achieve good results for the thick specimens in his experiments. This Three Layer technique will be discussed in more detail in the Finite Elements chapter of this thesis.

Chapter 3 - Experimental Setup and Procedure

The purpose of this chapter is to detail the setup and procedures used in the experimental portion of this study.

3.1 Materials

All the cracked panels used in this study were cut from a 2024-T351 plate (unclad) aluminum with a thickness of $6.35mm$ $(0.25in)$. The composite patches were made from an 18 ply lay-up of Boron/Epoxy composite. The adhesive used was AF-163-2M structural film adhesive. The aluminum was purchased by AFIT from Thyssen Copper and Brass Sales. Both the adhesive and the Boron/Epoxy (in prepreg tape form) was supplied by the Materials Directorate, Air Force Research Laboratory. Specimen grips and machining support was provided by the Air Vehicles Directorate, Air Force Research Laboratory. The material properties for the plate, composite and adhesive are shown in Table 4

Table 4. Material Properties

Material	2024-T3	Boron/Epoxy	AF-163-2M Adhesive
E_L/E_T (GPA)	72.4/72.4	210/25	NA
$\sigma_{ult_L}/\sigma_{ult_T}$	448/448	1590/83	NA
α_L/α_T $(10^{-6}/^{\circ}C)$	22.7/22.7	4.5/20	NA
G (MPA)	NA	NA	405.8
γ_{yield} (%)	NA	NA	≈ 9
ν	0.33	0.1677	NA

3.2 Specimen Design and Fabrication

There were several steps that had to be accomplished before a single specimen was assembled and ready for fatigue testing. The next sections discuss each step in the process.

3.2.1 Patch Design and Fabrication

The patch was designed using similar tools that would be available to aircraft maintainers [3]. The repair guidelines mentioned in Chapter 1 contributed heavily in the design process. A stiffness

ratio of 1.4 has often been used for thin panel repair; however, as shown by Schubbe [10], for thick plates, a stiffness ratio of ≈ 1 yields the greatest improvement in life. Starting from the equation for stiffness ratio:

$$E_r t_r / E_p t_p = 1 \tag{16}$$

where E_r, E_p are found in Table 4 and $t_p = 6.35mm$, the thickness of the repair is calculated as:

$$t_r = E_p t_p / E_r \tag{17}$$

The thickness of the repair is $t_r = 2.19mm$. The number of plies needed equals the total repair thickness divided by the thickness of an individual ply of Boron/Epoxy. The thickness of a ply of Boron/Epoxy is $0.127mm$.

$$\#\ of\ plies = t_r / 0.127mm \tag{18}$$

From this, it was determined that eighteen plies of Boron/Epoxy would be used in the patch, yielding a true stiffness ratio of:

$$S = 1.044 \tag{19}$$

The patch is tapered in the loading direction and rounded at the tips to minimize peel stresses at the patch tip. There are nine size steps in the repair, moving from larger ply to smaller in what is commonly known as a "wedding cake" configuration. The last step acts as a cover ply and is designed to both carry load and protect the underlying plies from harm. Each step consists of two plies of Boron/Epoxy. Table 5 shows the lengths of each ply tip to tip, starting from the bottom of the wedding cake to the top. The repair design is shown in Figure 12.

To fabricate the patch, aluminum templates were cut to match the size of each patch layer. A teflon backing was applied to each template to keep it from sticking to the tacky Boron/Epoxy prepreg tape. Each template was placed upon the tape, and plies were cut to match the template. After the required number of plies were cut, they were placed upon a teflon sheet and laid-up unidirectionally, i.e. all fibers in the loading direction. The patch was then cured, allowing for easier

handling, storability and to reduce CTE mismatch effects during bonding to the aluminum panel. The patches were cured in an autoclave at the Materials Directorate, AFRL. The cure process involved applying positive pressure of 344,738 Pa (50 psi) to the patch while ramping to $121°C$ ($250°F$) at a rate of $2.2°C/min$ ($4°F/min$). The patch soaked at $121°C$ for one hour; whereafter the temperature was allowed to drop at a rate of $2.8°C/min$ ($5°F/min$), completing the curing process. Figure 13 shows a picture of the autoclave and controller (hotbonder) used to fabricate the patches. After curing, the patch was non-destructively inspected using ultrasonic inspection equipment. The ultrasonic inspection system uses a transducer to send a high-frequency pulse through a test object. If any voids or flaws are present, the transmission in interrupted. Another transducer receives the resulting pulse and transmits this data to an amplifier and CRT display. The result is a two-dimensional contour map of the test object showing void size and location. This method of inspection is often commonly referred to as C-scanning. Figure 14 shows a picture of the ultrasonic inspection equipment.

Table 5. Patch Lay-up

Ply Number(s)	Length (mm)
1,2	178
3,4	166
5,6	154
7,8	142
9,10	130
11,12	120
13,14	110
15,16	100
17,18	184

3.2.2 Panel Dimension and Precracking

All of the panels were cut from a single aluminum plate, with the longitudinal (loading) axis aligned with the grain (rolled) direction. The nominal dimensions of each panel were 559x178x6.35 mm (22x7x0.25 in). Holes were drilled at the ends of the panels to allow for grip attachment. For

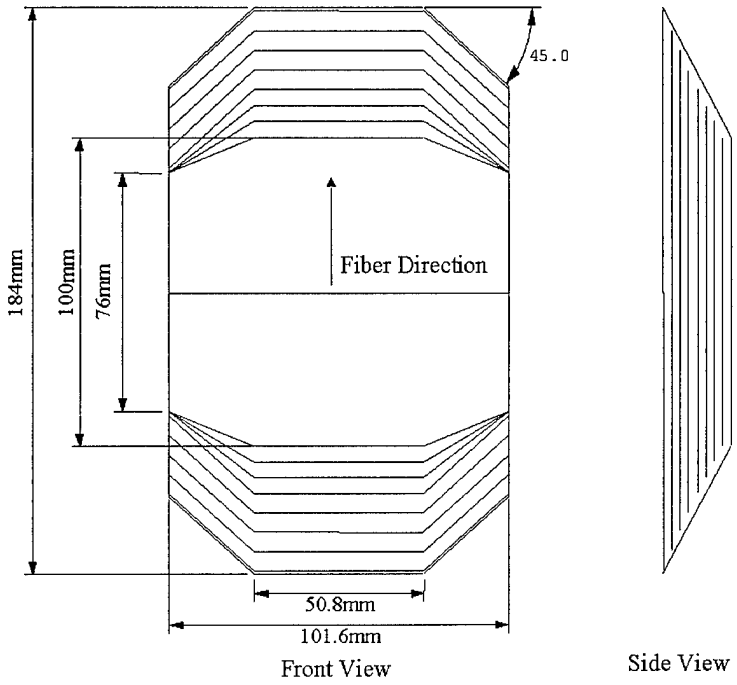

Figure 12. Patch Configuration

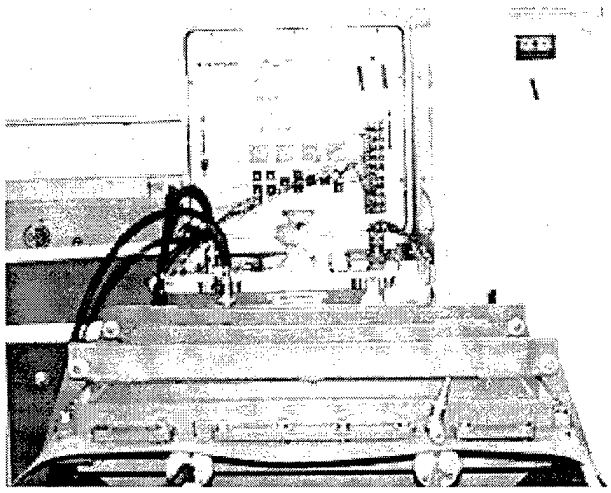

Figure 13. Autoclave and Hotbonder

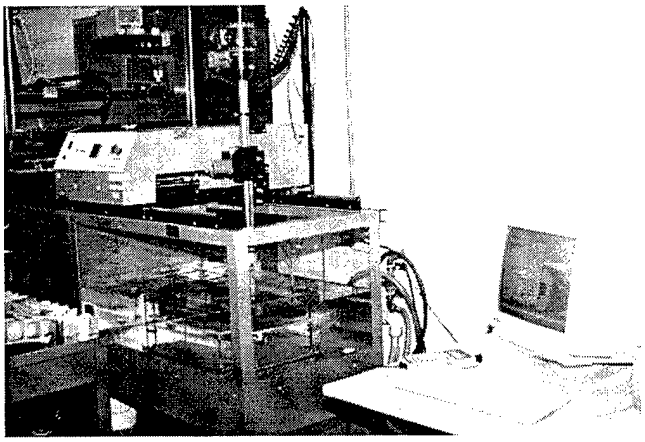

Figure 14. Ultrasonic Inspection System

precracking purposes, a 12.7mm (0.5 in) Electric Discharge Machining (EDM) cut was made in the center of each panel. The purpose of precracking is to provide a sharpened fatigue crack of adequate size and straightness. In accordance with ASTM Standards , the final K_{max} during precracking shall not be larger than the initial K_{max} for which data is to be taken [4]. The panels used in this study were all precracked using a technique known as load shedding. Load shedding requires that the load be systematically decreased until the desired precrack length is reached. The precracking loads used in this study are shown in Table 6.

Table 6. Precracking Loads

Total Precrack Length (mm/in)	Applied Stress (MPa)
12.7/0.5	100
15.24/0.6	90
17.78/0.7	80
20.32/0.8	70
22.86/0.9	60
25.4/1.0	NA

The precrack was grown from the starter notch to a nominal total length of 25.4 mm. The final precracking load equals half of the load to be applied during testing. This reduces the plastic zone size in front of the crack tip and the associated retardation effects, providing a worst case crack growth scenario during testing. This was desired as the author did not want load history to affect the test data.

3.2.3 Surface Preparation

The bonding surfaces of both adherends (the aluminum plate and the composite patch) must be properly prepared before the patch is bonded onto the cracked plate. The surface preparation process used for this was Grit Blast Silane.

The surface preparation for the aluminum plate involved several steps: 1) solvent degreasing, 2) mechanical abrasion of adherend, 3) silane agent preparation, 4) wetstanding procedure, and 5)

primer application and cure. The surface of the aluminum plate was degreased using the solvent Methyl Ethyl Ketone (MEK). MEK was repeatedly applied to the surface with lint free paper and wiped off until no more residue was noticed on the paper. The surface was then abraded using a scotch brite pad in a water-detergent solution to remove any oxide layers on the panel. The panel was then placed in an oven at $90°C$ ($200°F$) and allowed to dry. After drying, the panel was again wiped with MEK to remove any contaminants. The panel was then placed in a grit chamber and abraded with non-recycled 50 micron aluminum oxide grit to roughen the surface. Excess grit was blown off using a gaseous nitrogen jet. The wetstanding procedure involved a one hour mixing of $1ml$ silane coupling agent with a 99 ml distilled water solution. This solution was brushed onto the panel surface, completely wetting the surface for 10 minutes to ensure complete wetability of the bond area and to act as a water break test. If there were any contaminants left on the surface, the water break test would indicate this, and the surface preparation would be started again from the beginning. After the 10 minutes had passed, excess silane was removed from the panel using the gaseous nitrogen jet. The silane treated panels were then placed in an oven and allowed to dry for one hour at $93°C$ ($200°F$). After drying, the panels were sprayed with a corrosion inhibiting primer (American Cyanamid BR-127), cured at room temperature for 30 minutes and then at $121°C$ ($250°F$) for one hour. This completed the surface preparation for cracked aluminum plates.

Surface preparation of the composite patch required only two steps: 1) solvent degreasing and 2) mechanical abrasion of the surface. The Boron/Epoxy patch bonding surface was first wiped clean with MEK. Afterwards, the bonding surface was grit blasted to roughen the surface. Excess grit was blown off using the gaseous nitrogen jet. This completed the surface preparation for the patch.

3.2.4 Mating of Repair and Panel

To size the adhesive, the bonding surface of the composite patch was placed on a sheet of adhesive. The adhesive was then cut such that there was enough margin around the edge of the patch to allow for a good adhesive fillet after bonding. Artificial disbonds were made using $0.1mm$ (0.004 in) thick teflon tape. The tape was cut to size and carefully placed in the appropriate locations on the cracked aluminum plate. The patch plus adhesive was then placed on the panel, centered around the crack, with the fiber direction coinciding with the loading direction. The assembly was held in place using high temperature tape. The specimen was then placed in an autoclave. A two ramp cure cycle was used to cure the adhesive. The first ramp occurred under 26 $inHg$ (12.7 psi) vacuum pressure and took the specimen from room temperature to $82°C$ ($180°F$) at a ramp rate of $1.6°C/min$ ($3°F/min$). The high vacuum allowed any gases trapped in the bondline to expand and escape as the adhesive heated and became more fluid, a process known as debulking. When the temperature reached $82°C$, the vacuum pressure was dropped to 13 $inHg$ (6.4 psi), and the specimen was allowed to soak for thirty minutes. At this temperature, the adhesive is still fluid; and, by dropping the vacuum, any voids remaining in the bondline would be compressed, minimizing the effect they might have on the bond. After the soak, the temperature was increased at a rate of $2.23°C/min$ ($4°F/min$) to $120°C$ ($250°F$) and allowed to soak for one hour. During this time, the adhesive locks and gains its structural properties. After the hour has passed, the temperature is allowed to drop at a rate of $2.8°C/min$ ($5°F/min$), completing the cure cycle. After curing, the specimen was C-scanned to check bond quality. Figure 15 shows a diagram of the completed test specimen. Figure 16 shows a photograph of a completed specimen. Figure 17 shows a picture of a specimen in the ultrasonic tank.

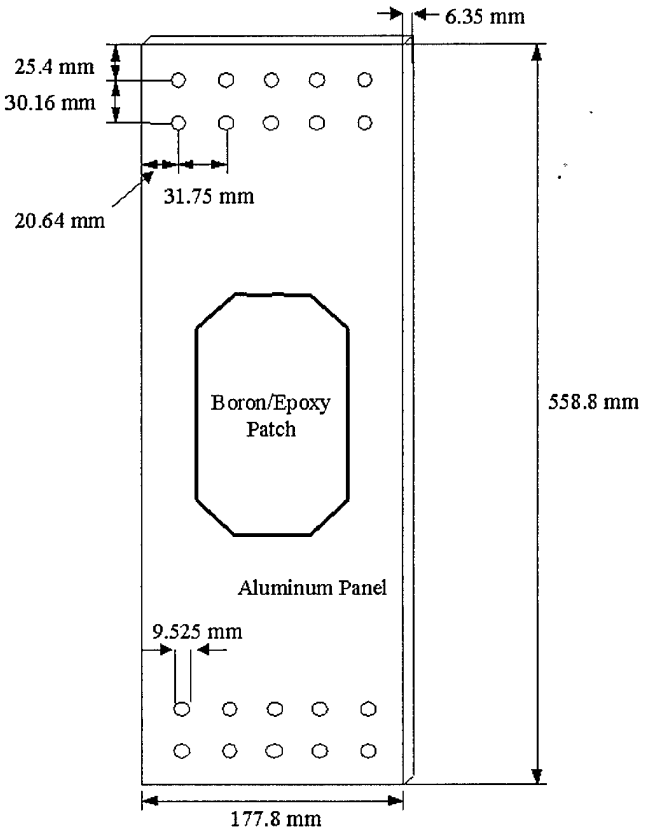

Figure 15. Specimen Configuration

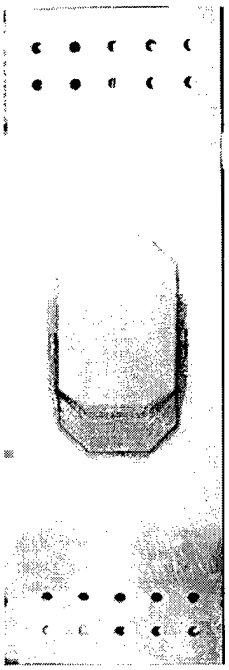

Figure 16. Photograph of Assembled Specimen

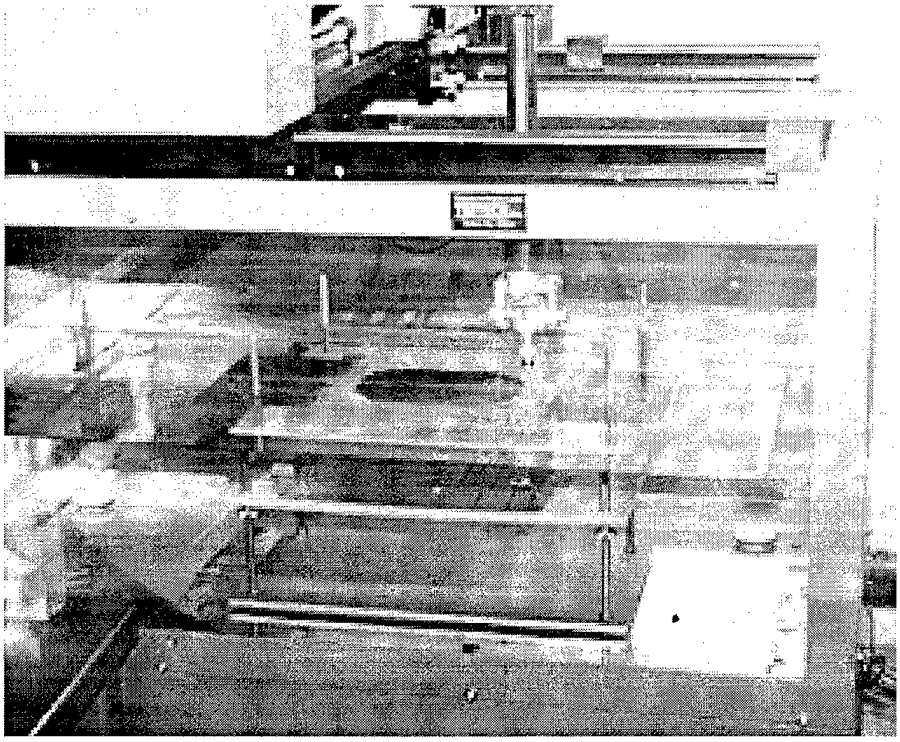

Figure 17. Specimen Undergoing Ultrasonic Inspection

3.3 Test Equipment

The following is a list of the test equipment used in this study:

- Mechanical Load System
- Crack Measurement System
- Thermal Imaging System
- Bending Measurement System

The mechanical loading system consisted of:

- 100 kip MTS 810 Servohydraulic Testing Machine
- MTS Testar IIs Controller
- Compaq Personal Computer (IBM compatible running Windows NT) with Testar IIs software.

The mechanical loading system was used for both the precracking and experimental testing phases of this study. The MTS Testar IIs system replaces the MTS 458.20 controller and employs a Graphical User Interface (GUI) in the Windows environment to allow for better test parameter control and easy programmability. The Testar IIs system uses the same feedback loop principle of previous MTS controllers. A photograph of the computer and Testar IIs system can be seen in Figure 18.

The two systems used to measure crack growth are listed below.

- Gaertner travelling telemicroscope with digital readout.
- In Situ Eddy current crack imaging system.

The travelling microscope was used on the unpatched side of the specimen to acquire optical crack measurements. A picture of the travelling microscope and digital readout are shown in Figure 19.

The eddy current system is a non-destructive inspection system for measuring crack length under the composite patch. The system was on loan from the Air Force Research Laboratory and consisted of:

- Phasec 2.2 eddy current system
- 50 kHz Nortec Absolute Probe
- Krant-Kramer eddy current scanner with color imaging capability

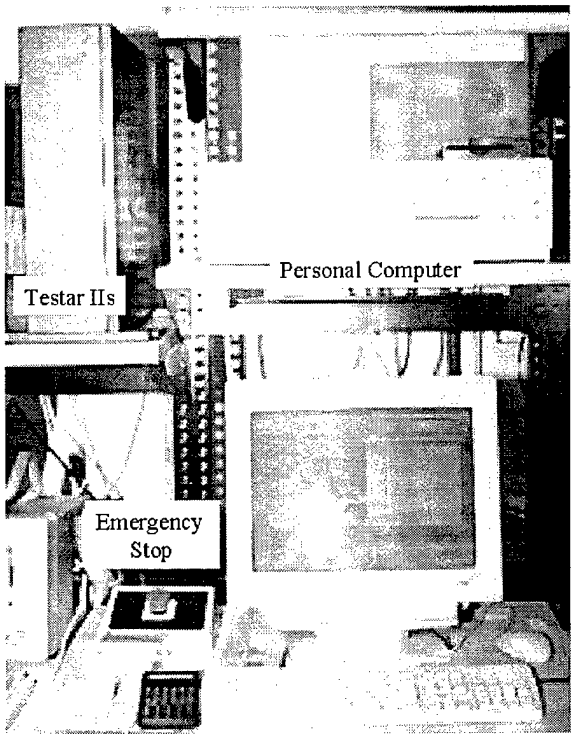

Figure 18. Personal Computer and Testar IIs Controller System

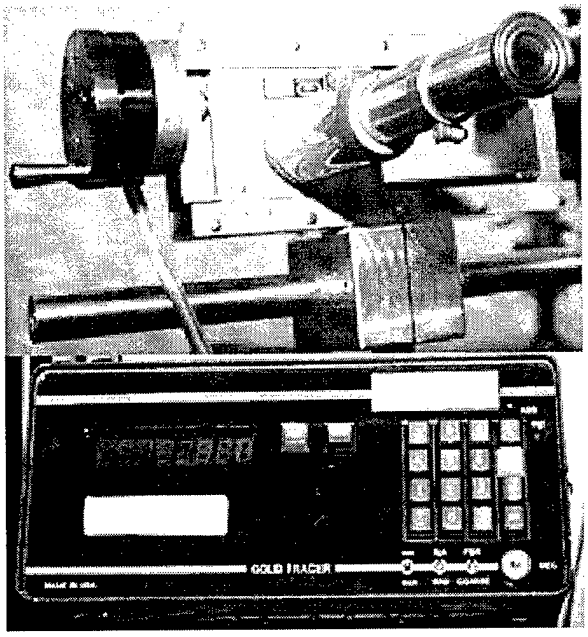

Figure 19. Gaertner Optical Microscope and Digital Readout

The eddy current system was calibrated using both a standard and calibration specimen developed by Schubbe [10]. A diagram and photos of the system are shown in Figure 20.

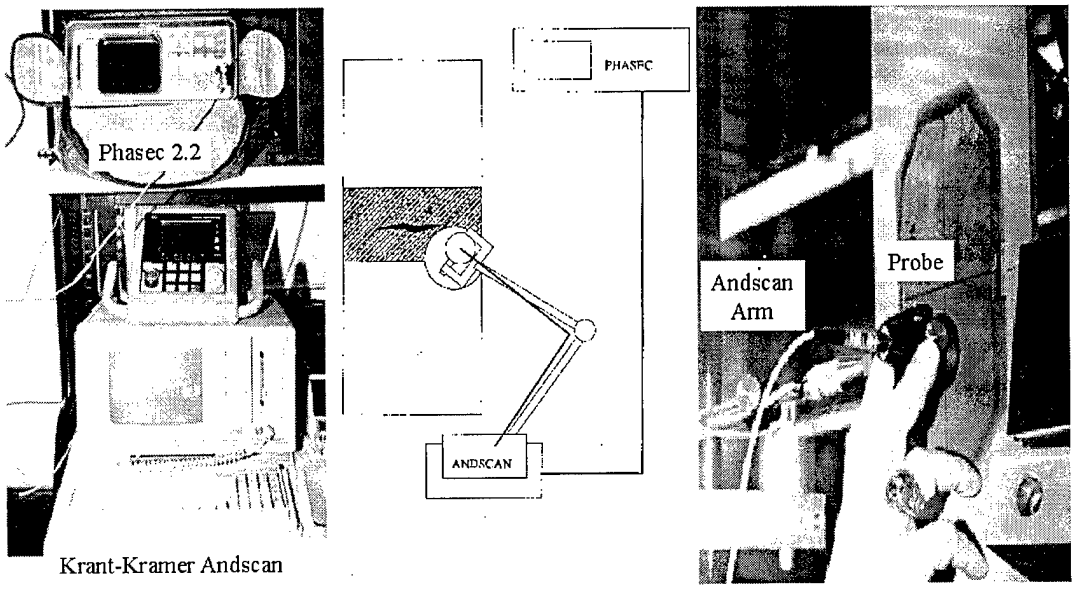

Figure 20. Eddy Current Inspection System

The thermal imaging system used was the Inframetrics Model 760 IR Imaging Radiometer. The system consisted of Model 760 Scanner and the Model 760 Control/Electronics Unit. On the control unit, a Liquid Crystal Display (LCD) was used to display the infrared image. The control unit also had an analog color video out terminal that could be connected to a separate monitor. The purpose of this system was to use thermography to locate and record disbonds and disbond growth in the bondline during testing. A photograph of the thermal system is shown in Figure 21.

The bending measurement system was the Faro Industrial Metrecom. The system consists of a mechanical digitizing arm and host computer. The arm measures points in space and was used to

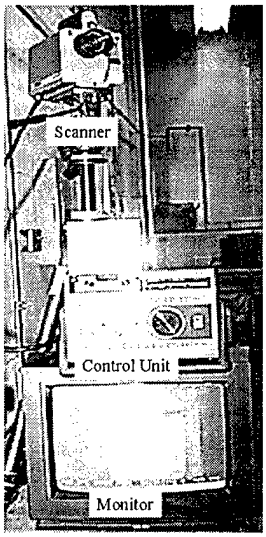

Figure 21. Thermal Imaging System

measure out-of-plane displacement of the aluminum panels after being repaired. A photograph of the mechanical arm is shown in Figure 22.

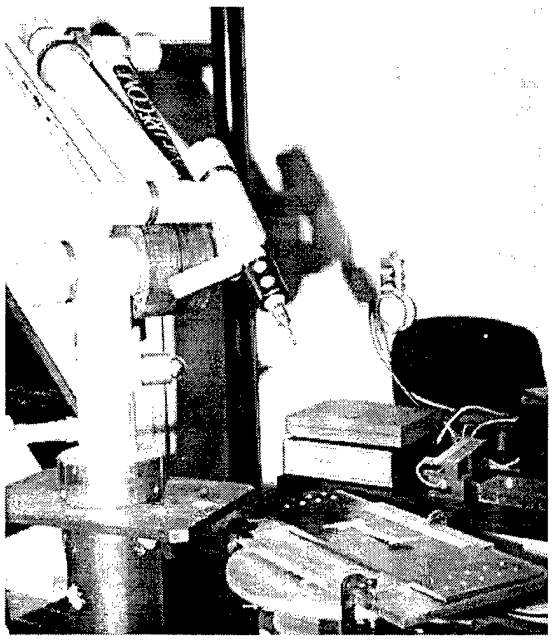

Figure 22. Mechanical Arm

3.4 Experimental Procedure

Before each specimen was placed in the load frame, out-of-plane displacement measurements were taken, and the unpatched side was polished using standard metal polish to allow for easier crack detection. Afterwards, the grips were bolted to the specimen and the entire assembly mounted in the load frame. The infrared camera was positioned facing the patch and the microscope was moved into place facing the unpatched face of the panel. Initial crack, length measurements were recorded using both the microscope and eddy current system. A baseline thermal image was also taken. Test parameters were then loaded into the computer. These parameters included:

- Mean Load (kips)
- Load Amplitude around the Mean (±kips)

- Frequency (Hz)
- Cycle Count
- Desired Waveform (Sine)

All tests were conducted under constant amplitude fatigue cycling conditions with a max stress (σ_{max}) of 120 MPa (17.4 kips), a stress ratio ($R = \sigma_{max}/\sigma_{min}$) of 0.1 and at a frequency of 7Hz. In terms of the input test parameters, the stresses relate to a mean load of 16.75 kips and a load amplitude of 13.71 kips. While the crack was under the patch, the tests were stopped and optical crack growth measurements were taken when $\Delta a \approx 01.27mm$ $(0.05in)$, thermal images and eddy current scans were taken when $\Delta a \approx 12.7mm$ $(0.5in)$. Moreover, the specimens were removed from the load frame at crack lengths of $2a \approx 63.5mm$ $(2.5in)$ and $2a \approx 101.6mm$ $(4.0in)$ for C-scanning. After the crack had grown beyond the patch, optical crack growth data was taken until the specimen reached failure. Upon failure, the failure mode was recorded and the specimen retired. A photograph of the test setup can be seen in Figure 23

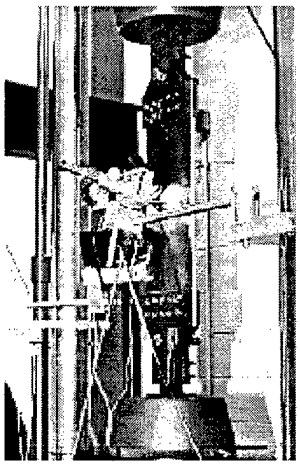

Figure 23. Specimen In Load Frame

Chapter 4 - Results and Discussion

4.1 Test Summary

The purpose of the experimental study was primarily to determine the effect of disbond location on fatigue crack growth of a repaired panel. The test matrix, shown in Table 7, was designed with this goal in mind. The test matrix consisted of 14 experimental tests covering the baseline cases of 1) No Repair and 2) Fully Bonded Patches (FBP), as well the as the four disbond cases shown in Figure 2, 1) Full Width Disbond (FWD), 2) Crack Tip Disbond (CTD), 3) Patch Tip Disbond (PTD), and 4) Center Disbond (CD).

This chapter will discuss the results of the experimental study.

Table 7. Test Matrix

Specimen Number	Description	Debond Size (%of total bond area)
1	Baseline/No Repair	NA
2	Baseline/No Repair	NA
3	Fully Bonded Patch	NA
4	Fully Bonded Patch	NA
5	Full Width Disbond	5%
6	Full Width Disbond	10%
7	Full Width Disbond	20%
8	Full Width Disbond	20%
9	Crack Tip Disbond	20%
10	Crack Tip Disbond	20%
11	Patch Tip Disbond	20%
12	Patch Tip Disbond	20%
13	Center Disbond	10%
14	Center Disbond	10%

4.2 Post Cure Curvature

Prior to repair, it can be assumed that the cracked aluminum plate is flat, i.e. it has no curvature. However, during the curing process, the coefficient of thermal expansion mismatch between the aluminum panel and the composite repair causes bending in the repaired panel. This bending is directly related to the magnitude of the post-cure residual thermal stresses. Out-of-plane dis-

placement data was taken for each of the repaired specimens to investigate the amount of bending encountered with the different debond cases.

Out of plane displacement data was taken along the centerline of the panel in the longitudinal (i.e. loading direction). Data points were taken up to a distance of $50.8mm$ $(2.0in)$ on both sides of the crack. A 2^{nd} order polynomial was fit to the displacement data to show a better representation of the curvature caused by the curing process. An example of this is shown for Specimen 4 in Figure 24. Similarly, curvature data was taken for each of the debond configurations. A comparison of the curvatures of the different debond configurations are shown in Figure 25.

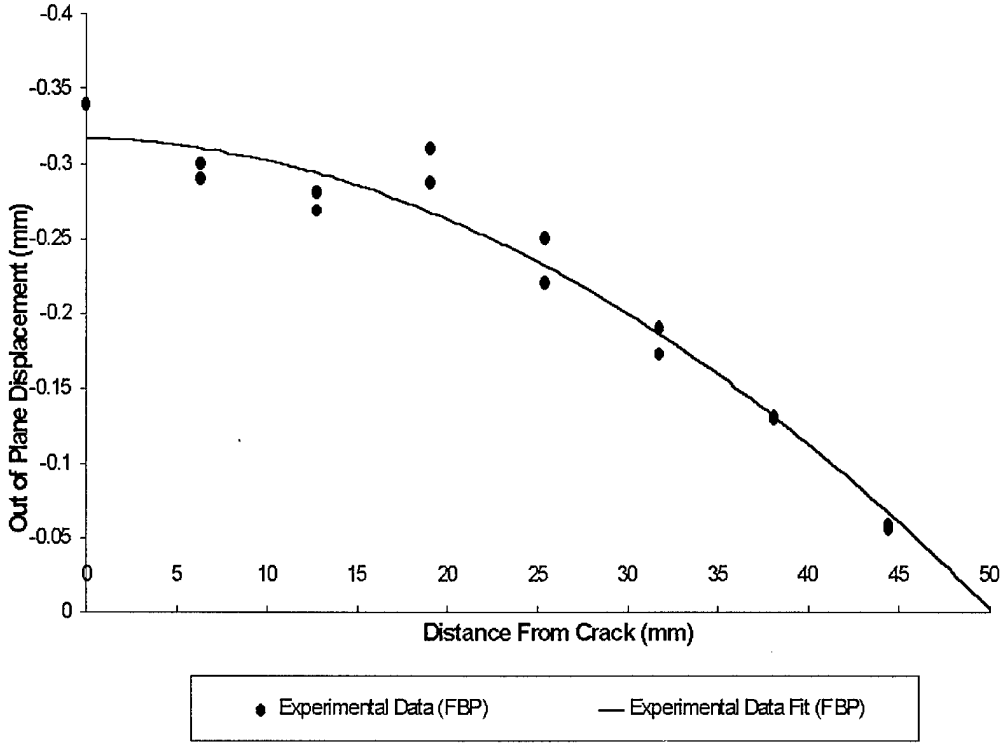

Figure 24. Curvature of FBP

From the data in Figure 25, it appears that the curvature of the FBP, FWD and CTD specimens are very similar. The two configurations that deviate are the PTD and CD, whose curvatures

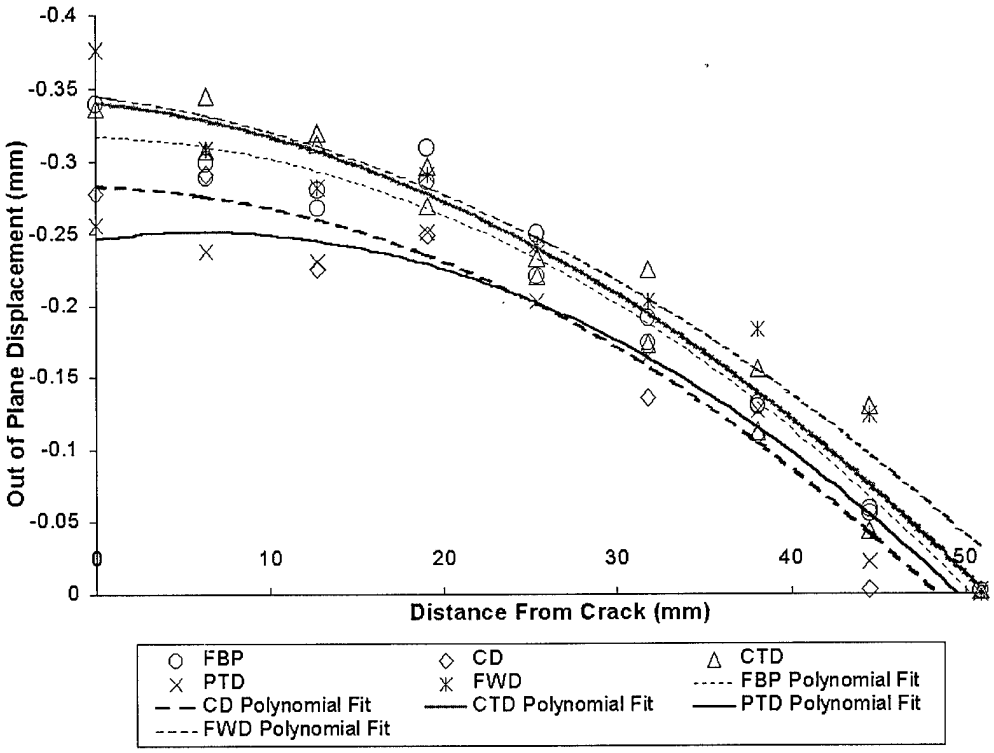

Figure 25. Curvature Comparison of Debond Configurations

are slightly less. The data would suggest that debonds in the immediate vicinity of the crack or that extend parallel to the crack have little effect on curvature. Cracks that extend away or perpendicular from the crack show the effect of decreasing the curvature, as is seen in the CD and PTD configurations. The radius of curvature (ρ) of each specimen can be calculated from the function for the parabolic fit and this equation:

$$\rho = \frac{[1 + (y')^2]^{\frac{3}{2}}}{|y''|} \qquad (20)$$

The radii of curvature for the specimens in Figure 25 are assembled in Table 8.

Table 8. Radius of Curvature

Specimen Number	Description	Radius of Curvature (m)
4	FBP	5.00082
8	20% FWD	5.55625
10	CTD	5.00099
12	PTD	5.00055
14	CD	5.00084

4.3 Effects of Debonds on Repair Efficiency

This section is divided into five subsections, each presenting the results of different repair configurations.

4.3.1 Baseline Tests

In order to have a baseline with which to compare the disbonds tests, panels with no repair and panels with fully bonded repairs were tested. Specimens 1 & 2, with no repairs and subjected to the loading conditions outlined in Chapter 3, had lives of 9101 and 9476 cycles respectively. Specimens 3 & 4, repaired with fully bonded composite patches, failed at cycle counts of 36147 and 38181. The fully bonded repairs extended the lives of the two cracked panels by about a factor of four as compared to the non-repaired cases. This data agrees with the trends observed by Denney [11], Schubbe [10] and Ryan and Mills [12] of decreasing life extension for increases in repaired panel thickness. This decrease in life can be attributed to higher crack tip stresses caused by greater

bending due to bonding of the patch to the panel. This phenomenon was also documented by Schubbe [10] for thick panel repair. Regardless, the increase in life is still significant. Figure 26 shows the comparison between crack growth versus cycles for the non-repaired and fully bonded specimens.

Looking at Figure 26, the first things noticed are the overall increase in life of the bonded repairs and the increase in critical crack length afforded by the patch. This is in agreement with the trends found in the literature. However, one trend not noticed is that of constant crack growth under the patch, as seen in experiments and analysis investigating thin repaired specimens [11, 12, 16]. Figure 27 shows this in better detail.

Table 9. No Repair vs. Fully Bonded Patch

Specimen Number	Description	Cycles to Failure
1	Baseline (No Repair)	9101
2	Baseline (No Repair)	9476
3	Basline (FBP)	38181
4	Baseline (FBP)	38061

The da/dN data shown in Figure 27 was generated using the secant method outlined in ASTM Standard E647 - 95a [4]. Crack growth rate for the repair in the present study grows linearly as crack length increases. After the crack grows past the edge of the patch, the crack growth rate increases exponentially until failure. This indicates that, unlike thin panel repair, ΔK_r is not constant while the crack is under the patch

Another item of interest is crack growth on the patched face, underneath the patch versus crack growth on the unpatched face. The data shown in Figure 28 is from Specimen 4 (FBP).

The asymmetric repair causes the crack underneath the patch to lag behind the unpatched face crack. As the crack grows, the lag becomes greater, illustrating how the asymmetric repair continues to bridge the patched face crack, while allowing the unpatched face crack to open.

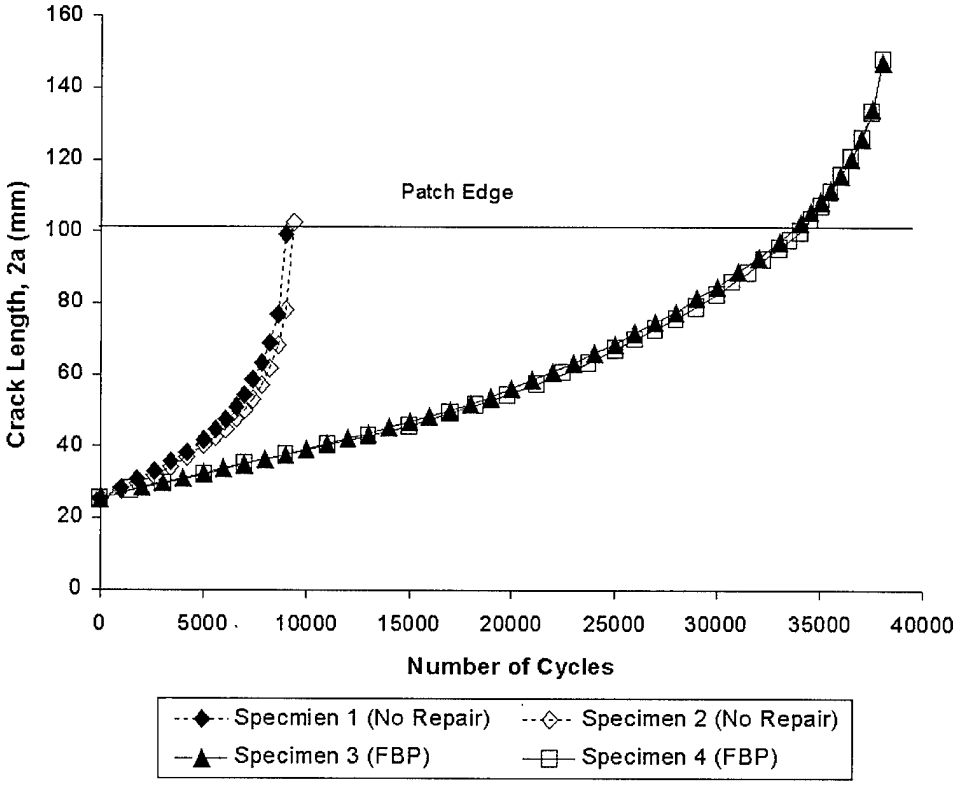

Figure 26. Baseline vs. Fully Bonded Repair

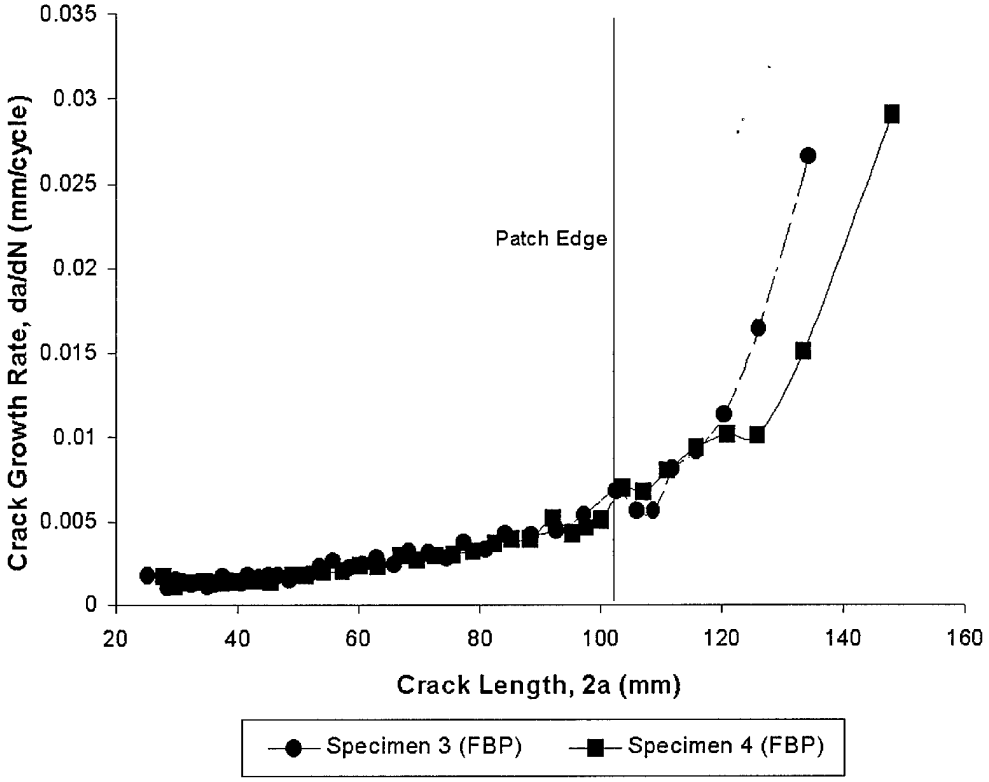

Figure 27. Crack Growth Rate vs Crack Length for FBP

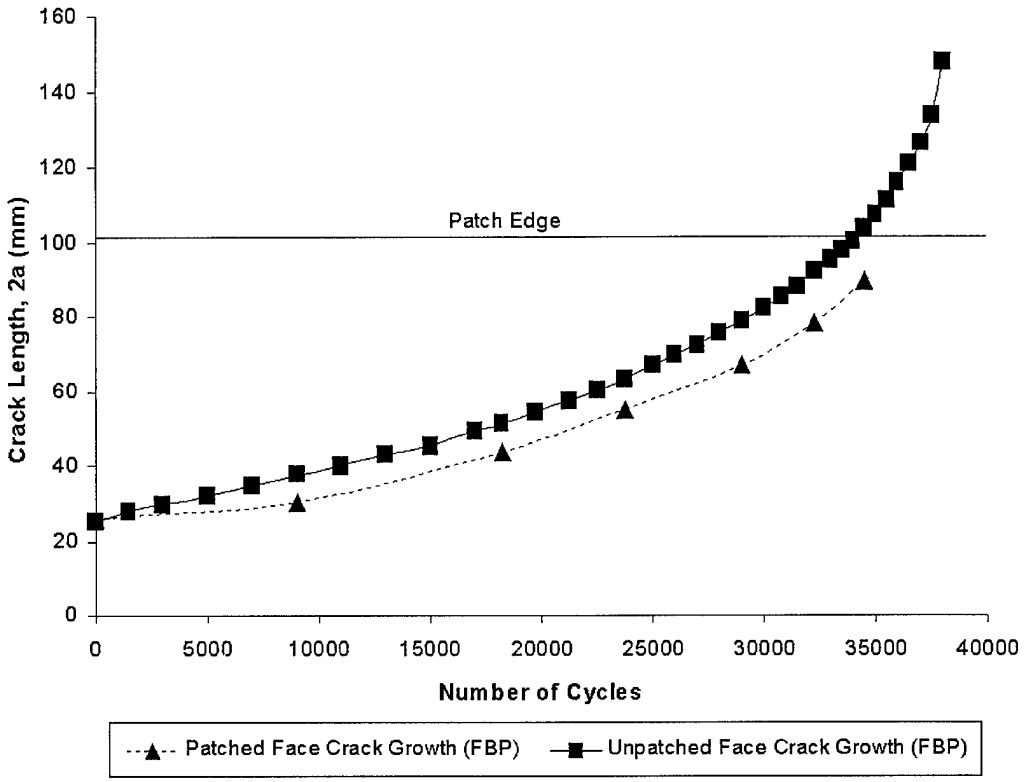

Figure 28. Patched Face vs. Unpatched Face Crack Growth (FBP)

Both thermal imagery and C-scans were used to document debond growth under the repair. Unfortunately, thermal imagery proved to be nearly useless for patches of the thickness used in this study. Normally, debond areas would act as an insulator on the patch material. During heating, these areas would show up as being cooler than surrounding bonded sections. However, in the case of the thick patches, debonds were only noticeable when they had become very large, late into the repair life. For this reason, C-scans, which are more accurate, were relied upon to record debond size and location. Figure 29 shows C-scans for three different crack lengths under Specimen 2 (FBP). From left to right, the first image is of the repair immediately after bonding to the panel, before any fatigue cycling had occurred. The second image is when the crack had grown half the distance from the precrack length to the patch's edge. The last image is when the crack had grown to the patch edge. The white ellipses in Figure 29 outline the debond areas. It can be seen that the debond grows in the shape of an ellipse. This is also in agreement with the literature. It should be noted that the crack lengths indicated in the figure are for the unpatched side. This is of interest mostly when examining the third image. According to eddy current data, the front face crack is 89.5 mm in length. The debond area however extends to the edges of the patch, a distance of 101.6 mm. If this is the case, the debond precedes the crack on the patched face rather than following in its wake.

There are two common failure modes associated with bonded repairs: 1) Patch failure mode and, 2) Adhesive Failure. Patch failure mode is associated with a failure of the patch. The Adhesive failure mode is associated with a failure of the adhesive, either in the interface between the panel and adhesive or the patch and adhesive. The adhesive failure mode is very undesirable as it is indicative of poor surface preparation, and a case of the adhesive being the weak link in the bonded joint. If the joint is to fail, the patch failure mode, as shown in Figure 30, is preferred.

Both Specimens 3 and 4 exhibit the patch failure mode. Example images of failed specimens can be seen in Appendix A.

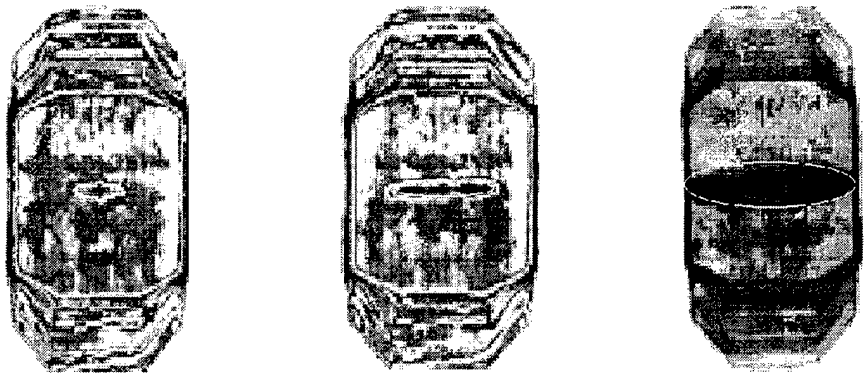

2a = 25.4 mm 2a = 63.5 mm 2a = 101.6 mm

Figure 29. Fully Bonded Patch C-scans

4.3.2 Full Width Disbonds

Both Denney [11] and Mills and Ryan [12] have conducted experiments with thin structure that show the FWD damage configuration has the greatest adverse impact on life. This is because there is no adhesive along the path of the crack, bridging or closing it. This allows for greater crack tip opening displacement and hence faster crack growth. With this in mind, Specimens 5-7 were prepared to investigate when debond size coupled with FWD configuration would affect repair life in thick structures. The results of this would then determine what debond size would be used in the remaining debond configurations. Figure 31 shows crack growth for the three FWD cases versus the unrepaired baselines.

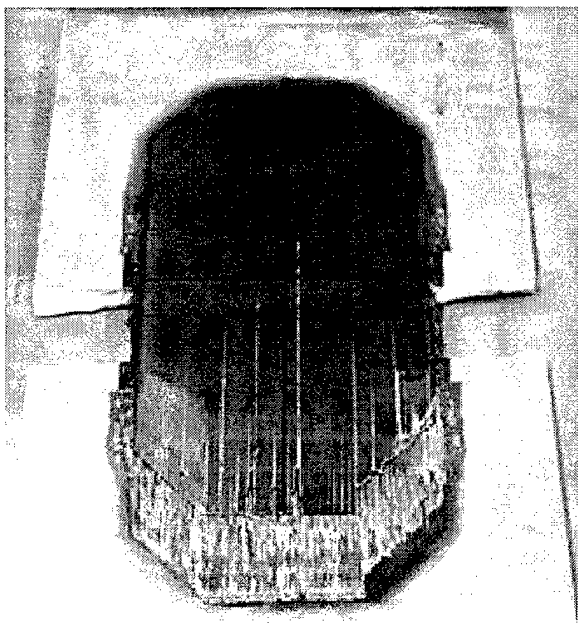

Figure 30. Exhibited Patch Failure Mode of FBP

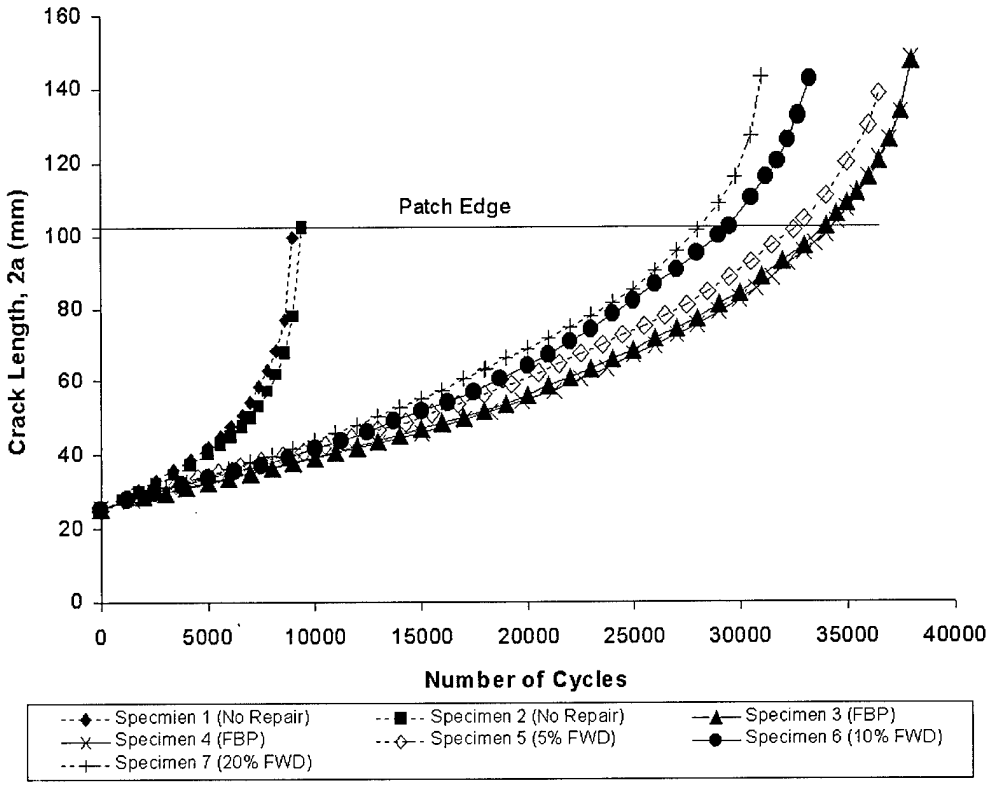

Figure 31. 5%, 10%, 20% FWD vs. Baseline

Figure 31 shows there is little difference between the baseline and the 5% FWD crack growth data. At 10% FWD and 20% FWD, the effects become a little more pronounced. The 20% debond area was chosen and used in subsequent tests, as it showed a potential significant impact on life over that of the 5% and 10% debond case. Dimensions of the 20% FWD are shown in Figure 32

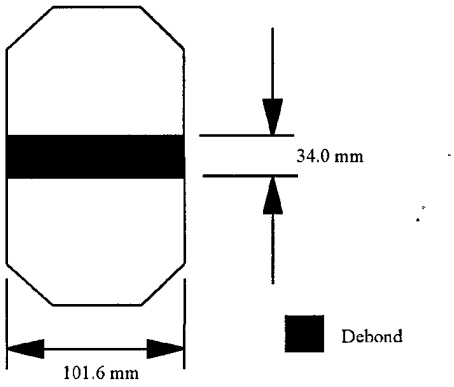

Figure 32. Full Width Debond Dimensions

A second 20% FWD test was then run to check repeatability. The two FWD cases exhibited life reductions of 18% and 24% respectively when compared to the average life of the baseline FBP. When compared to the unrepaired specimens, the two FWD cases yielded life extensions of 2.34 and 2.1 lifetimes, respectively. Much like the repaired thin structure, the FWD configuration has a very large impact on repair life. Figure 33 shows crack growth data for the 20% FWD specimens.

Plotting and inspecting the crack growth rate data for the two FWD specimens shows the same trend seen in the FBP specimens. Crack growth rate is not constant, while the crack is underneath the patch. Instead, it can be considered as growing linearly until the crack reaches the edge of the patch, at which time it increases exponentially until specimen failure. Figure 34 shows the crack growth rate data for the two 20% FWD specimens.

The large disbond area in the FWD does not seem to have affected the amount of lag between the patched face and unpatched face cracks when compared to FBP. Comparison of Figures 28 and 35 shows that the crack lag between the FBP and FWD case are nearly identical. C-scans for Specimen 8 are shown in Figure 36. The images are aligned from left to right in the same fashion shown in the FBP case. It can be seen from the images that the artificially induced debond does not grow in size as the crack lengthens. Lastly, both FWD specimens failed by the patch failure mode.

Table 10. Full Width Disbond vs. Baseline

Specimen Number	Description	Cycles to Failure
1	Baseline (No Repair)	9101
2	Baseline (No Repair)	9476
3	Basline (FBP)	38181
4	Baseline (FBP)	38061
7	20% FWD	31058
8	20% FWD	28875

4.3.3 Crack Tip Disbonds

Specimens 9 and 10 were constructed with debonds located just ahead of the precrack crack tip. Again, the total debond area under the patch equalled 20%. The dimensions for the CTD specimens are shown in Figure 37.

Crack growth data presented in Figure 38 shows that there was no noticeable effect on the overall repair life by the CTD damage configuration. By closely examining the data, it appears that crack growth of the two CTD specimens is slightly slower (albeit by very little) than that of the FBP case. In the case of the CTD specimen, the portion of the crack under the middle of the patch is bridged by adhesive, restricting the middle portion of the crack from opening and therefore also restricting the opening at the crack tips. The debond in the vicinity of the crack will grow under cyclic loading. When this debond has grown large enough in the middle of the patch-panel interface to begin interacting with the debonds around the crack tip, a full width debond case may

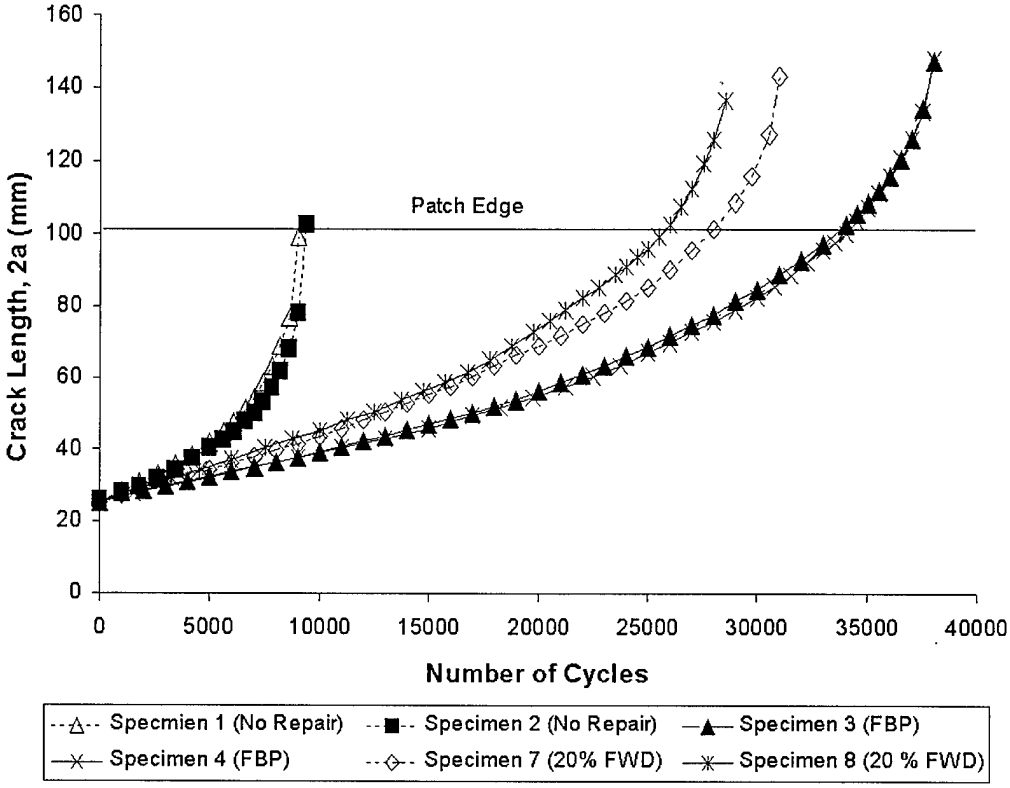

Figure 33. 20% FWD vs. Baseline

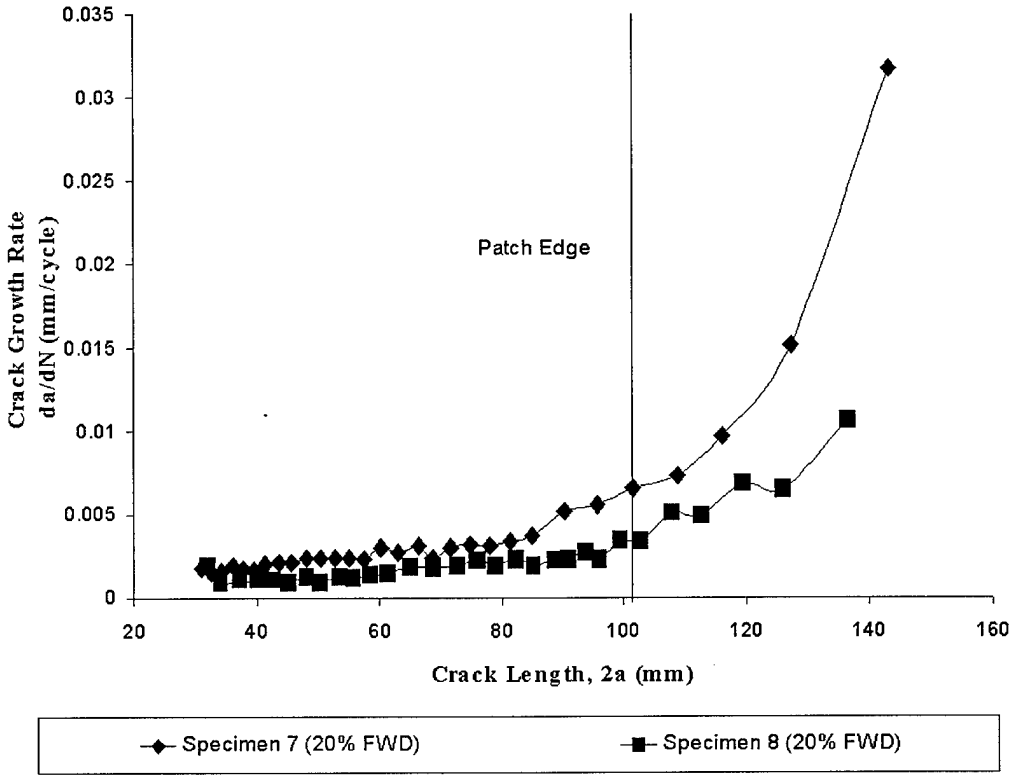

Figure 34. Crack Growth Rate vs. Crack Length for 20% FWD

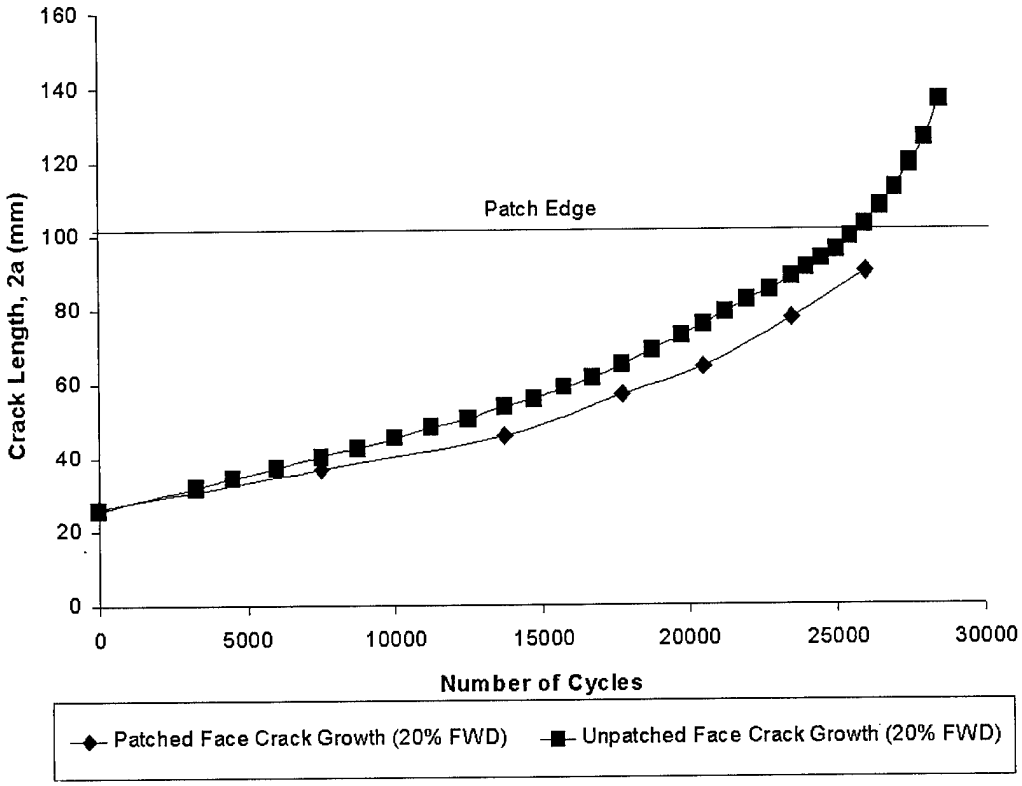

Figure 35. Patched Face vs. Unpatched Face Crack Growth (20% FWD)

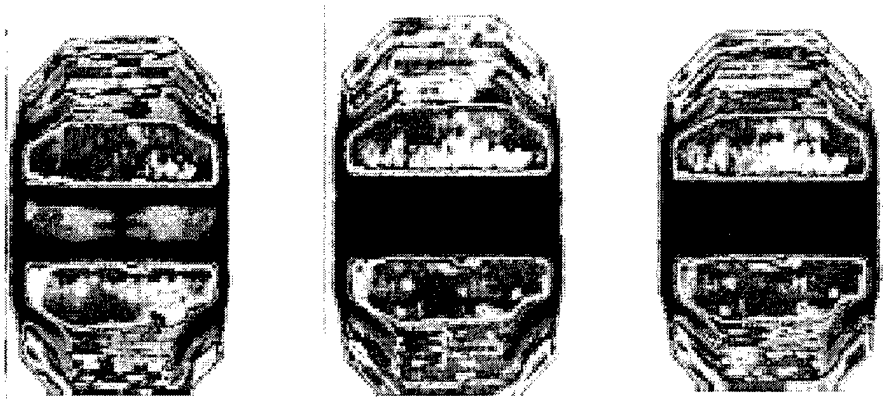

Figure 36. 20% Full Width Debond C-Scans

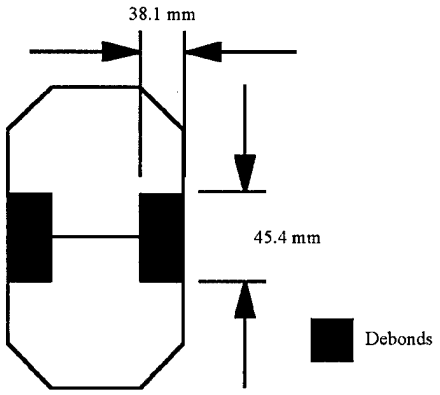

Figure 37. Crack Tip Debond Dimensions

develop. The data indicates that this does not happen until very late in the life of the repair, which would explain the acceleration in crack growth seen as the crack reaches the edge of the patch. The performance of the thick CTD specimens deviates from their thin counterparts, where decreased life was observed [11]. The results do however support observations by Baker [16] that disbonds in front of the crack tip have little effect on the rate of crack propagation.

Table 11. Crack Tip Disbond vs. Baseline

Specimen Number	Description	Cycles to Failure
1	Baseline (No Repair)	9101
2	Baseline (No Repair)	9476
3	Basline (FBP)	38181
4	Baseline (FBP)	38061
9	20% CTD	37139
10	20% CTD	38031

Plotting crack growth rate data shows the same linear growth observed in both the FBP and FWD cases. This data is shown in Figure 39.

The only difference noticeable in crack lag for the CTD specimen is the catching up of the front face crack to that of the back face as the crack nears the edge of the patch. Otherwise, there again seems to be little change in the lag observed in CTD specimens when compared to both the FBP and FWD specimens. The C-scan images for CTD specimen 10 are shown in Figure 41. From the images, it is seen that the debond around the center of the crack grows as crack length increases, similar to the growth seen in the FBP configuration. However, the debond size does not become very large until the crack reaches the edge of the patch. At this time, the center debond plus the crack tip debonds begin resembling the FWD case. No growth is observed in the artificiallly induced debonds. Specimen failure mode was observed to be the patch failure mode.

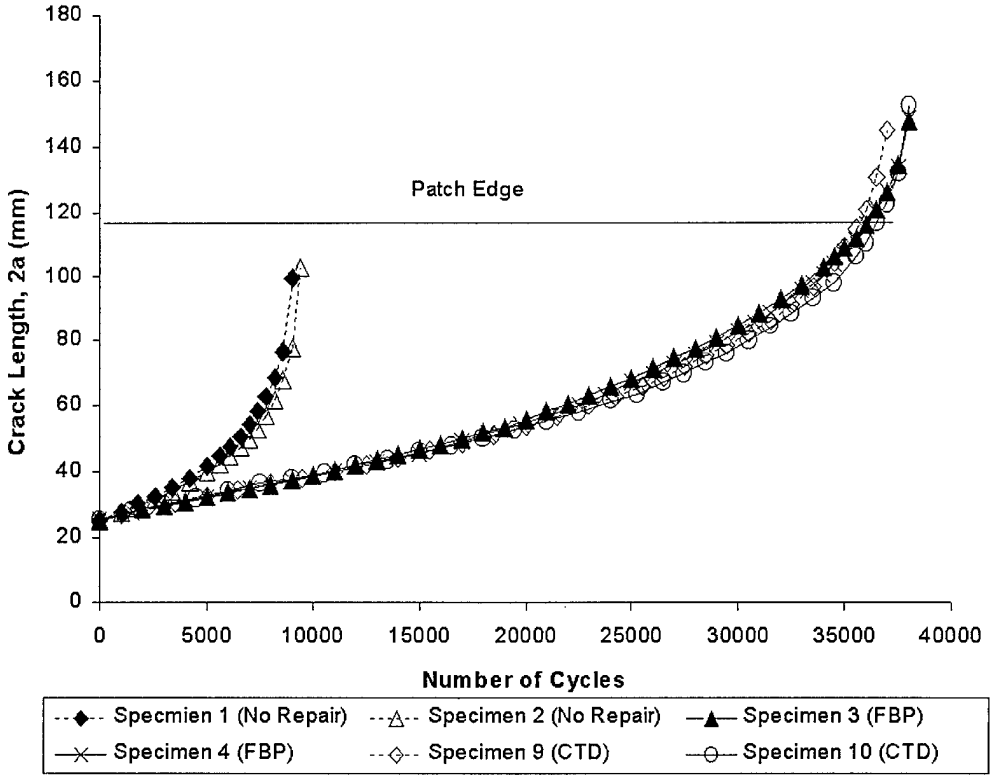

Figure 38. Crack Tip Debond vs. Baseline

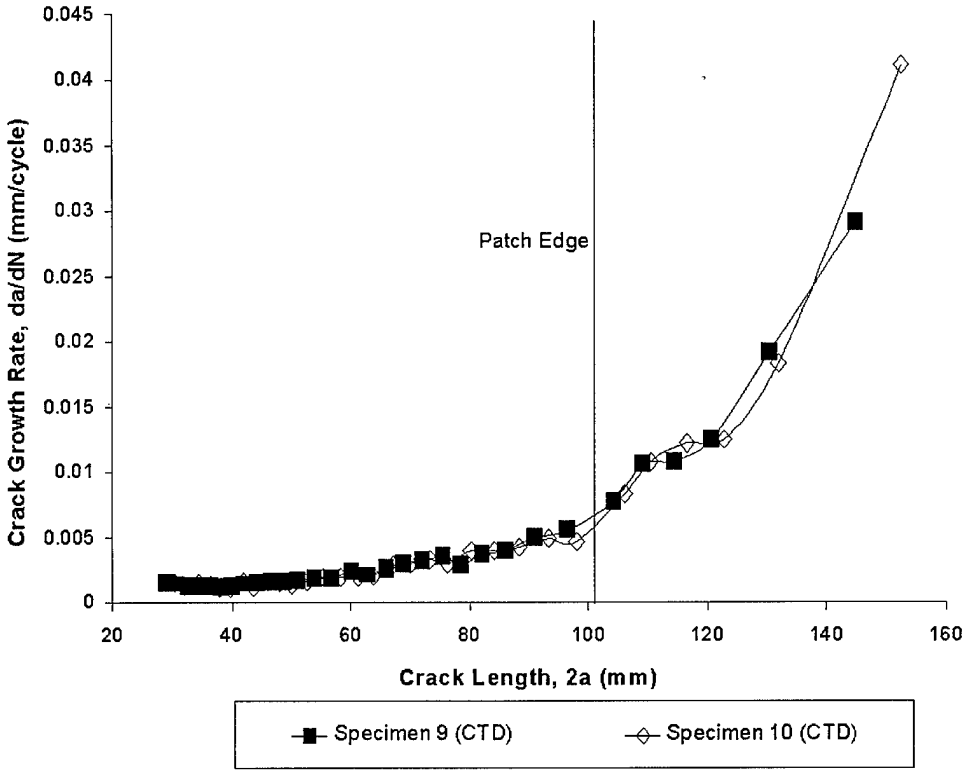

Figure 39. Crack Growth Rate vs. Crack Length for 20% CTD

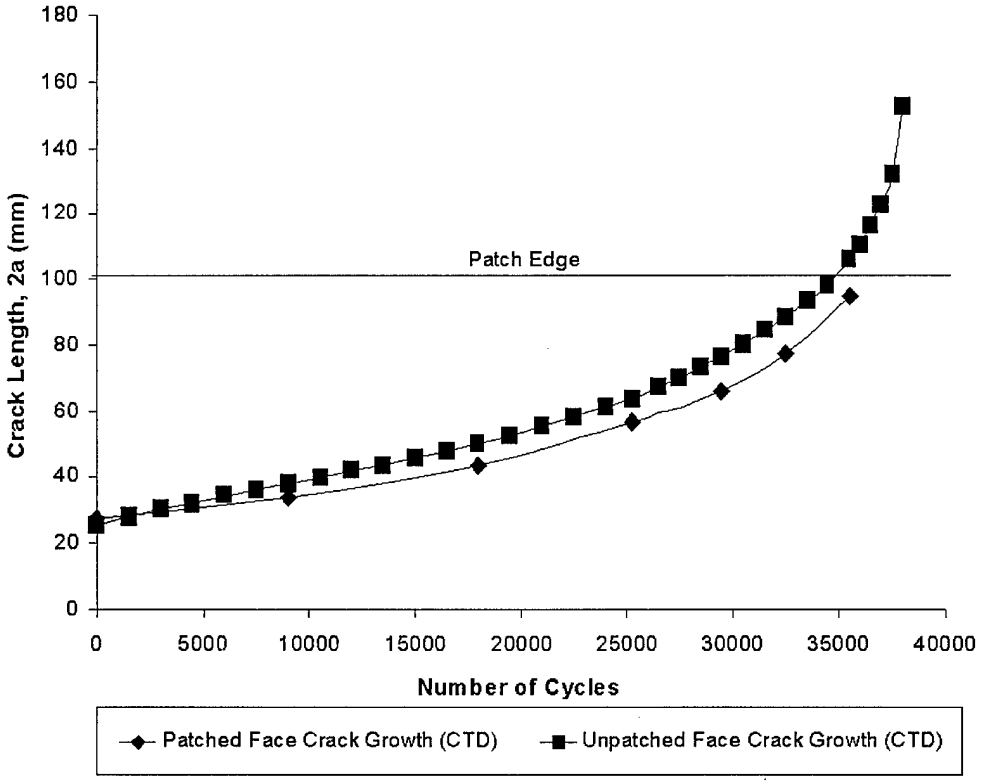

Figure 40. Patched Face vs. Unpatched Face Crack Growth (20% CTD)

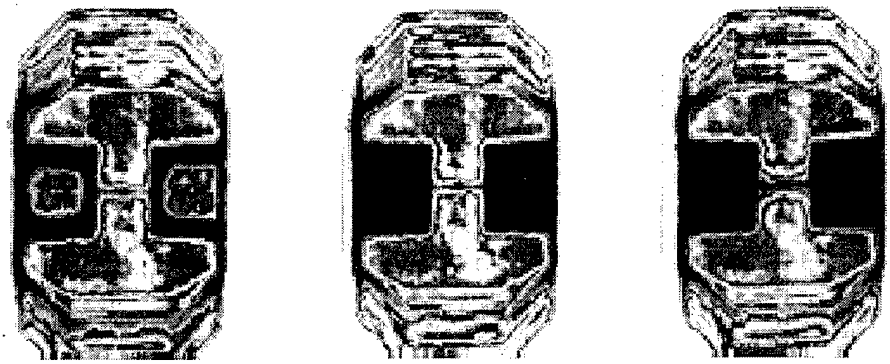

Figure 41. Crack Tip Debond C-Scans

4.3.4 Patch Tip Disbonds

Specimens 11 and 12 were constructed with debonds located at the upper and lower tips of the patch. The debond size equalled roughly 20% of the total bond area. Figure 42 shows the dimensions of the PTD configuration.

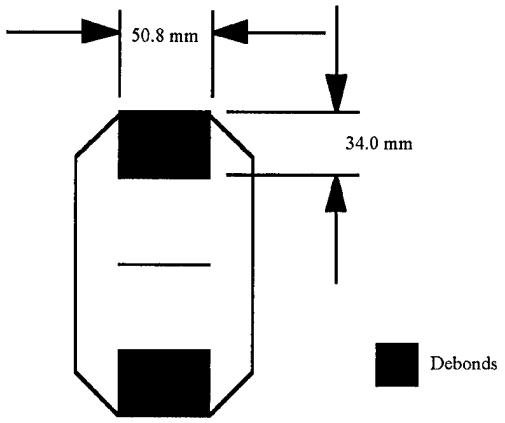

Figure 42. Patch Tip Debond Dimensions

Crack growth data, presented in Figure 43, shows that the two PTD specimens performed either as well as or better than that of the FBP. Specimens 11 and 12 failed at cycle counts of 42283 and 37005 respectively. This difference in life between the two tests is the largest seen in the test matrix, deviating by approximately 14%. Specimen 11 extended the repair life by a factor of 4.5 over the unrepaired baseline and an increase in life of 10% over the average life of the FBP. Specimen 12 extended repair life by a factor of 3.98 over the unrepaired baseline and a decrease in life of only 2% compared to the average life of the FBP. Figure 43 shows crack growth data for PTD vs. Baseline specimens.

By introducing debonds into the tips of the patch, the length of the patch has been effectively reduced. This shortening of the patch has two effects: 1) decreased bending due to adhesive cure and 2) less load attraction into the patch. Schubbe showed that bending was directly related to

Table 12. Patch Tip Disbond vs. Baseline

Specimen Number	Description	Cycles to Failure
1	Baseline (No Repair)	9101
2	Baseline (No Repair)	9476
3	Basline (FBP)	38181
4	Baseline (FBP)	38061
11	20% PTD	42283
12	20% PTD	37005

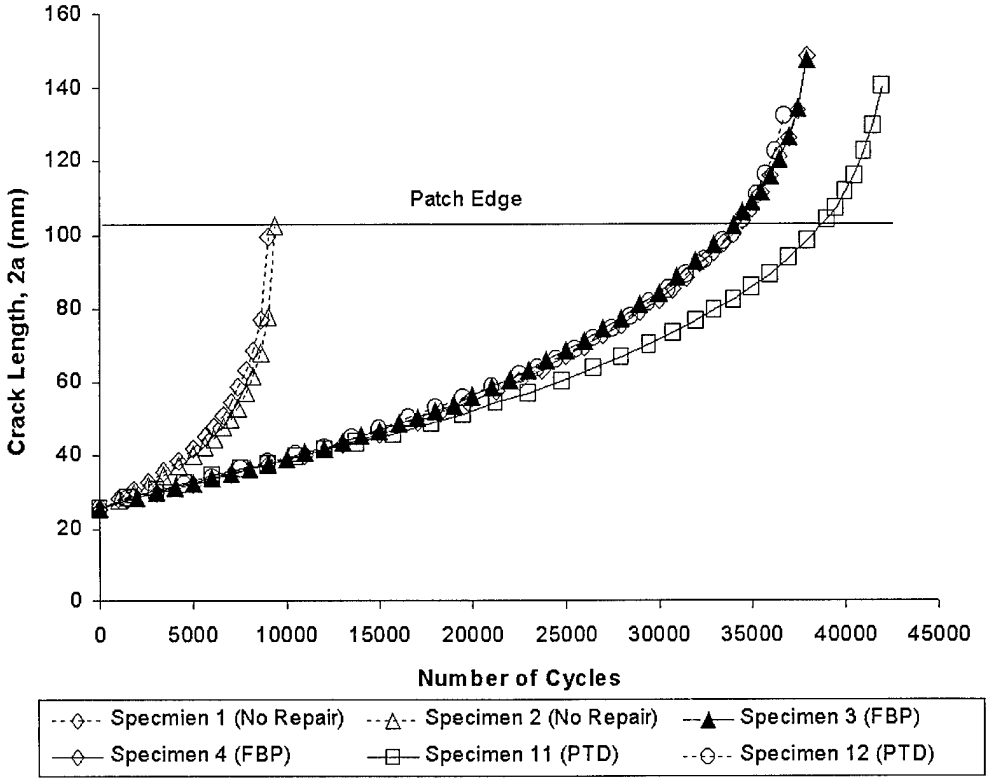

Figure 43. Patch Tip Debond vs. Baseline

residual thermal stresses induced during adhesive cure. The greater the bending, the higher the stresses. A reduction in patch length results in less bending, thus lower residual stresses and longer repair life [10]. He showed that shorter, wider patches were more effective in extending life in thick plates. By bonding a repair onto a panel, the local stiffness around the repair area is increased. This area of increased stiffness will attract load from its surroundings, increasing ΔK_r. Shortening the patch reduces the area of higher stiffness and also the amount of load attracted into it. This results in a reduction in ΔK_r and an increase in repair life. This is not to say that patch lengths should be as short as possible. Care must still be taken in designing the repair so that the length of the patch accommodates the load to be transferred while not succumbing to peel and cleavage fracture.

Plotting the crack growth rate data for the PTD specimens, the same linear growth as seen in the other debond cases is observed. Crack growth rate data is shown in Figure 44. Figure 45 shows front face crack and back face crack length versus cycle number for the PTD specimens. The curve shows the crack lag to again be similar to the previously presented cases.

C-scans for the Specimen 12 are presented in Figure 46. The debond areas are outlined in white. Of interest is the reduced debond growth around the middle portion of the crack. The debonds instead grew elliptically outward from the precrack crack tips. This trend was also observed in the C-scans for Specimen 11, which can be seen in Appendix B. The C-scans also show that the artificially induced debonds do not grow as crack length increases. Specimen failure mode was again the patch failure mode.

4.3.5 Center Disbonds

Specimens 13 and 14 were constructed with disbonds over the center of the crack. These disbonds were only 10% of the total debond area. The debond size was reduced in order to keep

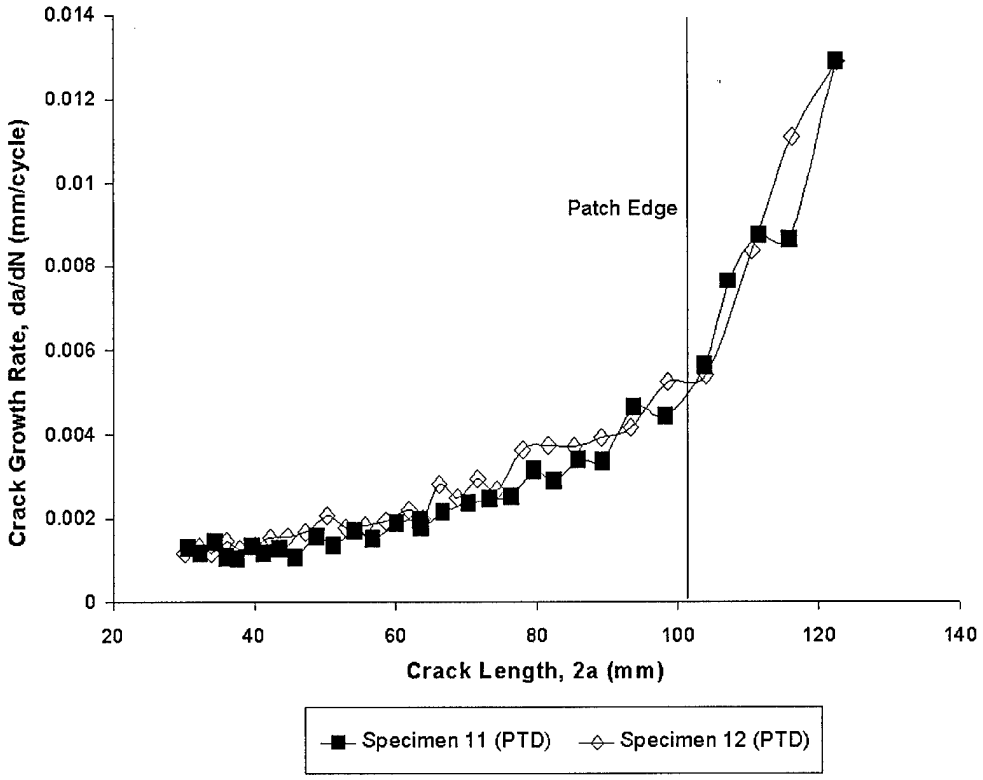

Figure 44. Crack Growth Rate vs. Crack Length for 20% PTD

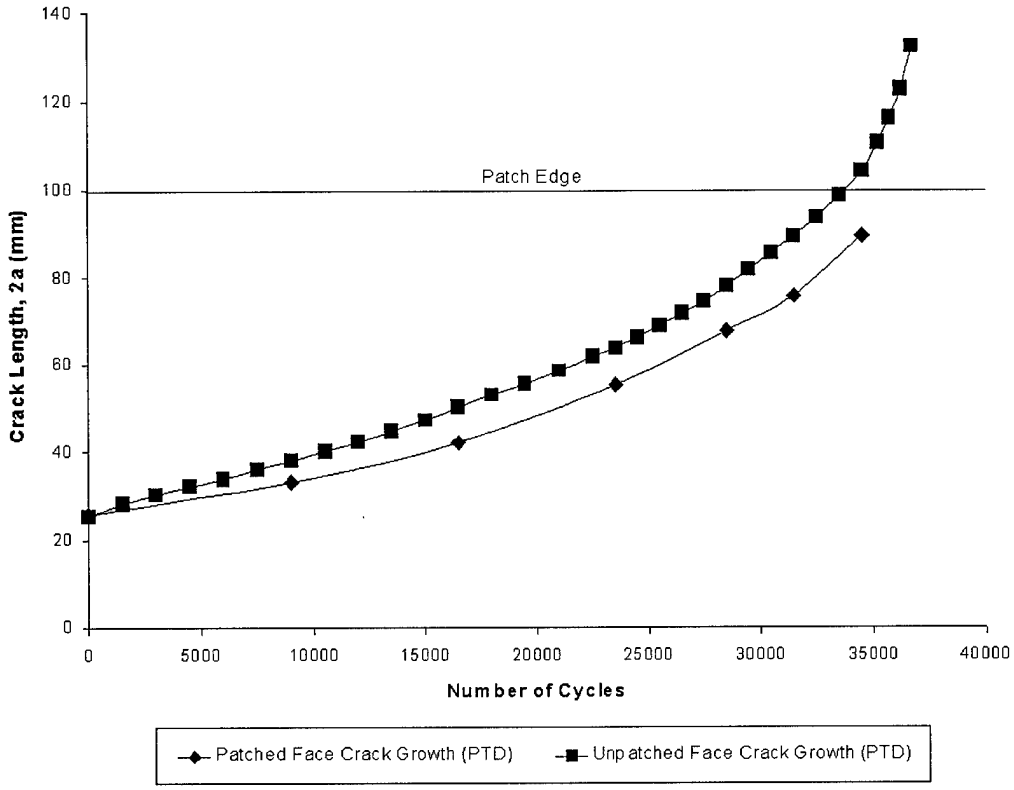

Figure 45. Patched Face vs. Unpatched Face Crack Growth (20% PTD)

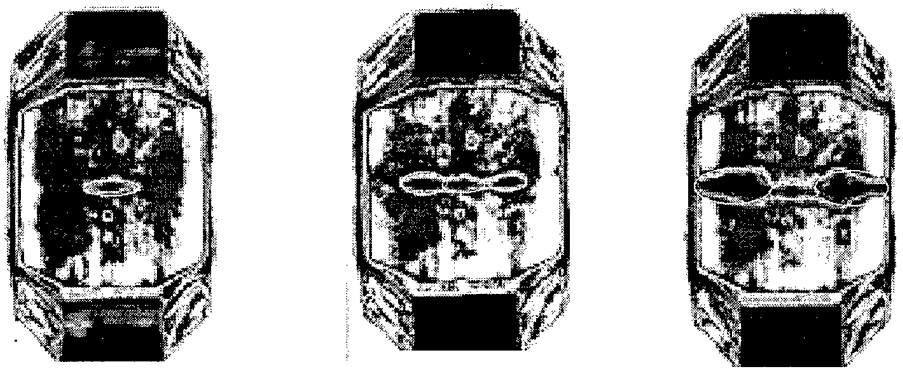

Figure 46. Patch Tip Debond C-Scans

the debond area under the uniform thickness region of the patch and to have the precrack crack tips covered by adhesive. The dimensions of the CD specimens are shown in Figure 47.

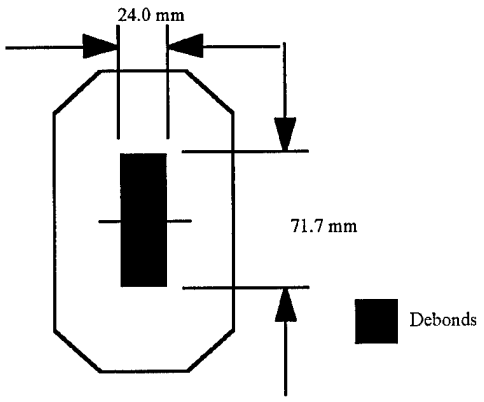

Figure 47. Center Debond Dimensions

Crack growth data shown in Figure 48 shows that the CD damage configuration has a noticeable adverse impact on repair life. Specimens 13 and 14 exhibited a 11.7% and 16.5% decrease in life as compared to the average life of the FBP specimens. Specimens 13 and 14 yielded life extension factors of 3.62 and 3.32 over the unrepaired panels. It is interesting to see that the CD specimens, despite the decrease in debond area, performed only marginally better than the 20% FWD specimens.

The CD configuration like, the FWD configuration, has no adhesive bridging the crack. This allows the crack to open resulting in faster crack growth. This supports observations and results obtained by both Baker [16] and Denney [11]. Moreover, Denney showed that increases in the longitudinal length of the debond in the CD configuration resulted in shorter repair life.

Crack growth rate data is presented in Figure 49. As in the previous debond cases, crack growth rate, hence ΔK_r, is not constant under the patch. Instead, it increases linearly until the crack reaches the edge of the patch, whereafter it increases exponentially until failure. Figure 50

shows crack growth on the patched and unpatched faces of the CD configuration as a function of cycle number. As in the previous cases, crack lag seems to be independent of damage configuration. C-scans for Specimen 14 are shown in Figure 51. Debond growth is shown to be the expected elliptical growth outwards from the center of the crack. The images also show that the artificially induced debonds do not grow as crack length increases. Both Specimens 13 and 14 failed by the patch failure mode.

Table 13. Center Disbond vs. Baseline

Specimen Number	Description	Cycles to Failure
1	Baseline (No Repair)	9101
2	Baseline (No Repair)	9476
3	Basline (FBP)	38181
4	Baseline (FBP)	38061
13	10% CD	33656
14	10% CD	31842

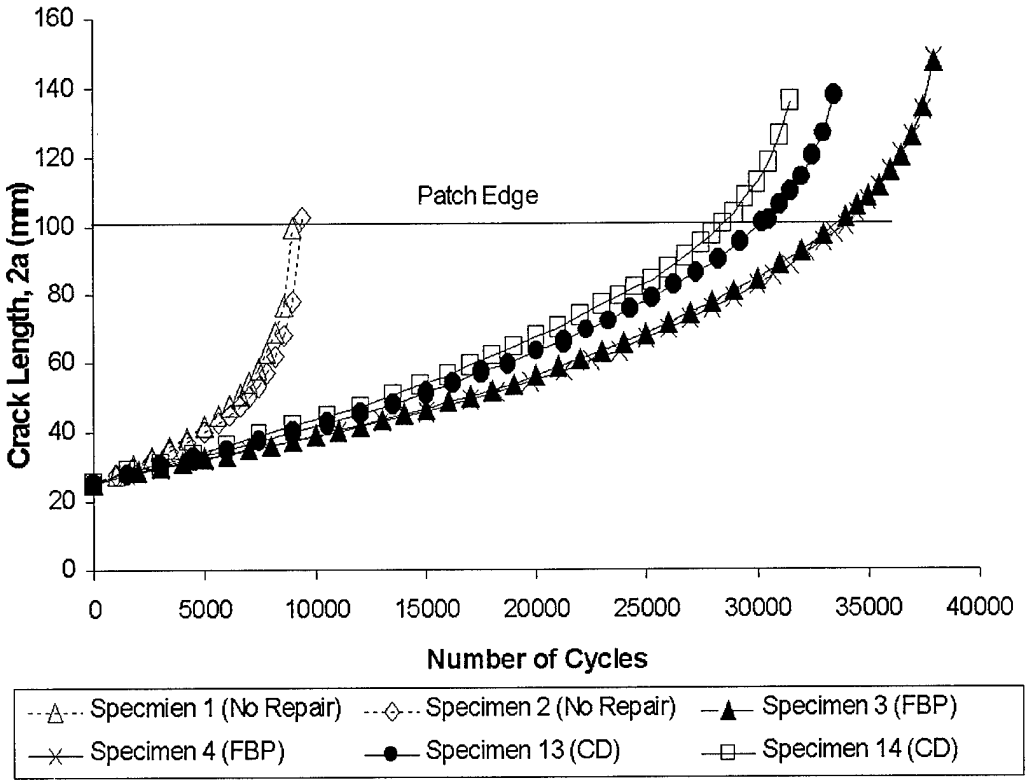

Figure 48. Center Debond vs. Baseline

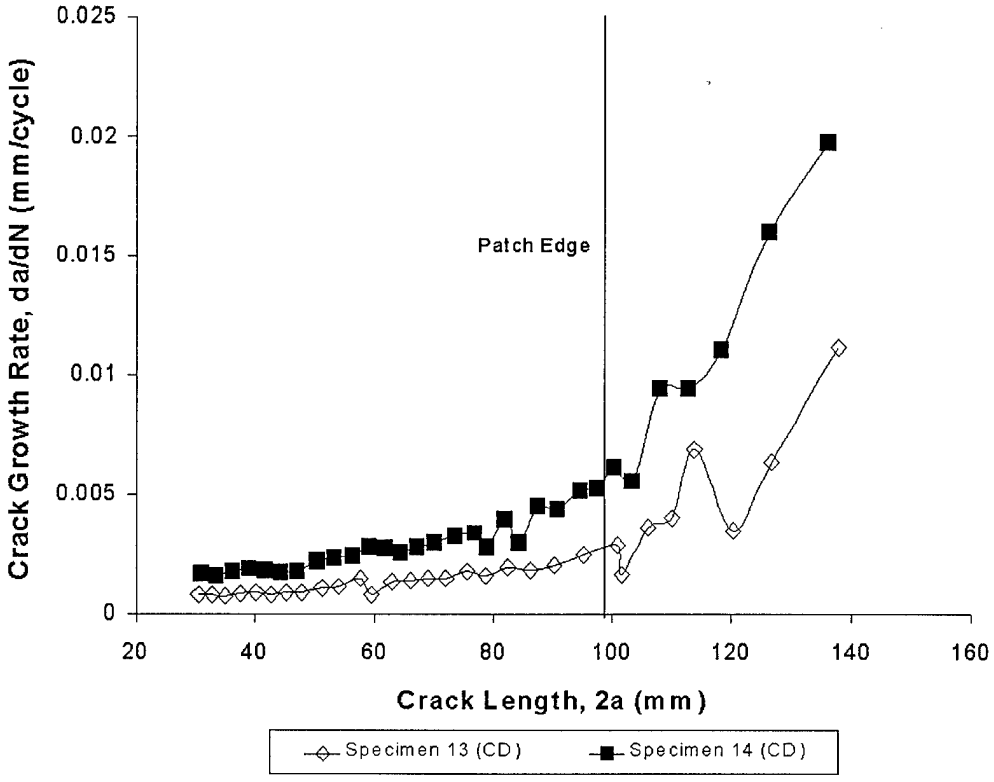

Figure 49. Crack Growth Rate vs Crack Length for 10% CD

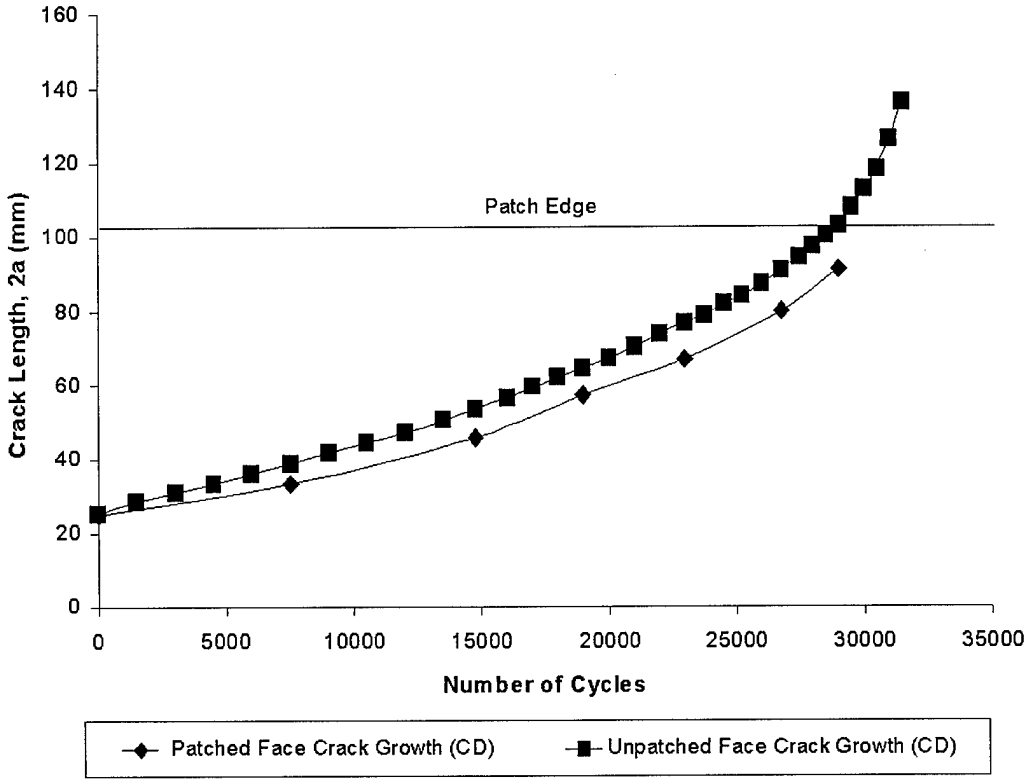

Figure 50. Patched Face vs. Unpatched Face Crack Growth (10% CD)

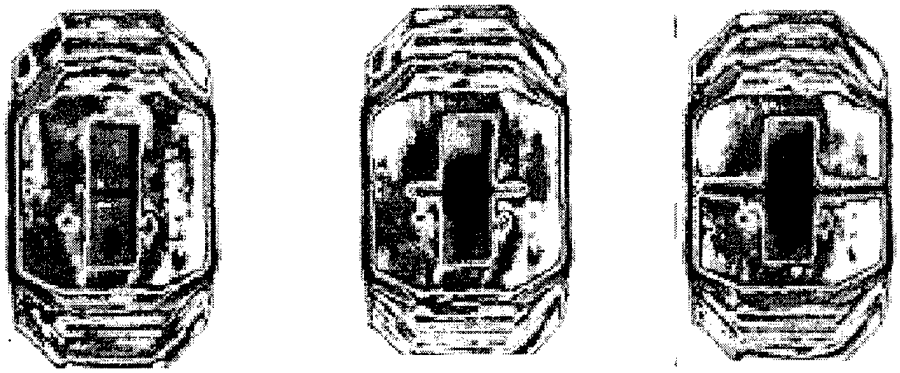

Figure 51. Center Debond C-Scans

Chapter 5 - Finite Element Analysis

This chapter presents the finite element analysis method used in analyzing the bonded repair. The ability of the present model to predict life is investigated by comparing its results with experimental data.

5.1 Three Layer Technique

The Three Layer Technique introduced by Naboulsi and Mall [32, 33] is a two dimensional (2D) finite element analysis that uses three layers of 2D Mindlin plate elements to model the aluminum plate, the adhesive and the composite patch. This technique is an evolutionary step from Sun's approach, which modeled the plate and patch with 2D Mindlin plate elements and the adhesive with spring elements [29]. One of the benefits of the Three Layer technique is that it allows the adhesive to be modeled as an elastic continuum, more accurately representing the structure. Another is that it provides an economical 2D numerical solution to a three-dimensional (3D) problem.

Due to symmetry, only one quarter of the repaired plate configuration was modeled. The quarter plate model consisted of 6040 four-noded Mindlin plate elements of which 1744 were used to model the patch, 1744 were used to model the adhesive and 2552 were used to model the aluminum plate. Model refinement in the crack-tip area consisted of ten 0.05 mm square elements leading the crack tip, ten 0.05 mm square elements trailing the crack tip, and ten 0.05 mm square elements ascending from the line of symmetry. The model and crack tip refinement are shown in Figures 52 and 53. In Figure 52, moving in the positive z-direction, the layers as shown are the aluminum plate, adhesive and repair. The areas of the model where symmetry is enforced are shown as Edges 1 and 2. The crack is modeled as free nodes along Edge 2 of the aluminum plate extending from the origin to the desired crack length.

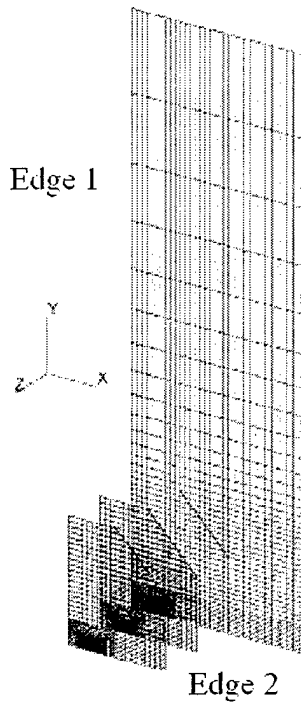

Figure 52. 3 Layer FEM Quarter Panel

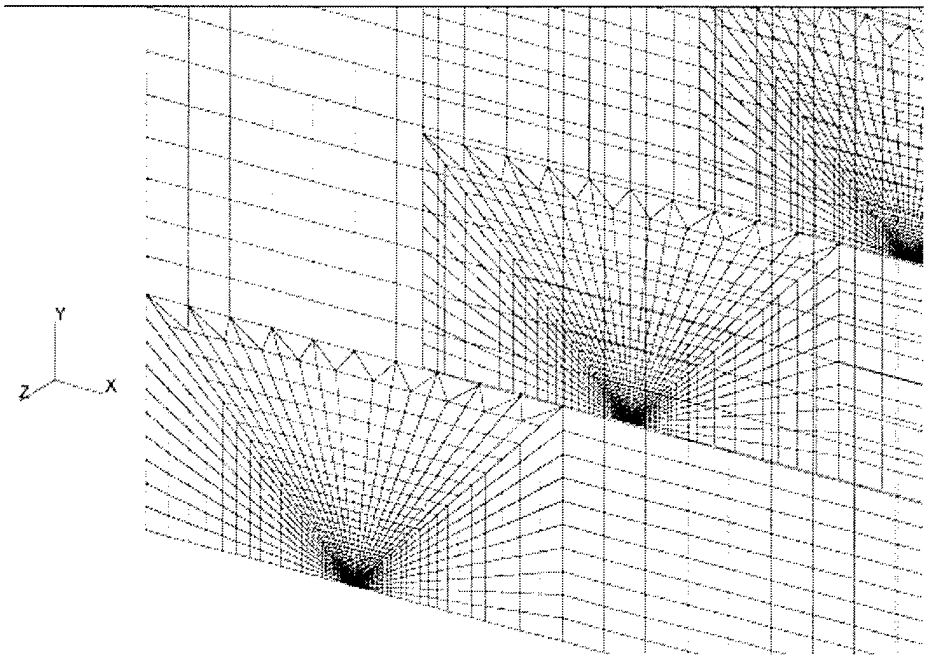

Figure 53. Crack Tip Refinement

Mindlin Plate elements are well suited to modeling thick plates, as they account for both bending deformation and transverse shear deformation [34]. Compatibility conditions were enforced through the three layers at each bonded interface with constraint equations based on Mindlin plate theory. Mindlin plate theory assumes a linear displacement field through the thickness:

$$u_x = \overline{u_x} + z\overline{\theta_y} \tag{21}$$

$$u_y = \overline{u_y} + z\overline{\theta_x} \tag{22}$$

$$u_z = \overline{u_z} \tag{23}$$

where $\overline{u_x}$, $\overline{u_y}$, and $\overline{u_z}$ are defined as the mid-plane displacements in the x, y and z directions and $\overline{\theta_y}$ and $\overline{\theta_x}$ are the rotations of the plate cross-section about the y and x axes. For the model used in this study, the plate elements were in the xy plane, the y axis was the direction of the uniaxial loading and the z axis was in the thickness direction of the plate. Each layer was constructed using Mindlin plate elements and as such were assumed to have linear displacement fields through the thickness. This being the case, each layer must then satisfy these equations:

$$u_x^i = \overline{u_x^i} + z^i\overline{\theta_y} \tag{24}$$

$$u_y^i = \overline{u_y^i} + z^i\overline{\theta_x} \tag{25}$$

$$u_z^i = \overline{u_z^i} \tag{26}$$

where i represents the plate (p), the adhesive (a) or the repair (r). The z^i coordinate represents the thickness of each plate element and is defined as:

$$-\frac{h^i}{2} \leq z^i \leq \frac{h^i}{2} \tag{27}$$

with the superscript i again representing either p, a or r. To have compatibility through the three layers, geometric constraints must be enforced at the interface of each layer. At the interface of the aluminum plate and adhesive, these are:

$$u_x^p = u_x^a \tag{28}$$

$$u_y^p = u_y^a \tag{29}$$

$$u_z^p = u_z^a \tag{30}$$

And similarly moving from the adhesive to the repair:

$$u_x^a = u_x^r \tag{31}$$

$$u_y^a = u_y^r \tag{32}$$

$$u_z^a = u_z^r \tag{33}$$

With results from the finite element model, the indirect modified crack closure method [31] was used to calculate the strain energy release rate G at the mid-plane crack tips. Assuming a decoupling of the Mode I and Mode II strain energy relation and using the through-the-thickness linear assumptions of the model, G_I was calculated at both the patched and unpatched surfaces of the aluminum plate. From G_I, the stress intensity factor K_I was then calculated for both the patched and unpatched faces of the aluminum plate.

5.2 Boundary Conditions

5.2.1 Rotation and Displacement

Due to specimen and loading symmetry, only one quarter of the repaired aluminum panel was modeled. In Figure 54, the dashed lines represent the lines of symmetry. These correspond to Edges 1 and 2 of the panel, adhesive and patch. Along Edge 1, symmetry requires that displacements in the x and rotations about the y equal zero. This condition applies to all three layers, thus:

$$u_x^p = u_x^a = u_x^r = \theta_y^p = \theta_y^a = \theta_y^r = 0 \tag{34}$$

Along Edge 2, with the exception of the crack in the aluminum panel, displacements in the y and rotations about the x must equal zero. This again applies to all three layers, thus:

$$u_y^p = u_y^a = u_y^r = \theta_x^p = \theta_x^a = \theta_x^r = 0 \tag{35}$$

Edge 3 of the aluminum panel was not constrained. Edges 3 and 4 of both the adhesive and patch were constrained using the through-the-thickness constraint equations discussed in the previous

section. Edge 4 of the aluminum panel was constrained in a manner to simulate the clamped loading condition used during the experimental phase of this study. Displacements in the x and z and rotation about the x were set equal to zero. Thus, along Edge 4:

$$u_x^p = u_z^p = \theta_x^p = 0 \tag{36}$$

Loads were applied to Edge 4 of the panel in the positive y direction to simulate the uniaxial loading applied during testing. Lastly, due to the nature in which the solver (ABAQUS) defines the Mindlin plate element, all rotations about the z direction were automatically set equal zero.

$$\theta_z^p = \theta_z^a = \theta_z^r = 0$$

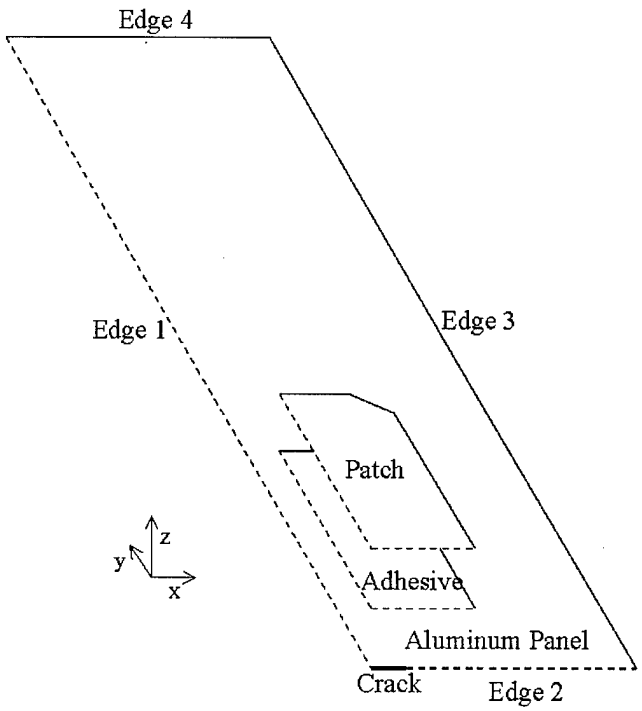

Figure 54. Repaired Panel Quarter Model

5.2.2 Temperature Condition

Residual thermal stresses have been shown to have a large impact on the stress state of thick repaired panels [10]. For this reason, the cool-down period after patch bonding was simulated in the analysis as $\Delta T = -100°C$. To determine whether this choice of temperature was an adequate approximation, a comparison of out-of-plane displacement was made between experimental data and model data for a fully bonded patch (Specimen 4). In the case of the physical specimen, out of plane displacement data was taken along the longitudinal (loading) centerline of the specimen on both sides of the crack up to a distance of 50.4 mm. This data fell under the region of uniform patch thickness. Similarly, for the FEM model, data was taken along the longitudinal centerline under the uniform thickness region of the patch a distance of 35 mm above the crack. After the experimental data was plotted, a 2^{nd} order polynomial was fit to the data to illustrate the curvature caused by the bonding process. The FEM data was then plotted with both the curve-fit and experimental data to show correlation. Figure 55 shows that the curvature of the finite element model and the actual specimen very closely agree with one another, validating the chosen value of $-100°C$ for ΔT.

5.3 Crack Growth Rate Comparison

To investigate the accuracy of the Three Layer technique, a comparison between experimental and finite element crack growth rate data for the 20% FWD case was made. To do this, finite element models were constructed of the bonded repair at three crack lengths: 1) $2a = 25.4mm$ $(1.0in)$ 2) $2a = 63.5mm$ $(2.5in)$ and 3) $2a = 101.6mm$ $(4.0in)$. The disbonds were simulated in the model by releasing nodes in the disbond area from some of the constraint equations. For example, in the case of connected nodes, conditions described in Equations 28 through 33 would be enforced through the thickness at the layer interfaces. However, for a disbond, there would

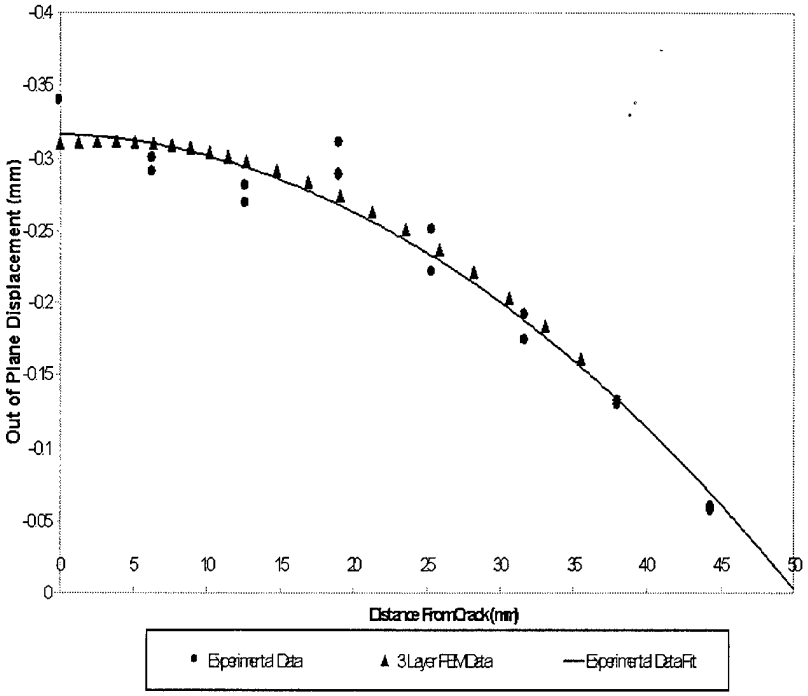

Figure 55. Comparison of Out-of-Plane Displacement of FBP Experimental Data and 3-Layer FEM Data

be no through the thickness transfer of shear loads, thus eliminating Equations 28, 29, 31, and 32. Only the conditions in Equations 30 and 33 would be enforced. This would be done to maintain the physical distance between each layer, and to prevent the layers from potentially overlapping in space. Figures 56, 57, and 58 show the aluminum plate layer of the three models and the refinement around the crack tips.

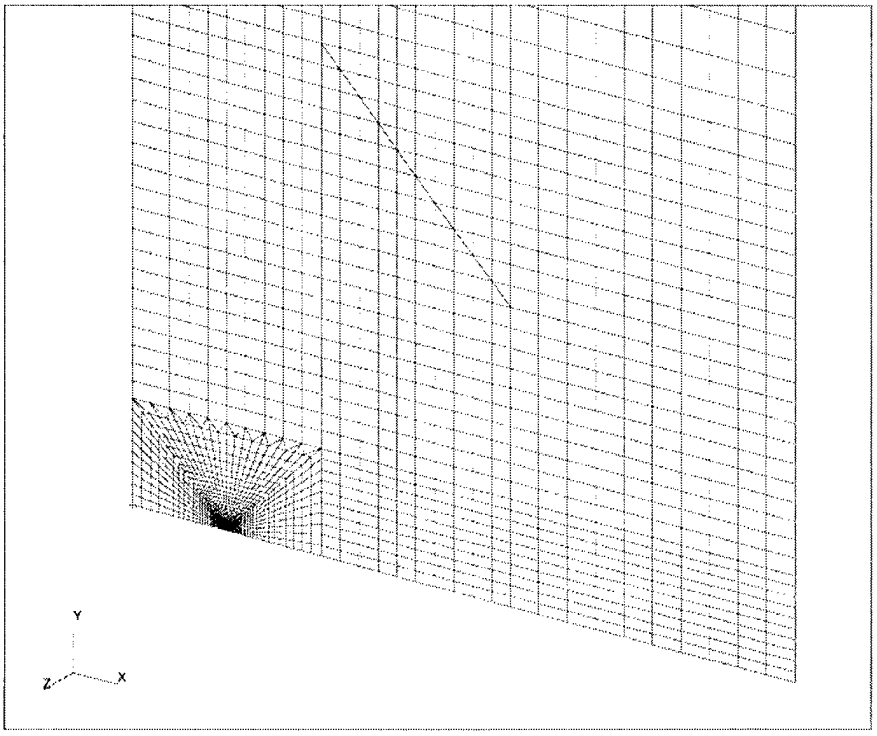

Figure 56. Finite Element Mesh of Aluminum Panel 2a=25.4mm

Each model was run separately under both thermal and mechanical loading conditions. The inclusion of a thermal condition was done to ensure that residual stresses caused by bonding would be included in the final result. The thermo-mechanical loading result was then obtained by linearly summing the thermal and mechanical results. Figure 59 shows an example stress contour and deformation plot of the thermo-mechanical loading case for the 20% FWD repair with $2a = 63.5mm$

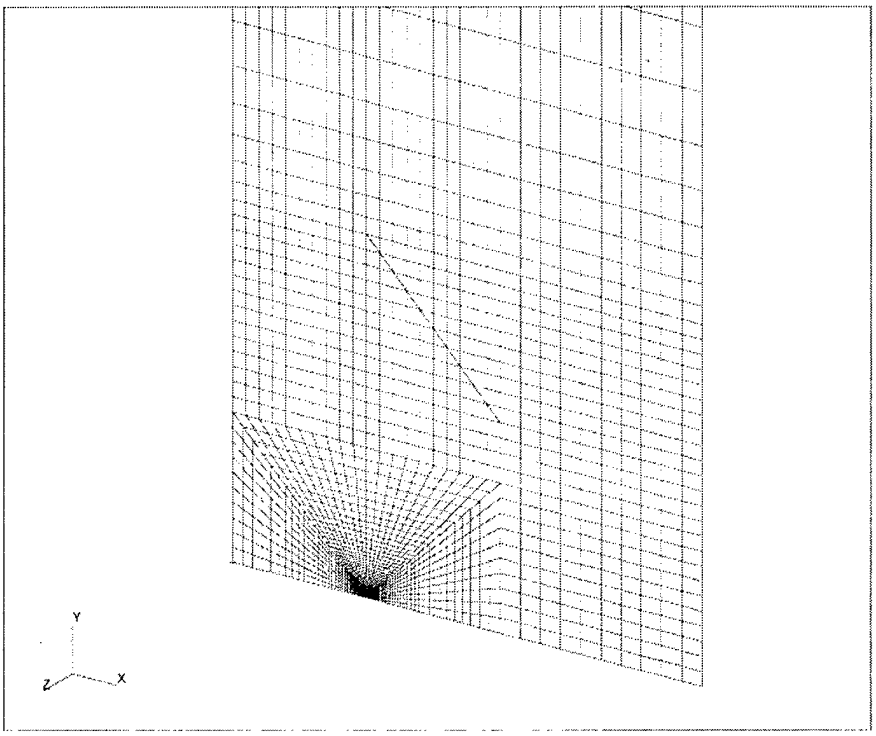

Figure 57. Finite Element Mesh of Aluminum Panel 2a=63.5mm

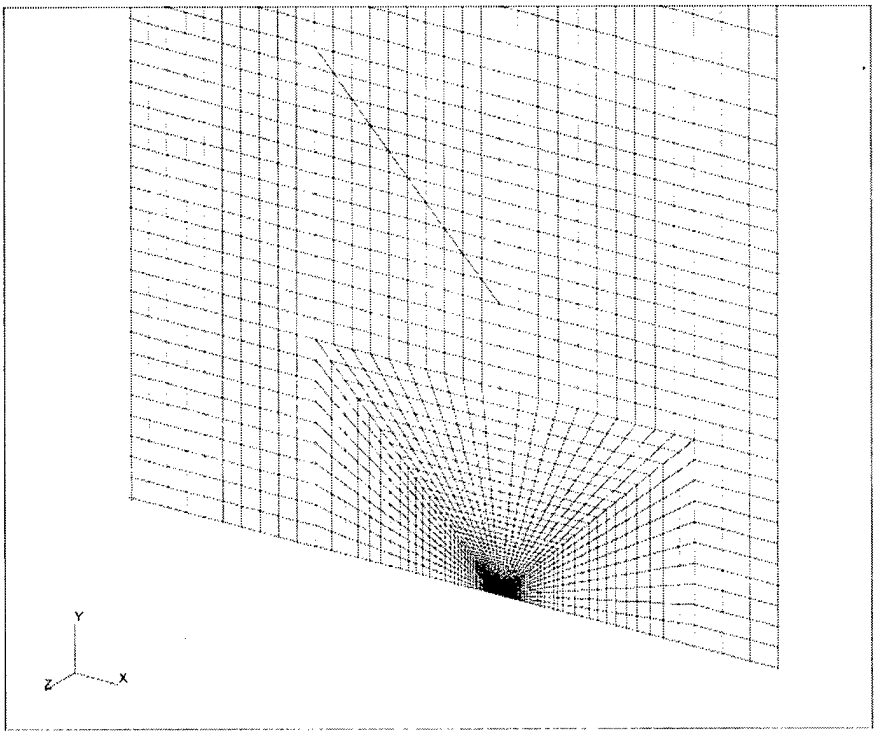

Figure 58. Finite Element Mesh of Aluminum Panel 2a=101.6mm

$(2.5in)$. Data from the thermo-mechanical loading was used with the indirect modified crack closure method [31] to calculate G and then the repaired stress intensity factor K_r. Using the Paris Law:

$$\frac{da}{dN} = c\Delta K_r^m \tag{37}$$

and, having determined ΔK_r for a known crack length, the crack growth rate da/dN for the 20% FWD was then calculated. The values used for c and m were developed by Schubbe [10] for specimens of the thickness and load conditions (frequency, load ratio, ΔK) used in this study. The constants c and m were $10.267 * 10^{-12} m/cycle$ and 3.408 respectively. ΔK_r has the units of $MPa\sqrt{m}$, and da/dN has the units $mm/cycle$. Crack growth rate data for both the unpatched and patched face are shown in Tables 14. FEM crack growth rate data for the unpatched face is compared with experimental data in Figure 60. Figure 60 shows that the Three Layer technique yields results that match the crack growth rate of Specimen 7 very closely while being conservative in its predictions compared to Specimen 8.

Table 14. 3 Layer Crack Growth Rate Data for Patched Face

Crack Length 2a (mm/in)	G **Patched Face** (N/m)	K **Patched Face** $(MPa\sqrt{m})$	$\frac{da}{dN}$ **Patched Face** $(mm/cycle)$
25.4/1.0	8.24E03	24.19	5.33E-4
63.5/2.5	1.13E04	28.10	8.89E-4
101.6/4.0	1.31E04	30.34	1.15E-3

Table 15. 3 Layer Crack Growth Rate Data for Unpatched Face

Crack Length 2a (mm/in)	G **Unpatched Face** (N/m)	K **Unpatched Face** $(MPa\sqrt{m})$	$\frac{da}{dN}$ **Unpatched Face** $(mm/cycle)$
25.4/1.0	1.19E04	29.06	9.96E-4
63.5/2.5	2.04E04	38.15	2.52E-4
101.6/4.0	3.45E04	49.59	6.16E-3

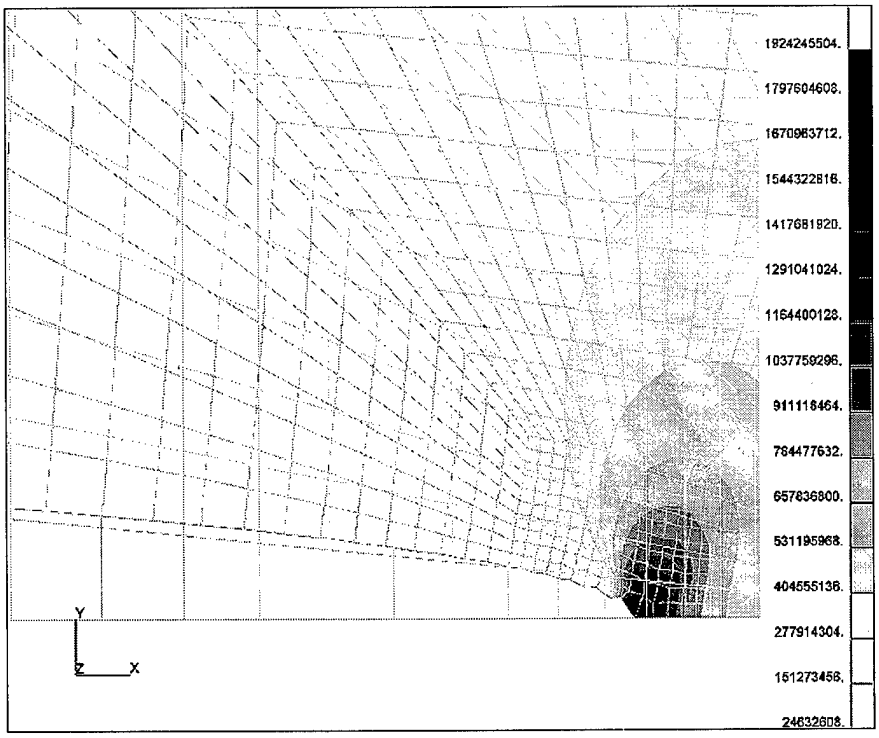

Figure 59. Displacment and Stress Contour of Crack Tip 2a=63.5mm

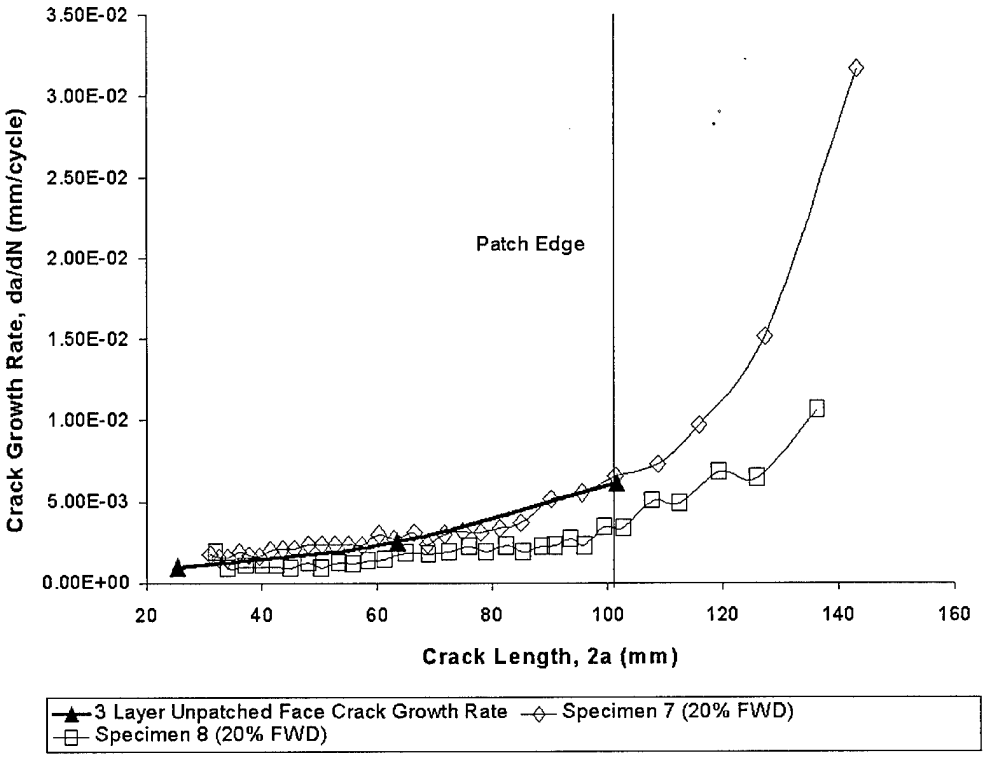

Figure 60. 3 Layer FEA and Experimental Crack Growth Rate Data Comparison for 20% FWD

Chapter 6 - Summary and Conclusions

The purpose of this study was twofold: 1) to investigate the effects of bondline flaws during the repair of thick unstiffened aluminum panels by bonded composite patches and 2) to determine the accuracy of current finite element modeling techniques in predicting the life of thick repaired structure. This was accomplished by conducting both an experimental and numerical study. The experimental study consisted of the fatigue testing of five different debond configurations of repaired thick aluminum structure. The artificially induced debonds were monitored during fatigue testing using C-scans to investigate any growth that might occur over the life of the repair. The numerical study involved the finite element modelling and crack growth rate determination of one of the debond cases. Finite element results were verified against experimental data.

6.1 Experimental Study

The five debond configurations studied were the Fully Bonded Patch (FBP), the Full Width Debond (FWD), the Crack Tip Debond (CTD), the Center Debond (CD) and the Patch Tip Debond (PTD). Panels with no repairs were also tested to develop the baseline for comparison. Repairs were designed using current industry "rules of thumb."

The experimental data showed that, for the repair design used in this study, the FBP configuration extended life by a factor of four when compared to the unrepaired panel. The CTD and PTD configuration performed similarly, yielding average life extension factors of 4.05 and 4.27 respectively. Crack growth rate under the FBP, CTD, and PTD configurations were observed as growing linearly. Crack tip lag between the patched and unpatched face of the specimens was consistent between the three configurations, exhibiting an independence from debond configuration. The results of the CTD configuration for thick repaired specimens differs from the results observed by Denney [11], who observed an adverse impact of the CTD configuration on repair life in his testing of thin

repaired specimens. The results are, however, in agreement with observations made by both Baker [16] and Mills and Ryan [12] in their testing of thicker structure. The results of the PTD configuration are similar to those seen in thin repaired tests, resulting in life extensions either greater than or equivalent to the FBP configuration. C-scan images taken of the CTD and PTD configuration showed that the size of the artificially induced debonds did not increase during the life of the repair.

The FWD and CD configurations yielded average life extension factors of 3.2 and 3.5 respectively, slightly less than the CTD and PTD configurations. In the case of the FWD, this equates to a 21% decrease in life compared as to the FBP configuration. For the CD configuration, this equals a 14% loss of life as compared to the FBP configuration. Crack growth rates and patched face versus unpatched face crack growth behaved similarly to the FBP, CTD and PTD configurations. C-scan images taken during fatigue testing showed no growth of the artificial debonds during the life of the repair. Results for these two configurations support those found in the literature [11, 12, 16].

The results from the experimental testing suggest that: 1) debonds away from the crack (CTD, PTD) have little impact on repair life and, 2) debonds located around the crack (FWD, CD) have a noticeable impact on repair life. In the case of the CTD configuration, the crack tip is exposed, i.e. in the debond area, but the majority of the crack is still covered by the adhesive and composite patch. The bridging of the crack reduces crack opening and thus crack growth. In the PTD configuration, the entire crack is covered by adhesive, bridging it and not allowing it to open. The PTD configuration can occasionally show improvements in life over the FBP case. This is caused by lower residual thermal stresses/less bending induced during cure due to the effective shortening of the patch. Both the FWD and CD configurations have debond locations over the crack. Being only partially bridged, these debond configurations allow greater crack opening resulting in the relatively shorter repair life.

6.2 Finite Element Analysis

The finite element analysis was conducted using the Three Layer technique developed by Mall and Naboulsi [32, 33]. The method uses separate layers of 4-noded Mindlin plate elements to simulate the cracked aluminum panel, the adhesive and the composite patch. The 3 layers are connected at the nodes by constraint equations that satisfy Mindlin plate assumptions. Displacement data generated by the model is used with the indirect modified crack closure method [31] to calculate strain energy (G) at the crack tip. From strain energy, both the stress intensity factor (K_r) and crack growth rate (da/dN) are then calculated.

For this study, the Three Layer technique was used to generate da/dN data for the 20% FWD configuration. This involved the modeling of the repaired panel at three different crack lengths. Debonds in the model were simulated as a releasing of constraint equations in the debond area. At each crack length, values for G, K and da/dN were calculated. The calculated crack growth rate data, when plotted versus experimental data, showed excellent correlation between the finite element model and the exhibited behavior of the FWD test specimen. The model is not perfect, however, as prior knowledge of debond size and location is required to generate reasonable results.

6.3 Recommendations for Future Research

A minimum goal for a good repair design is to provide a life extension factor to the repaired structrue of at least four. Using the current "rules of thumb" for single sided repair, this can be accomplished for thick structure if no debonds are present. However, in the event of poor process control, debonds can be introduced into a repair. From the results of this study, if the debond is located near the crack, this can greatly decrease the expected life of the repair. This then raises the issue of whether to remove the repair or leave it with the knowledge that it may have to be replaced sometime in the future, not an acceptable solution considering fiscal and monetary constraints. This

can be avoided by performing research in the area of repair design optimization for thick structures. New "rules of thumb" should be developed for thick structural repair.

Experimentation in this study was performed on unstiffened aluminum panels, something not usually found on actual aircraft structures. To get a better idea of how bonded repairs might perform in real world applications, studies should be done into the effectiveness of bonded repairs to stiffened structure. Baker [16] assumed that bending caused by residual thermal stress would be negligible because of localized stiffening caused by surrounding structure. This does not mean the stresses are not present, only that they have been moved away from the repair area into surrounding structure. The potential for damage to the surrounding structure caused by repair then becomes an issue. A study in this direction would provide information on both the efficiency of the bonded repair as well as its impact on surrounding structure.

Lastly, many applications for bonded repair technologies are being targeted at large transport aircraft. These aircraft typically cruise at altitudes of $10km$ $(35000ft)$ at temperatures of $-40°C$ $(-40°F)$. Experimental testing conducted by Baker [16] has shown the adverse effects on bonded repairs that can be caused by elevated temperatures, however little work has been done characterizing repair efficiencies at low temperatures. If bonded repairs are to be used on these aircraft, this area should also be investigated.

APPENDIX A - Appendix A: Post Failure Images

This appendix contains select post-failure images of specimens detailing disbond and failure mode characteristics. A representative of each disbond configuration is presented. Close inspection of the failed specimens shows where artificial disbonds were created in the bondlines.

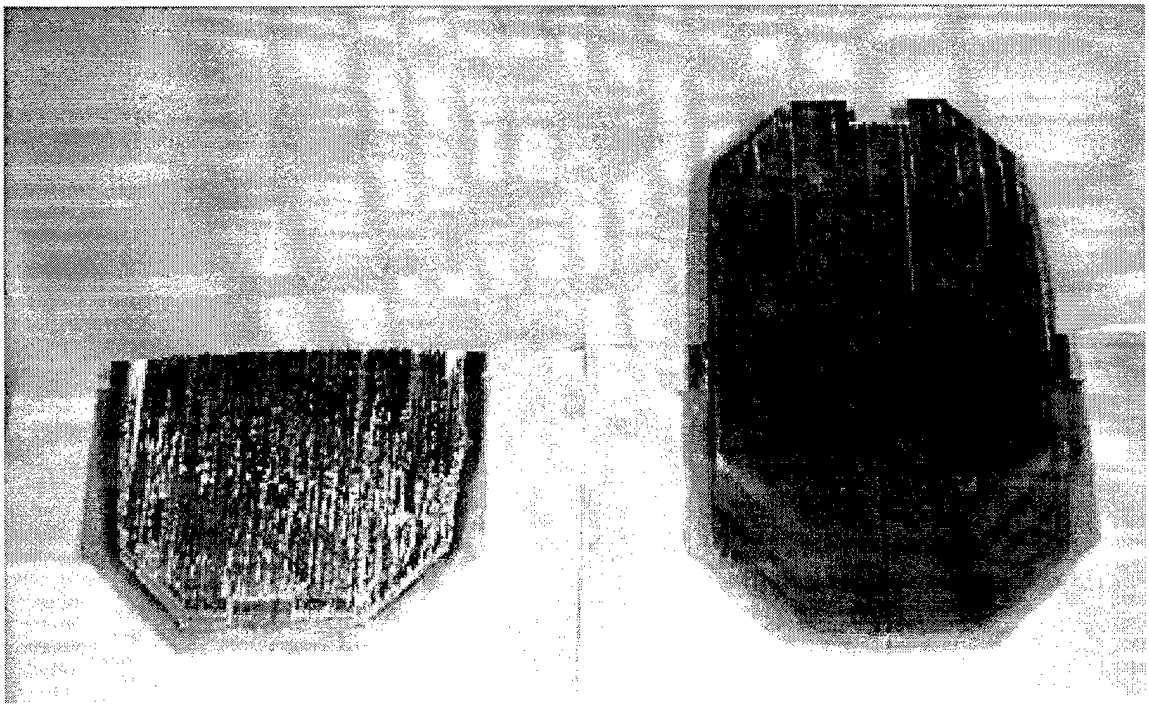

Figure 61. Post Failure - Fully Bonded Patch (FBP)

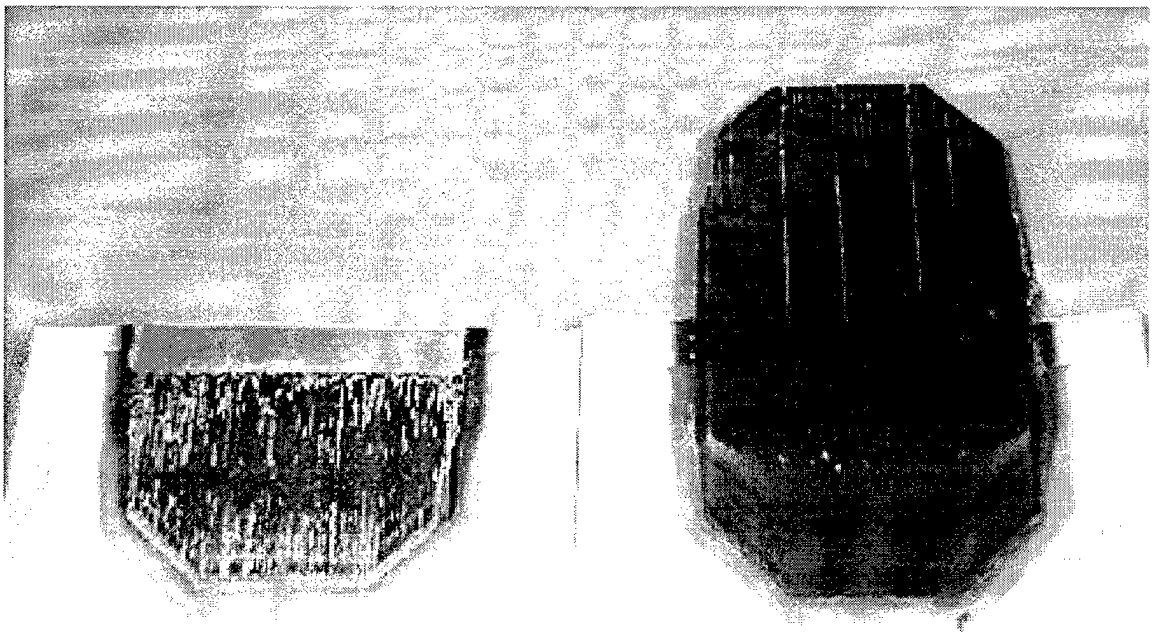

Figure 62. Post Failure - 20% Full Width Disbond (FWD)

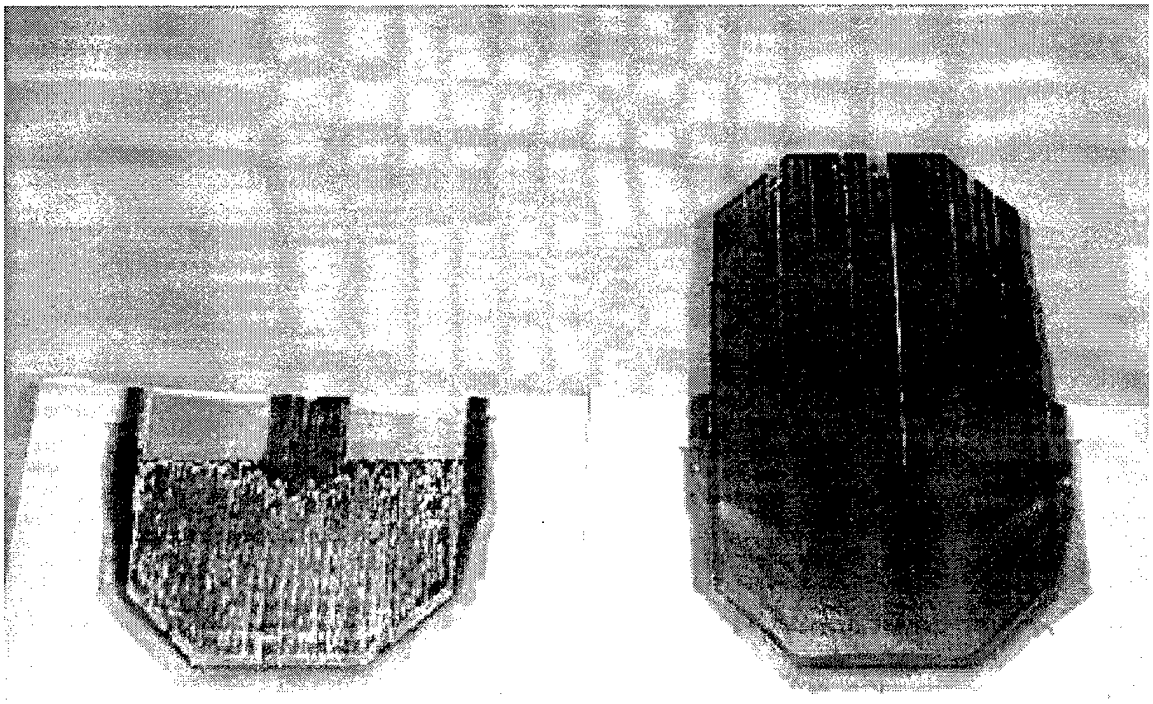

Figure 63. Post Failure - Crack Tip Disbond (CTD)

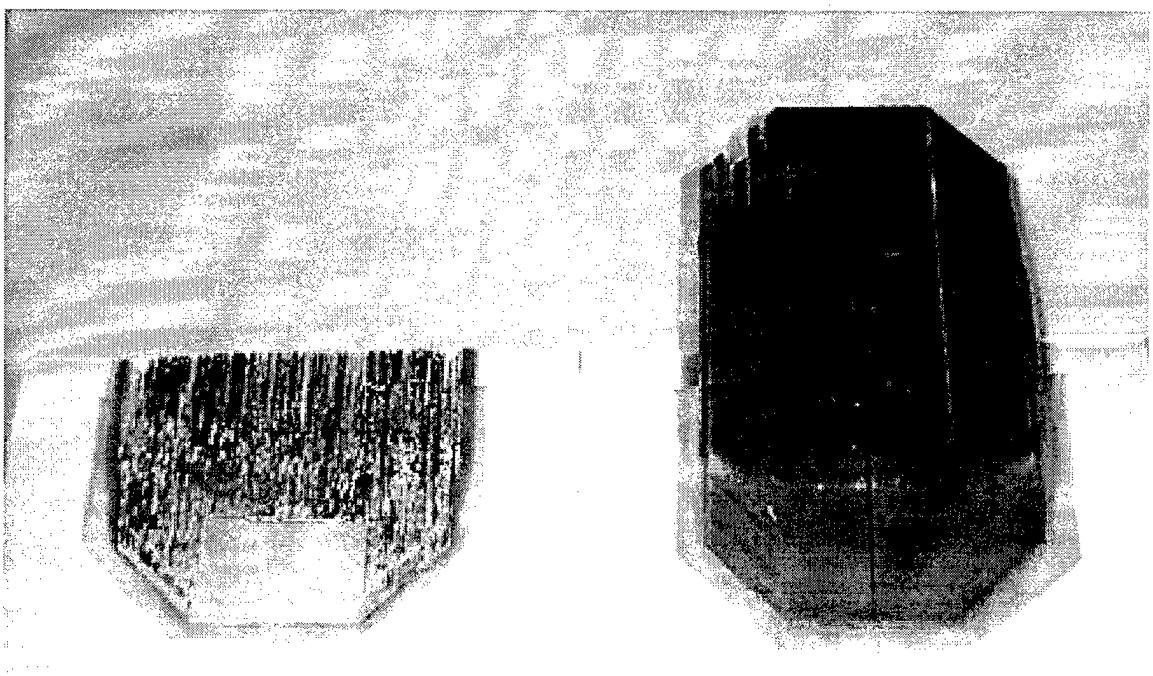

Figure 64. Post Failure - Patch Tip Disbond (PTD)

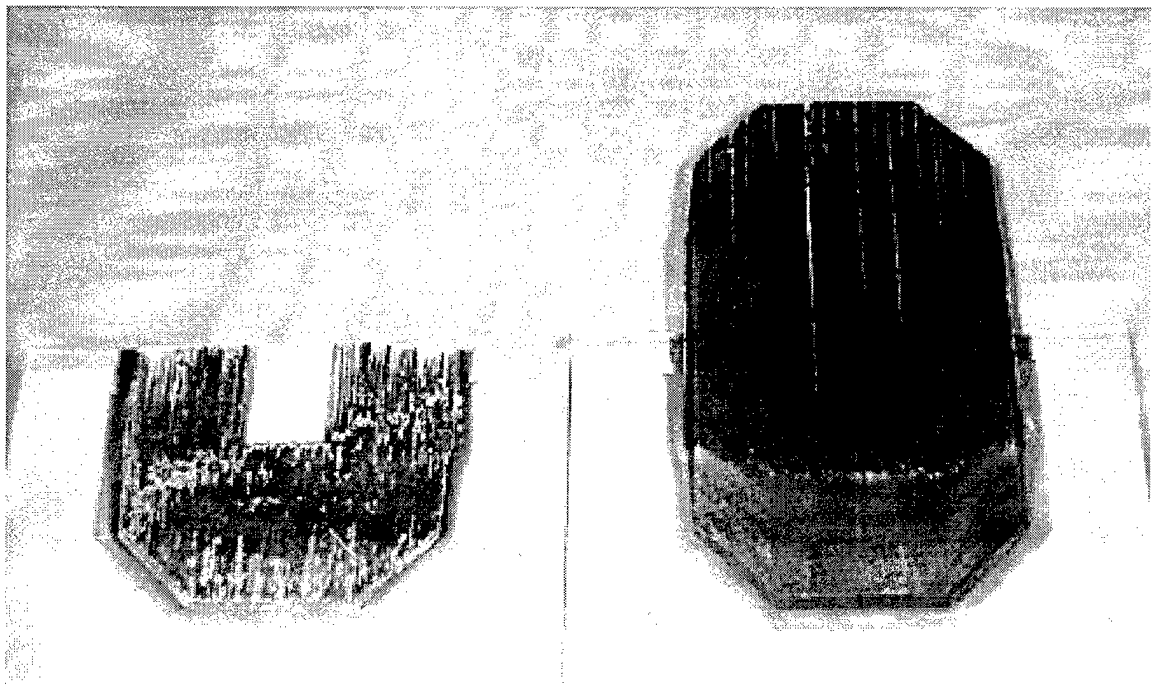

Figure 65. Post Failure - Center Disbond (CD)

APPENDIX B - Appendix B: C-Scan Images

This appendix contains select C-scan images of specimens detailing disbond size as a function of crack length.. A representative of each disbond configuration is presented. Three images from each disbond configuration are included. Tthe first image shows debond size and location at $2a = 25.4mm$, the second at $2a = 63.5mm$ and the third at $2a = 101.6mm$.

Figure 66. C-scan Fully Bonded Patch (FBP) 2a=25.4mm

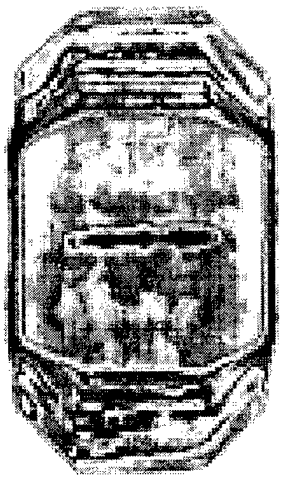

Figure 67. C-scan Fully Bonded Patch (FBP) 2a=63.5mm

Figure 68. C-scan Fully Bonded Patch (FBP) 2a=101.6mm

Figure 69. C-scan 20% Full Width Disbond (FWD) 2a=25.4mm

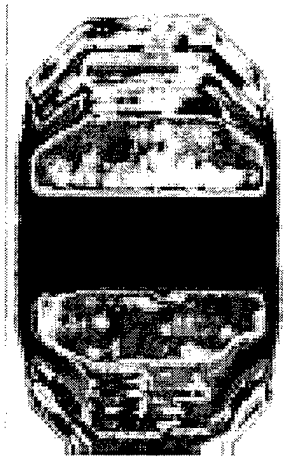

Figure 70. C-scan 20% Full Width Disbond (FWD) 2a=63.5mm

Figure 71. C-scan 20% Full Width Disbond (FWD) 2a=101.6mm

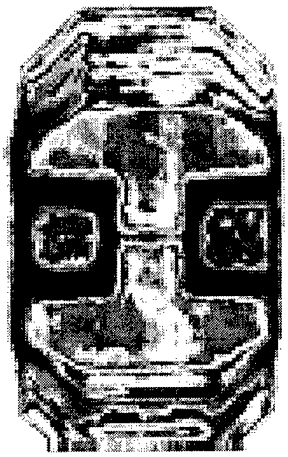

Figure 72. C-scan Crack Tip Disbond (CTD) 2a=25.4mm

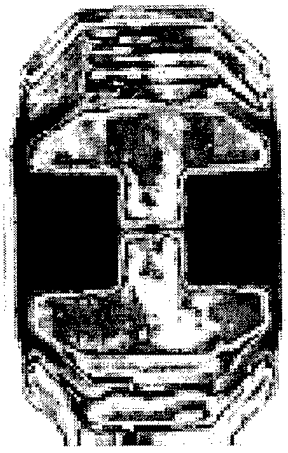

Figure 73. C-scan Crack Tip Disbond (CTD) 2a=63.5mm

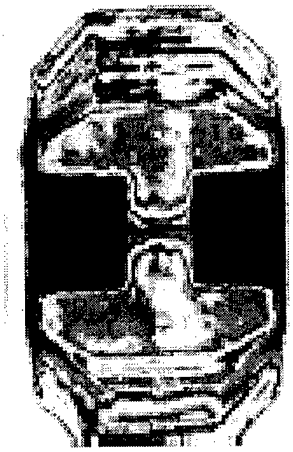

Figure 74. C-scan Crack Tip Disbond (CTD) 2a=101.6mm

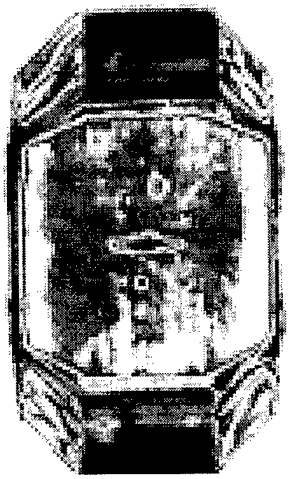

Figure 75. C-scan Patch Tip Disbond (PTD) 2a=25.4mm

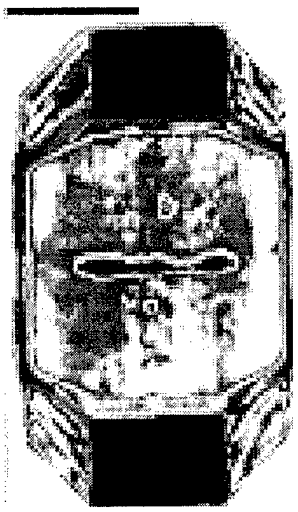

Figure 76. C-scan Patch Tip Disbond (PTD) 2a=63.5mm

Figure 77. C-scan Patch Tip Disbond (PTD) 2a=101.6mm

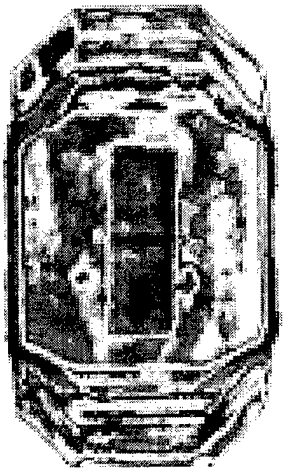

Figure 78. C-scan Center Disbond (CD) 2a=25.4mm

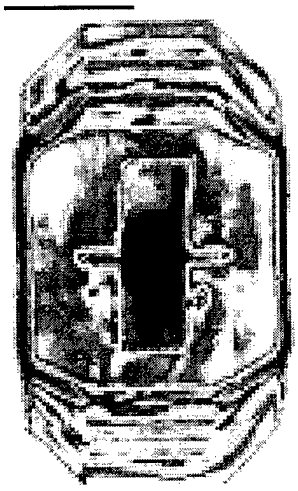

Figure 79. C-scan Center Disbond (CD) 2a=63.5mm

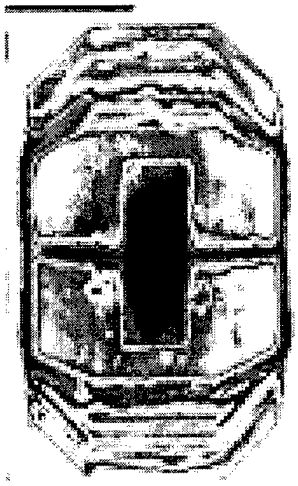

Figure 80. C-scan Center Disbond (CD) 2a=101.6mm

Bibliography

[1] Bureau of Accident Investigation. *Aircraft Accident Report: Aloha Airlines Flight 243, Boeing 737-200, N73711, Near Maui, Hawaii, April 28, 1988.* Report No. NTSB/AAR-89/03. Washington: National Transportation and Safety Office, 14 June 1989

[2] USAF Aging Aircraft Program Office. "Aging Aircraft: USAF Perspective

[3] Boeing Space and Defense Group. *Guidelines for Composite Repair of Metallic Structure.* Contract F33615-94-D-2006. Seattle, Wa: Boeing Space and Defense Group.

[4] American Society for Testing and Materials. *1993 Annual Book of ASTM Standards: Metals Test Methods and Analytical Procedures.* Vol. 03.01. Philadelphia: ASTM, 1993

[5] Baker, A. A., R. J. Chester, M. J. Davis, M. A. Retchford, and J. D. Roberts. "The Development of a Boron/Epoxy Doubler System for the F-111 Wing Pivot Fitting - Materials Engineering Aspects," *International Conference on Aircraft Damage Assessment and Repair.* August 1991.

[6] Walker, K., and R. Boykett. "Repair Substantiation Fatigue Testing Including Temperature and Frequency Effects for a Bonded Composite Repair to an F-111 Lower Wing Skin," *Proceedings of the 1996 USAF Aircraft Structural Integrity Program Conference.* 291-303. Materials Directorate, Wright Laboratory, Air Force Materiel Command, June 1997

[7] Hansen, L. G. "B-1B Shoulder Longeron Repair," *Proceedings of the 1993 USAF Structural Integrity Program Conference.* San Antonio, Texas: 30 November - 2 December 1993.

[8] Alford, R. E. and R. P. Bell. "C-141 Composite Material Repairs to Metallic Airframe Components," *Proceedings of the 1994 American Society for Nondestructive Testing Fall Conference.* Atlanta, Georgia: 19-23 September 1994.

[9] Grabovac, I., R. A. Bartholomeusz, and A. A. Baker. "Compoosite Reinforcement of a Ship Superstructure - Project Overview," *Composites, 24*: 501-509, (Number 6, 1993).

[10] Schubbe, Joel J. *Thickness Effects on Cracked Aluminum Plate With Composite Patch Repair.* Air Force Institute of Technology, (AU), Wright-Patterson AFB OH, May 1997 (AFIT/DS/ENY/97-4).

[11] Denney, Jason J. *Fatigue Response of Cracked Aluminum Panel With Partially Bonded Composite Patch.* JS thesis, AFIT/GAE/ENY/95D-7. School of Engineering, Air Force Institute of Technology (AU), Wright-Patterson AFB, OH, December 1995

[12] Ryan, J., and T. B. Mills. "TheEffects of Disbonds on Patching Efficiency Over Thicker Structure," *Proceedings of the 1998 USAF Structural Integrity Program Conference.* San Antonio, Texas: December 1998.

[13] Broek, David. *Elementary Engineering Fracture Mechanics.* Dordrecht: Kluwer

Academic Publishers, 1996.

[14] Kelly, L. J. "Introductory Chapter," *Bonded Repair of Aircraft Structures*. 1-18. A.A. Baker and R. Jones, editors. Dordrecht: Martinus Nijhoff Publishers, 1988.

[15] Eelason, E. B. "Bonded Doublers for Aircraft Structure Repair," *Aerospace Engineering*: 13-18 (July 1995).

[16] Baker, A. A. "Bonded Composite Repair of Metallic Aircraft Components - Overview of Australian Activities," *Proceedings of the 1994 AGARD Specialist's Meeting on Composite Repair of Military Aircraft Structures*. Seville, Spain: October 1994.

[17] Air Force Joint Technology Applications Office. *Composite Patches for Metallic Structures*. No. TT-89034. Wright -Patterson AFB OH, 29 August 1989 (AD-B143611).

[18] Ekstrom, M. "Bonded Repair of Aircraft Structures," *Materials Evaluation, 50*: 340-342 (March 1992).

[19] Fredell, R. S. *Damage Tolerant Repair Techniques for Pressurized Aircraft Fuselages*. PhD dissertation. Delft University of Technology, Delft, The Netherlands, June 1994 (WL-TR-93-3134).

[20] Reinhart, T. J. "Surface Treatments for Bonded Repairs of Metallic Components," *Bonded Repair of Aircraft Structures*. 19-29. A.A. Baker and R. Jones, editors. Dordrecht: Martinus Nijhoff, Publishers, 1988.

[21] Rose, L. R. F. "Theoretical Analysis of Crack Patching," *Bonded Repair of Aircraft Structures*. 77-105. A. A. Baker and R. Jones, editors. Dordrecht: Martinus Nijhoff, Publishers, 1988.

[22] Davis, M. J. "The Development of an Engineering Standard for Composite Repairs," *Proceedings of the AGARD SMP Specialists Meeting*. Seville, Spain: Octorber 1994.

[23] Shannon, R. W. and others. *Primary Adhesively Bonded Structure Technology*. Contract F33615-75-C-3016. Long Beach, Ca: Douglas Aircraft Co., McDonnell Douglas Corp., September 1978 (AD-A077891).

[24] Hart-Smith, L. J. "Design and Analysis of Bonded Repairs for Metallic Aircraft Structures," *Bonded Repair of Aircraft Structures*. 31-47. A. A. Baker and R. Jones, editors. Cordrecht: Martinus Nijhoff Publishers, 1988.

[25] Fredell, R. S., David Conley, and Shane Knighton, "Design Development of a Bonded Fuselage Repair for the C-5A," *Proceedings of the 1995 USAF Structural Integrity Program Conference*. 887-902. San Antonio, Texas: December 1995

[26] Kan, H. P., and M. M. Ratwani. *Composite Patch Repair of Thick Aluminum Structures - Final Report, Airtask No. WF41-400, PE 62241*. Report No. NADC-82139-60. United States Navy - Naval Air Development Center, Warminster, PA 18974, 1983.

[27] Labor, J. D., and M. M. Ratwani. *Development of Bonded Composite Patch Repairs for Cracked Metal Structure - Final Report.* Report No. NADC-79066-60 Vol. I. United States Navy - Naval Air Development Center, Warminster, PA 18974, 1980.

[28] Muki, Rokuro, and Eli Sternberg. "On the Stress Analysis of Overlapping Bonded Elastic Sheets," *Int. Journal of Solids and Structures*: 75-94 (1968).

[29] Arendt, C. and C. T. Sun. "Bending Effects of Unsymmetric Adhesively Bonded Composite Repairs on Cracked Aluminum Panels." *Annual Report for Air Force Office of Scientific Research, Grant No. F49620-93-1-0377, prepared by A.F. Grant, Jr.* A9-1-A9-7. Purdue University, School of Aeronautics and Astronautics, 1994.

[30] Irwin, G. R. "Fracture," *Handbook Physik, 6*: 551 (1958).

[31] Rybicki, E. F. and M. F. Kanninen. "A Finite Element Calculation of Stress Intensity Factors by a Modified Crack Closure Integral," *Engineering Fracture Mechanics, Vol. 9*: 931-938 (1977).

[32] Naboulsi, S., and S. Mall. "Modeling of Cracked Metallic Structure with Bonded Bomposite Patch Using Three Layer Technique." *Composite Structures, 35*: No. 7. 295-308, 1996.

[33] Naboulsi, S., S. Mall, and J. J. Denney. "Analysis of Fatigue Crack Growth in Imperfectly Bonded Composite Patch Repairs of Cracked Aluminum Panels." *Fatigue in New and Ageing Aircraft, ICAF 97*, R. Cook and P.Poole, editors. EMAS, 639-655, 1997.

[34] Cook, Robert D., David S. Malkus, and Michael E. Plesha. *Concepts and Applications of Finite Element Analysis*. New York: John Wiley & Sons, 1989.

Vita

Captain David S. Conley was born on 4 November 1970 in Saigon, Vietnam. He graduated from Rosborg Gymnasium, Vejle, Denmark in 1989. He then entered the University of Florida and graduated with a Bachelor of Science in Aerospace Engineering on 18 June 1994. Also on 18 June 1994, he was commissioned through the Air Force Reserve Officer Training Corp (ROTC). Captain Conley's first assignment was as a developmental engineer in the Fatigue and Fracture Section of Wright Laboratories, now known as Air Force Research Laboratories, where he worked in the development and fielding of bonded composite repairs to aging aircraft. Captain Conley entered the Air Force Institute of Technology in August 1997.

Permanant Address: 5960 S.W. 15th Street, Plantation, Florida 33317.

REPORT DOCUMENTATION PAGE

Form Approved
OMB No. 0704-0188

1. AGENCY USE ONLY *(Leave blank)*	2. REPORT DATE	3. REPORT TYPE AND DATES COVERED
	March 1999	Master's Thesis

4. TITLE AND SUBTITLE
Fatigue Response of RepairedThick Aluminum Panels With Bondline Flaws

5. FUNDING NUMBERS

6. AUTHOR(S)
David S. Conley, Captain, USAF

7. PERFORMING ORGANIZATION NAME(S) AND ADDRESS(ES)
Air Force Institute of Technology
AFIT/ENY Bldg. 640
2950 P. Street
Wright-Patterson AFB, OH 45433-7765

8. PERFORMING ORGANIZATION REPORT NUMBER
AFIT/GAE/ENY/99M-03

9. SPONSORING/MONITORING AGENCY NAME(S) AND ADDRESS(ES)
Dr. Tom Mills and 1Lt James Ryan
AFRL/VASE
Wright-Patterson AFB, OH 45433-7542

10. SPONSORING/MONITORING AGENCY REPORT NUMBER

11. SUPPLEMENTARY NOTES
Dr. Shankar Mall (937)255-3636 ext. 4587

12a. DISTRIBUTION AVAILABILITY STATEMENT
Approved for public release; distribution unlimited

12b. DISTRIBUTION CODE
A

13. ABSTRACT *(Maximum 200 words)*

This research investigated the fatigue response of precracked 558x177.8x6.35mm (22.0x7.0x0.25in) 2024-T351 aluminum panels repaired with single-sided partially bonded, unidirectional, eighteen ply boron/epoxy reinforcements. Disbonds were introduced into the bondline of each repair during the adhesion process using teflon inserts. Five different disbond configurations, with varying disbond locations and sizes, were tested. Each repaired panel was subjected to constant amplitude cyclic fatigue loading with a maximum stress of 120MPa. Results from the different configurations were compared against one another and against repaired panels with no debonds to assess the effect of disbonds on repair life. Results from the experimentation showed that even in the case of very large disbonds (20% of total bond area), the bonded repairs significantly extended the lives of the cracked panels. Disbond configurations with disbonds located away from the crack in the aluminum panel, performed comparably to the repaired panel with no disbonds. Disbond configurations with disbonds covering the crack in the aluminum panel yielded slightly lower lives than those obtained from repaired panels with no disbonds. Cyclic fatigue loading caused no increase in size of the artificially induced disbonds. Cyclic disbond growth was observed in the immediate vicinity of the crack. Finite element analysis using the Three Layer Technique was performed to assess the ability of current modeling techniques in predicting the life of cracked thick aluminum panels repaired with composite patches. Results from the finite element analysis were shown to very closely match experimental data.

14. SUBJECT TERMS
Fatigue Response, Bonded Composite Repairs, Cracked Aluminum Panels, Disbonds, Finite Element Analysis, Three Layer Technique

15. NUMBER OF PAGES
144

16. PRICE CODE

17. SECURITY CLASSIFICATION OF REPORT	18. SECURITY CLASSIFICATION OF THIS PAGE	19. SECURITY CLASSIFICATION OF ABSTRACT	20. LIMITATION OF ABSTRACT
Unclassified	Unclassified	Unclassified	UL